ISSN 1173-5996

Performance of Unprotected Steel and Composite Steel Frames Exposed to Fire

by

Clayton Wastney

Supervised by:

Associate Professor Andrew Buchanan

and

Associate Professor Peter Moss

Fire Engineering Research Report 02/11

May 2002

This report was presented as a project report as part of the ME (Fire) Degree at the University of Canterbury

School of Engineering
University of Canterbury
Private Bag 4800
Christchurch, New Zealand

Phone 643 364-2250
Fax 643 364-2758
www.civil.canterbury.ac.nz

Abstract

This report examines the performance of unprotected steel and steel composite beams as a component of steel framed buildings subjected to severe fire. The question of whether thermal protection is necessary for all structural steel is asked.

The behaviour of structural steel and composite beams is analysed at elevated temperatures using the non-linear finite element computer software SAFIR (Franssen et al: 2001). SAFIR is used to first study the two-dimensional behaviour of beams with theoretical support conditions, and then with more realistic support conditions by the addition of columns.

Steel and composite construction are both common and popular forms of construction used around the world. Structural steel commonly has thermal protection for fire resistance, which according to full-scale experimental fires (Clifton: 2001) may not be necessary. At this stage it is not well understood how the fire resistance mechanisms of unprotected steel works, nor how the changes in material properties influence the behaviour of the composite or steel beam. It is the intention of this report to provide some detail on single span two-dimensional beam behaviour in relation to material properties, support conditions and thermal exposure.

A 610 UB 101 steel beam both with, and without a 120mm thick composite concrete floor slab is exposed to three-sided heating, simulating the effects of a compartment fire. It was found that the theoretically idealised beam with supports having axial and moment restraint performed poorly compared to beams with axial restraint only. It was also found that the beam without axial restraint at one support had a run-away failure mechanism. With the addition of columns the beam had varying degrees of axial and moment restraint at the supports, causing much lower midspan deflections during the early stages of the fire. This compares well with the findings of the real fire single beam test of the Cardington fires (Clifton: 2001).

It was also found that when the EC3 Proportional and EC3 Yield Limit stresses were reached in the steel section, displacements, axial force and bending moments along the section were affected.

ACKNOWLEDGEMENTS

I would like to thank the following people who have helped me with my project:

- Associate Professor Andrew Buchanan for supervising my project and always being available to offer invaluable assistance and guidance.

- Associate Professor Peter Moss for being the associate supervisor for my report. Also for providing me with invaluable assistance in finite element modelling, help with this reports proof reading, and particularly for supplying me with a means of extracting data from the SAFIR results.

- Di McBride for methodically proof reading this report.

- Linus Lim for invaluable ideas and help with the finite element modelling that has made this report possible.

- Mike Spearpoint for help with the set-up of Fortran compiling software, which was needed for data extraction.

- Jean-Marc Franssen, for the use of the finite element software, SAFIR, without which this research would not have been possible.

- The New Zealand Fire Service for their financial assistance in providing me with a scholarship.

- Nathanial Petterson, for listening to, and comparing research related complaints into the wee small hours of the morning.

- And finally, to my fiancée Karen for her unwavering support over the year.

Contents

List of figures

List of tables

Glossary of terms

Ambient.....Being at room temperature (20^0C)

Catenary action.....Load carried by 2-dimensional tension only, such as draped rope carrying its own weight when held loosely at either end.

Connection.....The supports, or method of connection to columns at the ends of beams. Typical real connections are either bolted or welded, but are often idealised as either pinned or fixed in design.

Degradation (thermal) .....The progressive loss of strength of a given material such as steel and concrete while heated.

Elastic behaviour.....When the strain, or deflection of a member is still proportional to the stress applied.

Elastic limit.....The end of the linear portion of the stress strain curve for a given material

Elastic yield strength.....The maximum stress that a given material can take before deflecting plastically.

Finite element method (FEM).....The method of thermal and structural calculations as used by the computer software SAFIR. The modelled item (i.e. beam) is represented by a grid of elements, which for each a constant temperature, stress, and deflection is calculated. Collectively these elements represent a distribution of the temperature, and stresses through the section.

Fixed connection.....An idealised welded connection; restrained against rotation, horizontal, and vertical movement.

Fully fixed.....Beam or column fixed at both ends.

Structural capacity.....The ability for a structure to still carry loads without collapse despite large deflections, i.e. retaining at least one viable load path.

Mechanism.....A structural system is called a mechanism when structural capacity is no longer maintained. Mechanisms form when sufficient plastic hinges have formed; the beam will have very large deflections with little decrease in strength of members.

Member.....A component of a structural frame, being either a beam or column.

Membrane action.....Load carried by 3-dimensional tension only, such as a draped sheet carries its own weight when held loosely at all edges.

Midspan.....The midpoint of a beam's span.

Non-linear behaviour.....Plastic deflections; when the strain or deflection of a member is no longer proportional to the stress applied.

Pinned connection.....An idealised bolted connection; restrained against horizontal, and vertical movement, but not rotational movement.

Plastic deformation.....The non-linear region of the stress-strain curve for a given material. Strains increase rapidly with relatively little increase in stress.

Plastic hinge.....A plastic hinge forms when a beam has yielded through the whole cross section at a certain location, and no further stress increase can occur at this location. The beam must redistribute any additional loads to other parts of the beam. The beam is able to rotate about this new plastic hinge in order to redistribute these loads.

Poisson's ratio.....The absolute value of the ratio of the axial strain over the axial strain of a material with an axial force.

Proportional limit.....The elastic limit, or the end of the linear portion of the stress-strain curve for a given material.

Protected structural steel.....Structural steel with thermal insulative material applied for fire protection

Roller.....An idealised connection; restrained against vertical movement, but not rotational or horizontal movement.

Sliding support.....An idealised connection; restrained against vertical and rotational movement only, but not horizontal movement

Specific heat.....The rate of temperature rise of a given material to a given amount of heat energy.

Steel composite beam.....A steel beam connected to the concrete slab above, such that both must deflect together without slipping.

Stiffness.....The resistance of a structural member to deflection due to loading.

Strain.....The shortening or elongation caused by an applied stress

Stress.....A compressional or tensile axial force per unit area.

Thermal conductivity.....The rate that heat energy is able to transfer (conduct) through a given material.

Unprotected structural steel.....Structural steel without any thermal insulative material applied for fire protection

Young's modulus.....The slope of the linear portion of the stress strain plot for a given material.

Nomenclature

c_p	Specific heat
λ_{steel}, $\lambda_{concrete}$	Thermal conductivity of steel and concrete respectively
T	Temperature
Δl	Change in member length
l	Original member length
f_y	Steel ambient yield stress
f_r	Concrete tensile strength
$f_{y,T}$	Steel yield stress at a given temperature
ν	Poisson's ratio
E_{steel}, E_{conc}	Elastic modulus of steel and concrete respectively
ρ	Density
f_p	Ambient proportional stress limit
$f_{p,T}$	Proportional stress limit at a given temperature
$k_{y,T}$	Reduction factor for yield stress limit at a given temperature above ambient
$k_{p,T}$	Reduction factor for proportional stress limit at a given temperature above ambient
$k_{E,T}$	Reduction factor of Young's modulus at a given temperature above ambient

1 Introduction

1.1 Performance of structural steel in fire

Structural steel's poor performance in fire has long been attributed to a loss of strength and stiffness due to thermal degradation. Because of this, it has become common practice to thermally protect all structural steel, or less conservatively make use of unprotected structural steel. However the design of unprotected steel for fire has concentrated often only on the design of each structural component in isolation. This design method is supported by most countries current fire tests where isolated elements are tested in standard furnaces.

Despite this, it has been observed in real fire events and tests that unprotected structural steel in fire can have greater fire resistance where it is a part of a frame, particularly where steel acts compositively with a concrete slab. Bailey et al (1999) state that there is growing support that design of individual unprotected steel members is overly conservative, and neglects fundamental observations of interactions of structural components and those members restraining them.

Recent full-scale fire testing of a typical steel framed office building at the Cardington Research facility (Clifton, 2001) has shown that the interaction of all the structural components together within a steel framed building can not be overlooked. Steel beams in composite action with a concrete slab when heated from below by fire have been shown to support loads well beyond the expected failure temperature of the steel alone. Clearly in this situation the concrete slab is offering additional strength after the steel beam has failed. Other fire tests at the Cardington Research facility with the structural steel was not acting compositively with a concrete slab other surprising results were shown. These results were that even after the steel beam had undergone excessive deflections structural capacity was maintained (Clifton, 2001).

It is well recognised that unprotected structural steel members perform poorly when subjected to fire as compared to an equivalent protected steel or concrete member (Buchanan: 2001). The cause of the steel's reduced performance at higher temperatures can mainly be attributed to a reduction of strength and stiffness. Structural steel typically has a very high ratio of surface to cross-sectional area compared to typical structural concrete members. This combined with steels high thermal conductivity leads to more rapid heating. A protective coating of concrete or other insulative material can be applied to structural steel members, providing thermal insulation and increasing performance in fire.

Unprotected structural steel has been shown to survive for the duration of severe fires (FSEC, 1991), resulting in large deflections, but no collapse. The severity of fire that can be resisted by unprotected steel appears to be a function of not only the stiffness of the member considered, but also the stiffness of the complete frame (Clifton, 2001).

Traditionally when designing unprotected steel for fire, the connections are not greatly considered, nor are the effects of stiffness of the surrounding structure. This report looks in detail at typical real connection types, particularly of steel beams connected to columns, showing the importance of allowing for the large axial forces associated with steel in fire. It is shown that the stiffness of the fire-exposed member is linked to the restraint offered by the complete frame.

1.2 Research impetus

Steel is one of the most frequently used construction materials, particularly for high-rise buildings owing to it's high strength and stiffness relative to the weight. Arguably, one of steels greatest limitations in construction is its relatively poor performance in fire. This report aims to gain more insight into the more efficient use of unprotected structural steel. It is envisaged that with a greater understanding of not only fire, but also the stiffness effects imposed by the surrounding structure, more efficient and safe use of unprotected structural steel will be possible.

1.3 Objectives of research

- To revisit previous research of both unprotected steel and composite steel beams with idealised connections, confirming and expanding on findings.

- To model these beams again, but with more realistic connection constraints.

- Clarify the relationship between the large deflections of unprotected steel beams and the cooler structure.

The thermal and structural analysis of this report is conducted with the use of the two dimensional non-linear finite element computer program; SAFIR (Franssen et al, 2001).

1.4 Organization of this report

This report consists of a total of 9 chapters, the purpose of each of the following chapters being outlined within this section.

- Chapter 2 contains the report literature review. Summaries of previous research, experiments, concerning the performance of unprotected steel, along with the findings of the Broadgate phase 8 fire are covered within this chapter. The findings of previous research and the observations of unprotected steel in real fires from this chapter shall be used for comparisons in later chapters.

- Chapter 3 contains a discussion of the material properties as used within this report, and also by the computer software SAFIR (Frannsen et al, 2000). SAFIR is used for the finite element modelling within this report.

- Chapter 4 contains a description of the physical dimensions of the building elements modelled by SAFIR within this report. Details of the beam dimensions, loads, and the materials used are defined here.

- Chapter 5 discusses the analysis methods used to simulate the building elements as defined in chapter 4. Chapter 5 is broken down into two main sections: the first being the discussion of the thermal analysis, and the second being the structural analysis used by the computer models.

- Chapter 6 presents the results of the modelled unprotected steel and composite steel beams with idealised connection types exposed to the ISO fire. A discussion at the end of this chapter compares the results found with those of earlier research by Seputro (2001) and Welsh (2001) who looked at these same beams, but exposed to a slower heating fire.

- Chapter 7 presents the results of the modelled frames. The frames consist of unprotected steel or composite steel beams exposed to the ISO fire, the beams are connected to protected columns of varying stiffness. A discussion at the end

of this chapter compares these results with the results found in chapter 6, and with observations of beams with frame actions from the literature source discussed in chapter 2.

- Chapter 8 contains the final conclusions of the report.

- Chapter 9 lists the references sourced within the report.

- Appendix 1 contains further details of the Eurocode stress-strain relationships of steel and concrete at elevated temperatures.

- Appendix 2 contains example thermal input files for the computer software SAFIR (Fanssen et al: 2001) as used within this report .

- Appendix 3 contains example structural input files for the computer software SAFIR (Fanssen et al: 2001) as used within this report .

2 Literature review: Unprotected steel in fire

2.1 Broadgate phase 8 fire

This section is a summary of findings published within "Structural Fire Engineering Investigation of Broadgate Phase 8 Fire" by Fire Safety Engineering Consultants (FSEC) Ltd., 1991.

On June 23rd, 1990 a fire developed in the partially completed fourteen-storey Broadgate building. As the building was still under construction, fire and smoke detection systems were not yet operational, and the automatic sprinkler system was not active. Protection for beams and trusses was not complete, and columns had not been fitted with fire protective cladding. The fire began inside a contractor's hut located on the ground floor, remaining unchecked for some time, spreading smoke throughout the building. The total cost of damage caused by the fire was 25 million pounds. Only 2 million of this has been estimated as damage to the structural steel frame or concrete floor.

The fire duration was approximately 4.5 hours, of which 2 hours could be described as severe burning. Flames out of the contractor's hut window were at least 1000^0C. Despite this, metallurgical testing has shown that the peak temperature of the steel framework was only around 600^0C. Most of the structural steel work was exposed to the fire, due either to incomplete fire protection installation, or removal of what protection was in place by pressurised water from fire hoses. The most significant structural damage was axial shortening of columns and large deflections of trusses and beams, producing dishing of floors of up to 600mm in some areas. Because the steel temperatures did not get to above 700^0C, and the loads within the unoccupied building were low; most of the deformed structural members were able to perform without transferring loads to cooler parts of the structure. Typical column damage is shown in Figure 1.

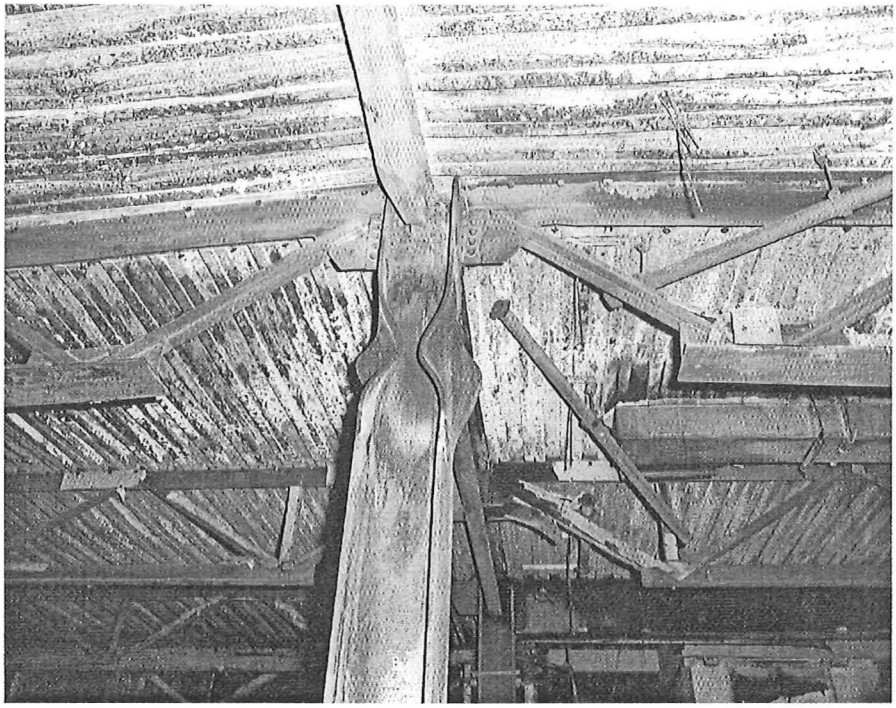

Figure 1) Axial shortening and yield at the top of a column from the Broadgate fire, image taken from FSEC Ltd (1991).

It was found that restraint conditions of members were important in the performance of heat-affected parts of the frame. For instance, small columns located close to a much larger column were found to have suffered more damage than the same sized smaller column without other adjacent larger columns. This is because as the smaller column would heat faster than the much larger column, its rate of axial expansion would be greater. This expansion would be restricted by the stiffness of the much larger column if it were present, causing large compressive stress within the smaller column. Similar effects were observed with beams and trusses that were fixed against rotation at end supports.

This differing rate of temperature change within different sized members is not considered in standard fire resistance tests, where each member is tested independently. The Broadgate fire has demonstrated that there is a need to consider the stability of the frame as a whole in fire engineering. Loss of capacity of individual members is not relevant, but most important is the maintenance of a reliable load path during, and after the fires duration for structural stability.

2.2 Cardington test fires

This section is a summary of findings published within "Notes prepared for a seminar on The Behaviour and Design of Multi-Storey Steel Framed Buildings For Severe Fires"; HERA Report R4-105, by Clifton C. (2001).

In 1995 and 1996 a full-scale modern office building was constructed and tested with fire in the BRE large scale testing facility at Cardington, in the United Kingdom. In total six fire tests were conducted, ranging from fire testing individual beams within a frame, to the burnout of a fully furnished office as shown in Figure 2.

1. Single beam tests

A composite beam connected to the rest of the cold structure was subjected to the standard ISO 834 test fire. It was found that the restraint conditions offered by the cold frame and the slab gave very different results for the beam's midspan deflection. The midspan deflection was found to be almost constant. Even when the steel temperature of the beam was up to 875^0C the deflection was found to have been equal to span/30. At this time the test was stopped because of electrical breakdown of data collection equipment.

2. Complete office fire

The last test involved the testing of a completely outfitted $135m^2$ office, complete with typical furniture. The steel columns were fire protected but the beams were not. The fire temperatures were recorded at being over 1200^0C, and the steel beams were recorded to have a peak temperature of up to 1100^0C with still no collapse, but considerable deflections. The steel beams would have only have had 3% of their strength at 1100^0C (Eurocode 3), with such little remaining strength left in the steel, the beams could only contribute as catenary tension members. It is also clear that the concrete floors were supplying strength to the structural system by membrane action.

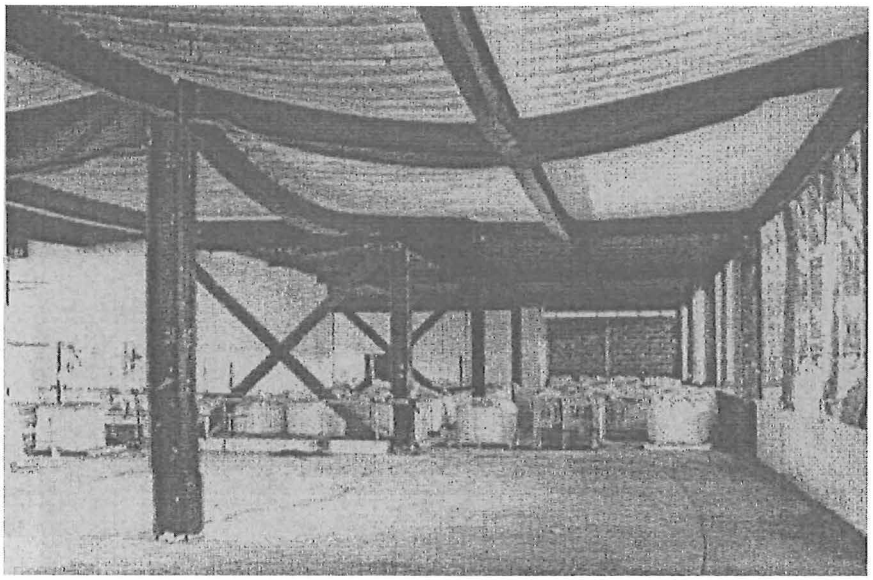

Figure 2) Steel beams acting as catenary members while the composite beam acts as a membrane after fire testing at Cardington (Clifton, 2001).

2.3 Other Research

Previous research by Seputro (2001), Welsh (2001), and Rotter and Usmani (2000) has shown that an unprotected steel beam's fire endurance is strongly dependant upon the support conditions. Rotter and Usmani (2000) suggest that the axial restraint from supports to the beams thermal expansion is the most crucial factor in determining the resistance of steel in fire. Either compressive stress within the section or thermal elongation occurs within the beam, depending on whether or not there is axial restraint at the supports (Rotter and Usmani, 2000). For other background on this topic see Becker (2000), or O'Callaghan and O'Connor (2000).

2.4 Summary

Both the Broadgate fire and the Cardington fire tests indicate that in a frame with unprotected structural steel exposed to fire, the support conditions offered by the frame are important. Further, it maybe overly conservative to fire rate each structural member individually. It maybe unnecessary to protect all structural steel members against fire, particularly where beams act in composite action with concrete slabs. Unprotected structural steel may undergo considerable deflections in severe fires, but as fire design should be treated as an ultimate limit state; deflections are not important. Rather we should be concerned with maintaining viable load paths for the duration of the fire, ensuring the building will be safe against collapse for fire fighting effects for the duration of the fire.

3 Material properties at elevated temperatures

This chapter describes the material properties as a function of temperature as used by SAFIR to simulate the non-linear temperature dependant material properties of both steel and concrete.

3.1 Steel thermal properties

This section describes the thermal properties of steel as used by SAFIR taken from the Eurocode (EC3: 1995).

3.1.1 Thermal conductivity; λ

Thermal conductivity is the measure of how rapidly the given material will conduct heat. For steel; thermal conductivity is a function of both temperature and the composition of the steel. The Eurocode suggests the following linear approximation for thermal conductivity for most structural steel, as shown in Figure 3.

$\lambda = 54 - (0.0333 \times T)$ (W/mK) for $800^0C > T \geq 20^0C$ **Equation 1**

$\lambda = 27.3$ (W/mK) for $1200^0C > T \geq 800^0C$ **Equation 2**

Where T is the steel temperature.

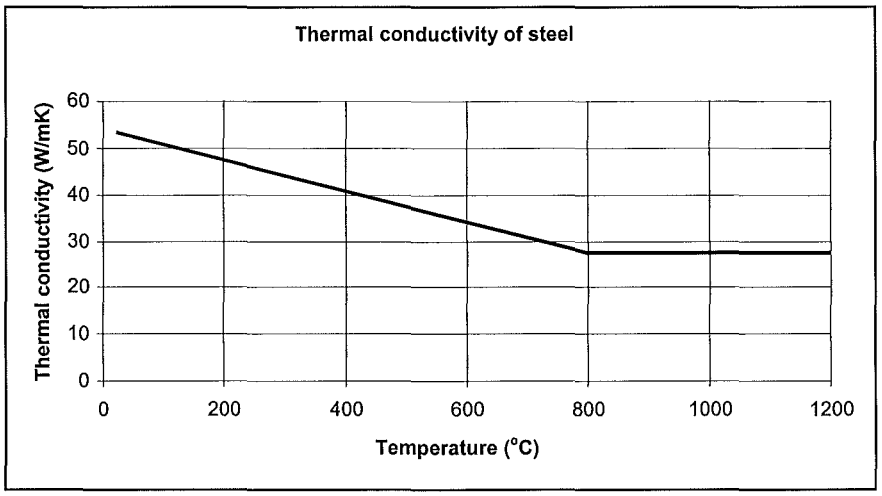

Figure 3) EC3 Thermal conductivity of steel as a function of temperature.

3.1.2 Specific heat; c_p

Specific heat is the measure of the materials ability to absorb heat. For steel, specific heat is a function of temperature and is independent of the composition of steel. The Eurocode suggests the following approximation for thermal conductivity for most steel (in J/kgK):

$c_p = 425 + 0.773\ T - 1.69 \times 10^{-3}\ T^2 + 2.22 \times 10^{-6}\ T^3$ for $600^0C > T \geq 20^0C$ **Equation 3**

$c_p = 666 + 13002/(738 - T)$ for $735^0C > T \geq 600^0C$ **Equation 4**

$c_p = 545 + 17820/(T - 731)$ for $900^0C > T \geq 735^0C$ **Equation 5**

$c_p = 650$ for $1200^0C > T \geq 900^0C$ **Equation 6**

Where T is the steel temperature.

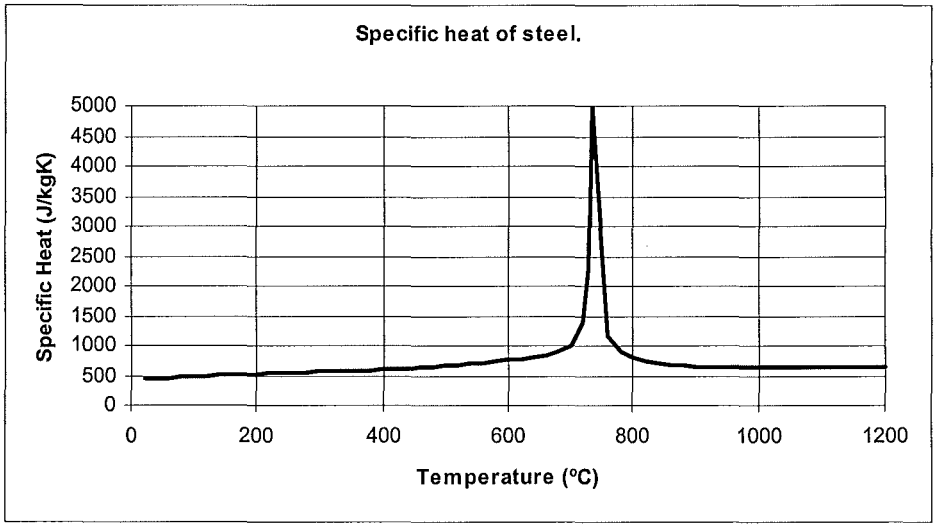

Figure 4) EC3 Specific heat of steel as a function of temperature

The sharp peak in the Eurocode suggested specific heat equations of steel at 730^0C as seen in Figure 4, is due to a metallurgical change in the steel crystal structure.

3.1.3 Thermal elongation

Thermal elongation is defined as the increase in member length divided by the members initial length; $\Delta l/l$. SAFIR determines thermal elongation of steel using the following Eurocode equations:

$\Delta l/l = 1.2 \times 10^{-5} T + 0.4 \times 10^{-8} T^2 - 2.416 \times 10^{-4}$ For $750^0C > T \geq 20^0C$ **Equation 7**

$\Delta l/l = 1.1 \times 10^{-2}$ For $860^0C > T \geq 750^0C$ **Equation 8**

$\Delta l/l = 2 \times 10^{-5} T - 6.2 \times 10^{-3}$ For $1200^0C > T \geq 860^0C$ **Equation 9**

Where T is the steel temperature. These equations are shown graphically in Figure 5.

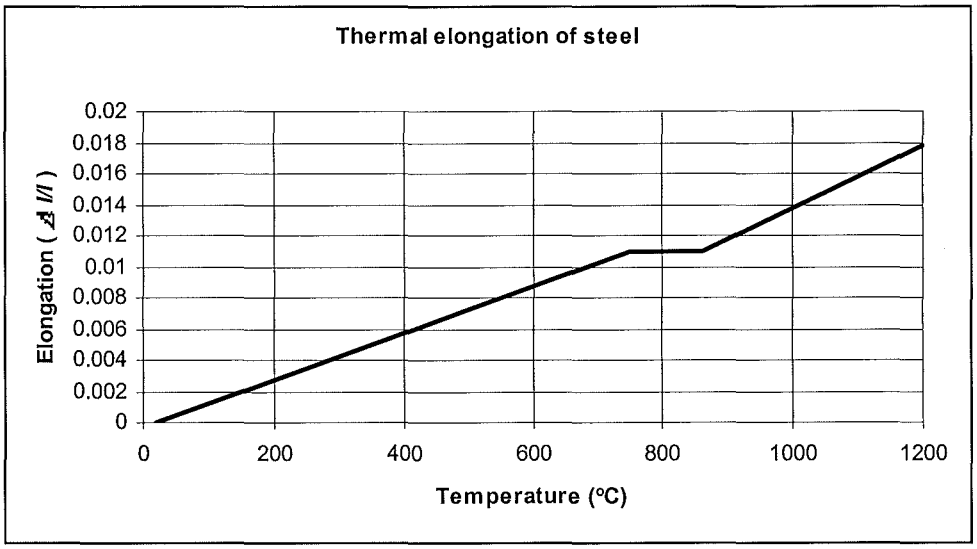

Figure 5) EC3 Thermal elongation of steel as a function of temperature.

3.2 Steel mechanical properties

This section describes the structural properties of steel as used by SAFIR taken from the Eurocode (EC3: 1995).

3.2.1 Proof and yield strength and the proportional elastic limit

Steel at ambient temperatures typically has a very well defined yield strength, however at elevated temperatures the point of yield is no longer well defined. Buchanan (2001) reports that the use of proof strength maybe used as the effective yield strength of steel at elevated temperatures. Proof strength is taken as the point of the stress strain curve intersecting with a line passing through 1% strain at the same slope as the linear portion of the stress strain curve, as shown on Figure 6.

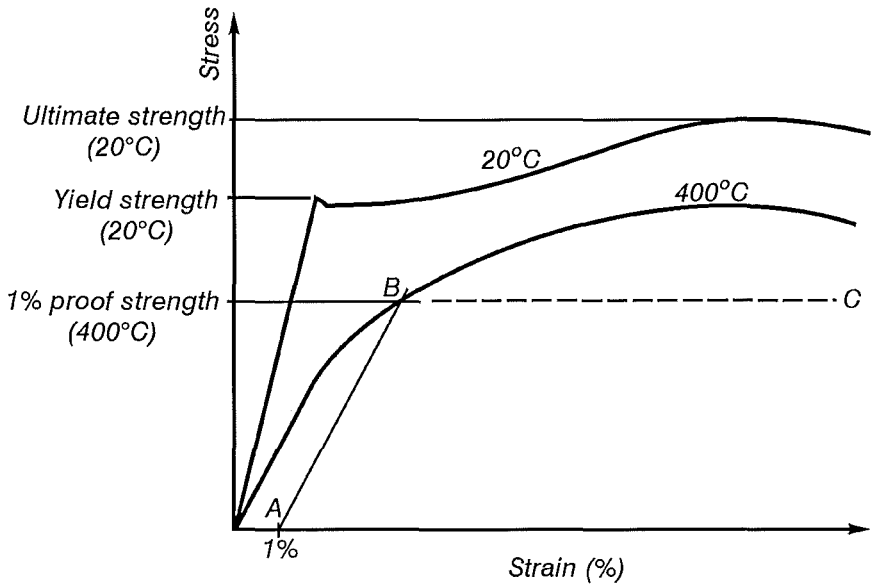

Figure 6) Stress strain curves for steel illustrating yield strength and proof strength, taken from Buchanan (2001).

The proportional limit is the point of the stress strain curve where strain is no longer linear with stress. That is, the proportional limit is the limit of elastic behaviour of steel at elevated temperatures.

3.2.2 *Ambient properties*

The following ambient material properties have been used for all steel considered within this report. The software SAFIR requires the user to specify the ambient material properties.

Table 1) Properties of steel at ambient temperatures

Property	**Notation**	**Ambient value**	**Unit**
Steel beam yield strength (610 UB 101)	f_y	300	MPa
Reinforcing mesh yield strength	f_y	430	MPa
Poisson's ratio	ν	0.3	-
Elastic modulus	E_{steel}	210	Gpa
Density	ρ	7850	kgm^{-3}

3.2.3 *Properties at raised temperatures*

The mechanical properties of steel change as both strength and stiffness steel drop with increased temperature. The temperature dependence of these properties has been taken from the Eurocode (EC3: 1995). These reduction factors, as shown in Figure 7, are used to determine the steel resistance to tension, compression, moment, and shear forces.

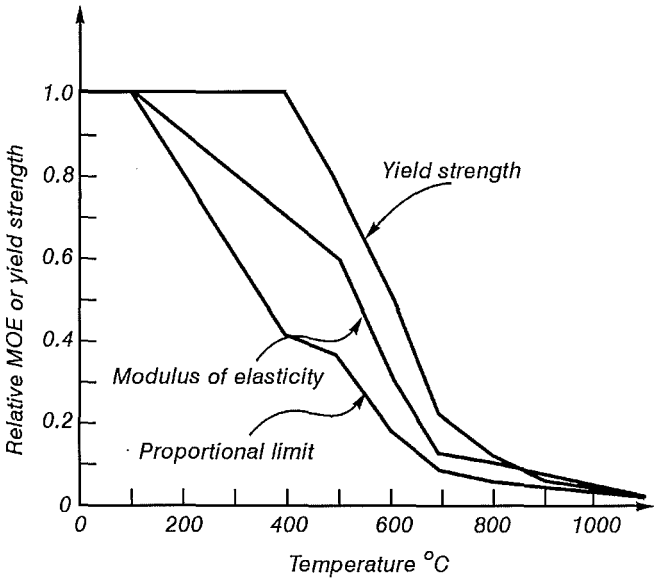

Figure 7) Reduction in steel's yield strength and modulus of elasticity with temperature

The meaning of each reduction factor is summarised below:

Table 2) Reduction factors of steel properties at elevated temperatures

Reduction factor	**definition (symbolised)**	**Meaning**
$k_{y,T}$	$f_{y,T}/f_y$	Temperature related effective yield strength relative to ambient temperature yield strength
$k_{p,T}$	$f_{p,T}/f_y$	Proportional limit relative to ambient yield strength
$k_{y,T}$	E_T/E	Elastic modulus relative to the ambient elastic modulus

3.3 Concrete Thermal properties

This section summarises the thermal properties of concrete assumed by SAFIR as recommended by the Eurocode (EC2 1993). A siliceous aggregate concrete is assumed.

3.3.1 Thermal conductivity

Thermal conductivity is dependant upon the aggregate type and the temperature of the concrete. The following equation is the Eurocode (EC2 1993) recommended thermal conductivity equation for siliceous aggregate, and is shown graphically in Figure 8.

$\lambda_c = 2 - 0.24\ T/120 + 0.012(T/120)^2$ (W/mK) for $1200^0C > T \geq 20^0C$ **Equation 10**

Where T is the temperature of the concrete.

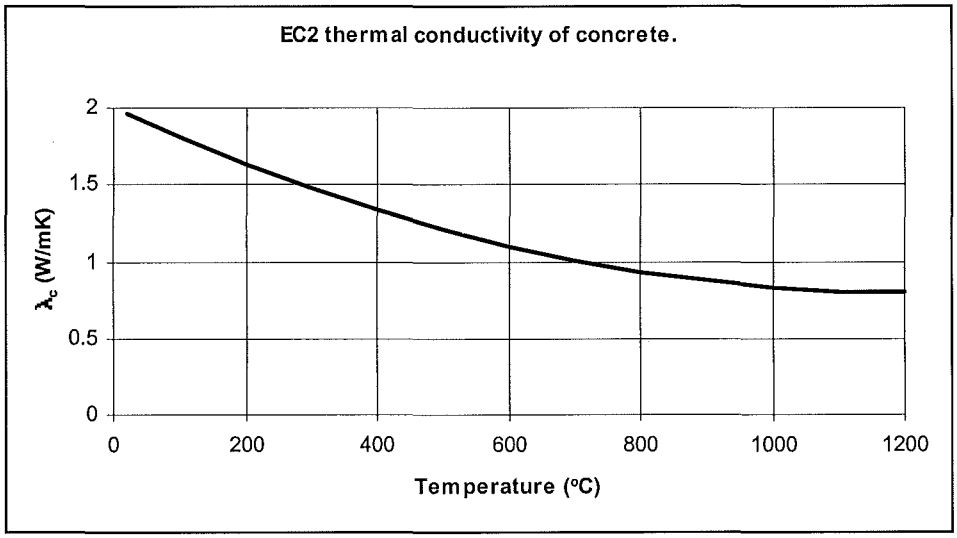

Figure 8) EC2 Thermal conductivity of concrete as a function of temperature.

3.3.2 *Specific heat*

The specific heat of concrete varies mainly with the moisture content. The moisture within the concrete causes a peak between 100^0C and 200^0C due to the water being driven off. The Eurocode recommends the following relationship for calculation of concrete's specific heat.

$c_p = 900 + 80\,T/120 - 4(T/120)^2$ (JkgK) For $100^0C > T \geq 20^0C$, and; $1200^0C > T \geq 200^0C$ **Equation 11**

Where T is the temperature of the concrete.

However, as shown by Figure 9, there is a peak between 100^0C and 200^0C due to water being driven off. This peak must be included with the above equation in the temperature range of 100^0C to 200^0C.

$c_{p,\,peak} = 1875$ (JkgK) For 2% moisture by weight; $100^0C > T \geq 20^0C$ **Equation 12**

$c_{c,\,peak} = 2750$ (JkgK) For 4% moisture by weight, $100^0C > T \geq 20^0C$ **Equation 13**

Where T is the temperature of the concrete.

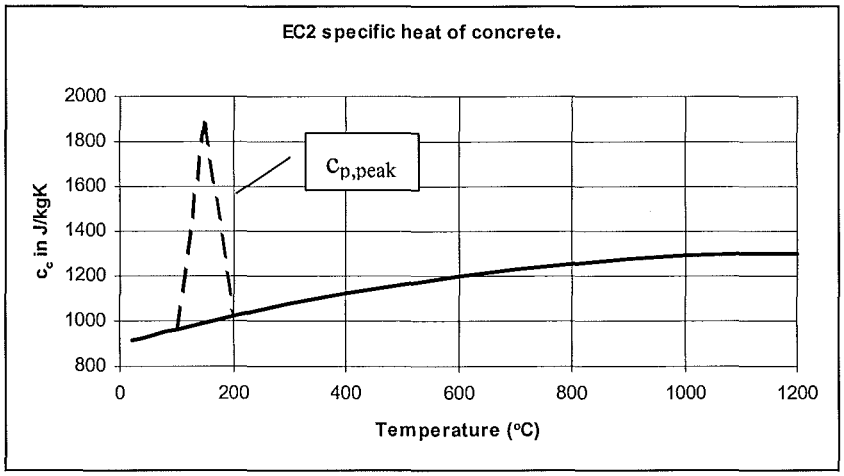

Figure 9) EC2 Specific heat of concrete as a function of temperature.

3.3.3 *Thermal elongation*

Eurocode (EC2: 1993) recommends the following equation for siliceous concrete. This thermal elongation and temperature relationship is non-linear until 700^0C, where it becomes constant. This equation is shown graphically in Figure 10.

$(\Delta l/l) = -1.8 \times 10^{-4} + (9.0 \times 10^{-6})T + (2.3 \times 10^{-11})\, T^3$ For $700^0C > T \geq 20^0C$ **Equation 14**

$(\Delta l/l) = 14 \times 10^{-3}$ For $1200^0C > T \geq 700^0C$ **Equation 15**

Where T is the temperature of the concrete.

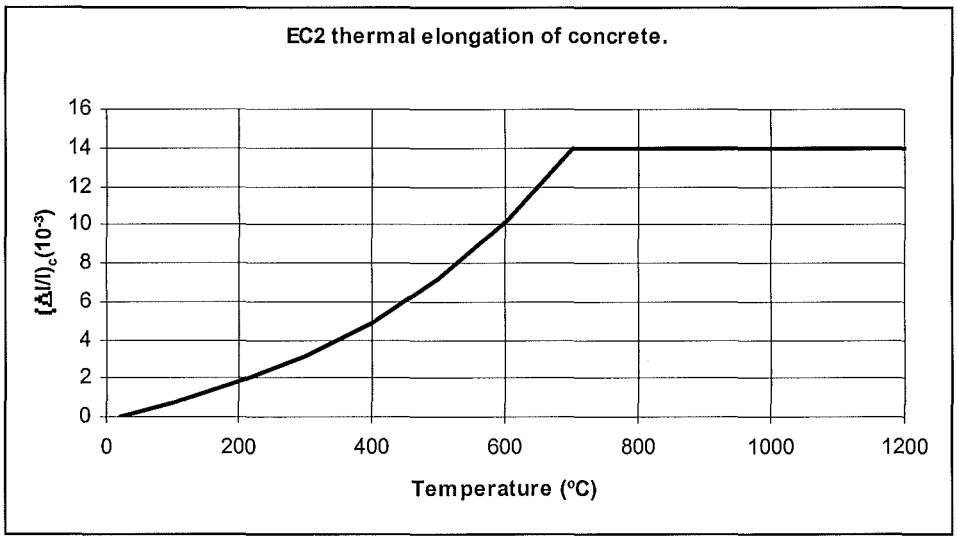

Figure 10) Thermal elongation of concrete as a function of temperature.

3.4 Concrete mechanical properties

3.4.1 Ambient properties

The following properties have been assumed for the siliceous concrete at ambient temperatures and entered directly in to each SAFIR simulation for concrete.

Table 3) Assumed concrete mechanical properties at ambient temperature

Property	**Notation**	**Ambient value**	**Unit**
Type of concrete	Not applicable	Siliceous concrete	*Not applicable*
Concrete crush strength	f'_c	30	MPa
Concrete tensile strength (or rupture strength)	f_r	0	MPa
Concrete elastic modulus	E_{conc}	23.5	GPa
Poisson's ratio	ν	0.02	*Not applicable*
Density	ρ	2300	kgm^{-3}

The concrete is assumed to crack when the tensile strength is reached. If the concrete tensile strength is not zero the energy released by cracking can cause computational errors for the SAFIR software. This problem, along with the reality that the tensile strength of concrete is typically negligible has led the author to use a concrete tensile strength of zero throughout.

3.4.2 *Properties at raised temperatures*

The stress-strain relationship for siliceous aggregate concrete at elevated temperatures is illustrated in Figure A.4 and Table A.3 in the Appendix. The reduction of the characteristic compressive strength of siliceous aggregate concrete as a function of the temperature *T,* is allowed for by the coefficient $k_c(T)$ for which:

$$f'_{ck}(T) = k_c(T)f'_c(20^{\circ}C) \qquad \textbf{Equation 16}$$

Where: $k_c(T)$ *is as per* Table A.3

4 The building modeled by this analysis

The beam studied within this report is based upon a 610 UB 101 steel beam spanning 8.0m acting compositively with a 120mm thick profiled concrete slab. This beam is an internal primary gravity beam from a typical New Zealand office building. The primary beam spacing is 8.9m centres, with secondary beams spaced at 2.50m centres. The existing 17 storey office building has all structural steel members thermally protected for fire, and the suspended ceiling also provides additional fire protection to the beams. Rather than analysing the beam in its real situation, this report intends to examine the fire resistance of this particular steel beam as if it were not fire protected, with no allowance for the hung ceiling. The beam will be analysed both as a composite beam, and as a steel beam only, with a variety of support conditions.

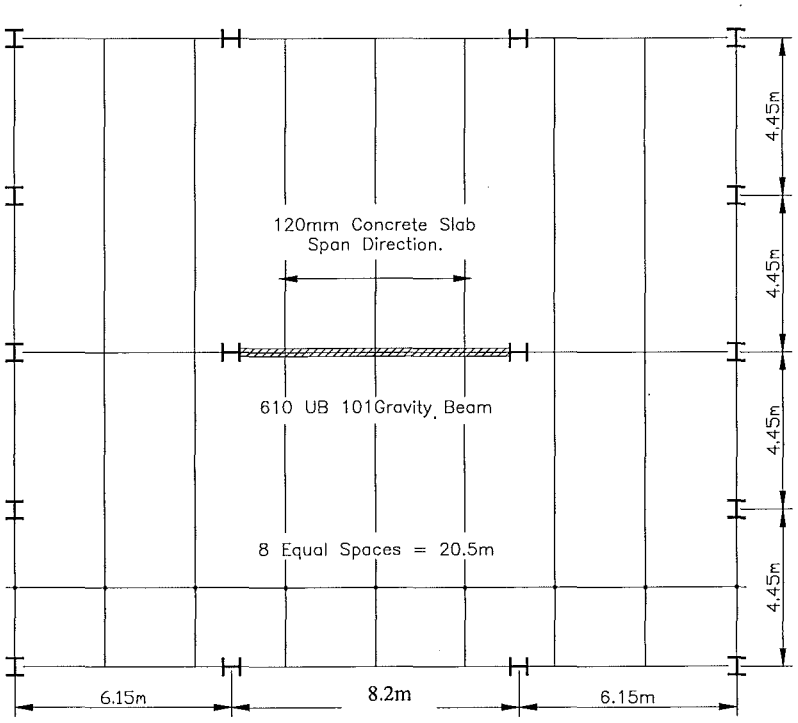

Figure 11) Layout plan of building, from Welsh (2001)

This is the same beam analysed by both (Welsh: 2001) and (Seputro: 2001), the objective of this study is to expand on their earlier findings.

4.1 Beam dimensions

4.1.1 Steel beam

A 610UB101 steel beam with no composite action with the concrete slab from above was used for the steel beam only scenarios. The dimensions of this beam are tabulated below:

Table 4) Dimensions of steel beam

Beam size	610UB101 steel beam (no composite action)
Depth of section	602 mm
Flange width	228 mm
Flange thickness	14.8 mm
Root radius	14.0 mm
Gross cross-sectional area	13000 mm^2
Second moment of area	761 x 10^6 mm^4
Depth to neutral axis	301 mm
Plastic section modulus	2900 x 10^3 mm^3

4.1.2 Composite beam

The composite beam scenarios used a 610UB101 steel beam with composite action with a profiled concrete slab. The dimensions of the steel beam were as detailed in Table 4. Figure 12 shows a typical cross-section through the steel beam and composite beam, complete with the Diamond Hi-Bond proprietary profile decking.

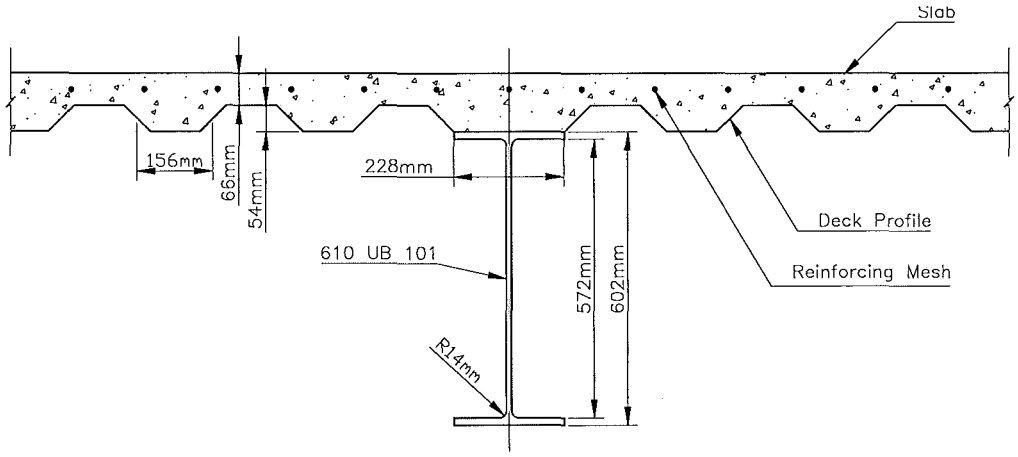

Figure 12) Cross-section through the composite beam used in model, taken from Welsh (2001)

NZS 3404:1997 (clause 13.4.2.1) states that for the calculation of the structural capacity of a composite beam in the positive moment region, the width of slab above the beams centreline shall be taken to have an effective width of the lesser of 0.25 times the span of the beam, or 0.25 times the span of the concrete deck between beams (beam to beam centreline distance). The span of the beam considered is 8m and the beam to beam centreline distance is 8.9m, hence in accordance with NZS 3404:1997 the width of the structural slab considered shall be 2m, or 1m either side of the steel beam centreline. Dimensions of the composite beam as used within this report are detailed below:

Table 5) Dimensions of composite beam

Steel beam size	610UB101 steel beam
Effective width of slab	1000 mm
Gross cross-sectional area of concrete	13000 mm^2
Second moment of area of composite beam	1.893 x 10^9 mm^4
Depth to neutral axis of composite beam	242 mm
Depth of concrete slab (through deck profile)	120mm
Depth of concrete slab (between deck profiles)	65mm
Mesh size	665 (Dimond Industries, 1997)
Concrete cover above mesh	25mm (Dimond Industries, 1997)

4.2 Loads applied to beams

The loads applied to the beam analysed within this report are the same as analysed earlier by Seputro (2001) in the case of the steel beam, and by Welsh (2001) in the case of the composite beam.

4.2.1 Composite beam

The following is the loading as used by Welsh (2001) for the composite beam loads.

Table 6) Calculation of composite beam loads from Welsh (2001).

Component of load	**Value**	**Unit**	**kN/m**
Slab + Deck	2.5	kPa	22.25
610 UB 101	0.99	kN/m	0.99
Self imposed dead load. (SDL)	2.00	kPa	17.8
Live Load	2.5	kPa	
Adjustment for $Q_u = \psi Q$	0.4*2.5	kPa	8.9
Total	5.62	kPa	50.00

4.2.2 Steel beam

The steel beam is required to have a reduced load for the purposes of this report as the existing beam is unable to carry this load without composite action, as is the case for the existing beam. The load used for all non-composite beam analyses will be arbitrarily set as 25 kNm^{-1} for convenient comparison with findings of Seputro (2001).

5 Analysis method using the SAFIR finite element software

5.1 General

The thermal and structural analysis of this report is conducted with the use of the two dimensional non-linear finite element computer program; SAFIR (Franssen et al, 2001).

SAFIR uses the Finite Element Method (FEM) to study one, two or three-dimensional structures. For the purpose of this report only a two-dimensional analysis was used. This is justified for unprotected steel beams provided they are compact, and buckling does not occur. Rotter and Usmani (2000) have shown that a compact steel section will yield forming plastic hinges before buckling occurs. The stress strain relationships are as defined in Chapter 3 of this report.

5.2 Thermal analysis

SAFIR first calculates the temperature profile through a given cross-section. As the analysis used is only two-dimensional, a representative temperature profile with time is calculated for the cross-section. Heat can only transfer through the cross-section and not along the length of the beam. The fire temperature is assumed to follow the ISO fire curve, with the sides and bottom perimeter of the beam exposed to fire, but no fire on the top of the top flange. The fire temperature is consistent on the sides and bottom perimeter of the beam. This is a reasonable assumption for a post flashover fire, where one can assume the fire compartment is a well-stirred reactor. It is this post flashover phase of the fire that is of greatest interest for structural stability of steel. Grids of finite elements are used to calculate the temperature distribution across each cross section considered.

5.2.1 Steel beam

The first thermal analysis was that of a 610UB101 steel beam with no composite action with a concrete slab from above. This thermal analysis is similar to the thermal analysis used by Seputro [2001] for the testing of idealised connection types and axial spring connections.

The steel beam was described by SAFIR by using 280 nodes and 206 elements for the cross-section. Details of the thermal analysis cross representation are shown in Figure 13

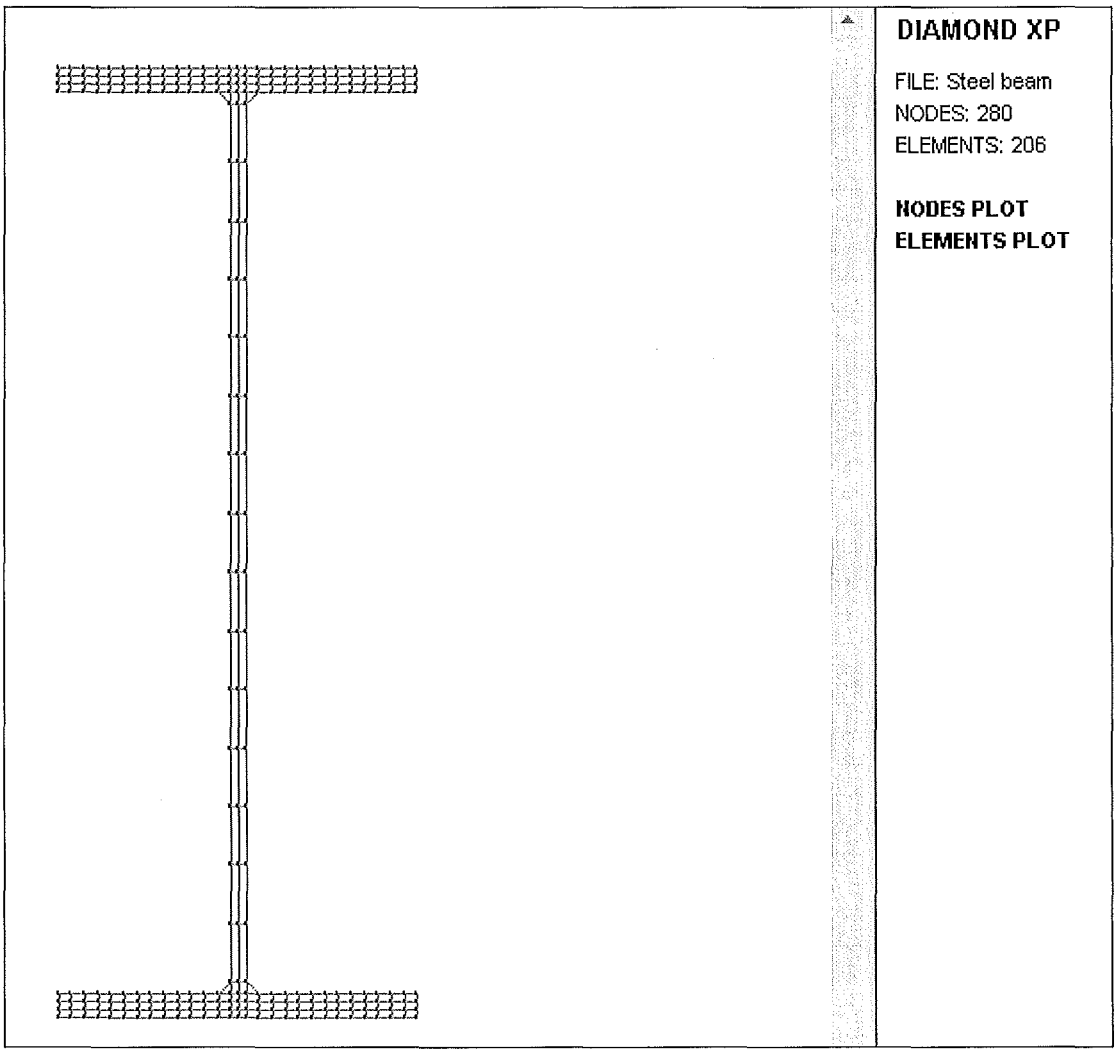

Figure 13) Nodes and elements used to represent steel beam without composite action

5.2.2 Composite steel beam

The second thermal analysis was a 610UB101 steel beam with composite action with a profiled concrete slab as shown in Figure 12.

The thermal analysis used within this report differs from the thermal analysis used by Welsh (2001) in that the profiles of the concrete slab is not idealised as an upper and lower layer of concrete (see Figure 14), but rather the profiled shape of the deck is maintained. The reason for the more complicated analysis was to achieve a more realistic temperature distribution to the steel mesh within the concrete slab.

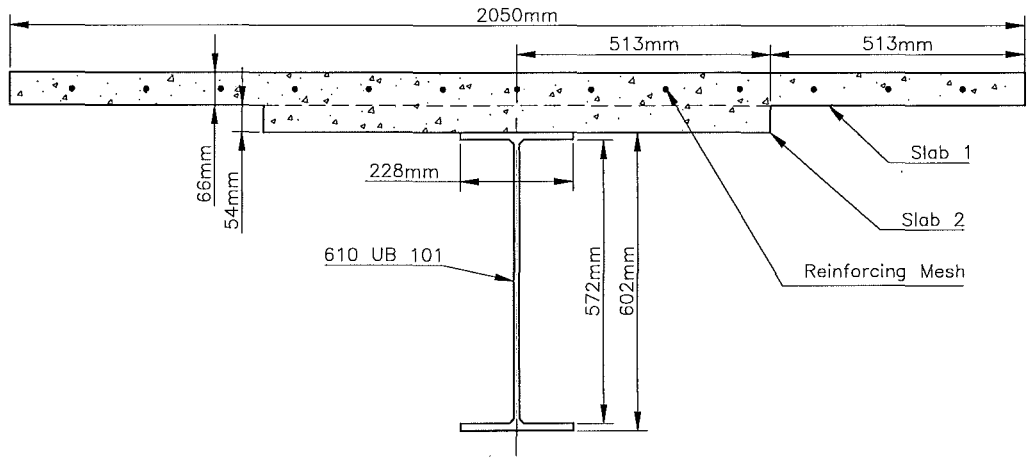

Figure 14) Composite beam as modelled by Welsh (2001).

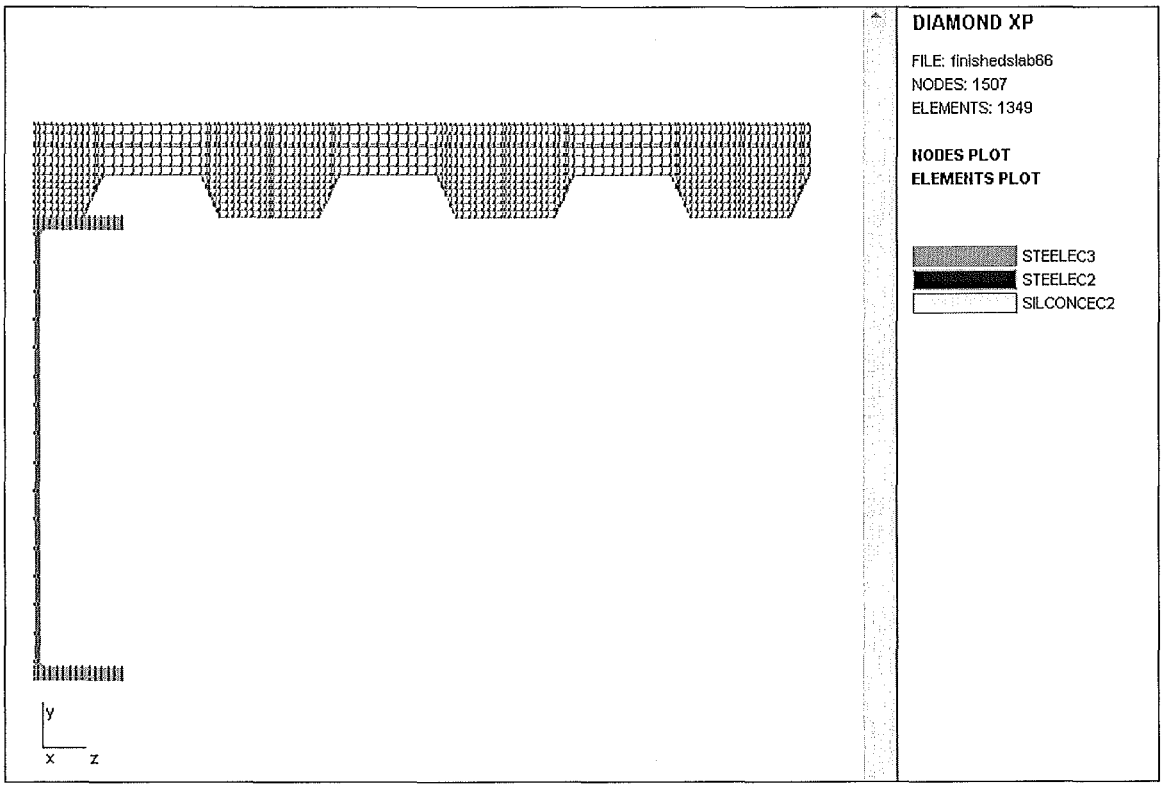

Figure 15) Refined profile deck as used for thermal analysis of the steel beam with a composite beam within this report

As shown by Figure 15, symmetry was used about the beam centerline, any boundary surface of the thermal analysis that does not have an associated boundary temperature is assumed to be a line of symmetry by SAFIR. All isotherms will be perpendicular to these surfaces. The top of the slab was exposed to a constant temperature of 20^0C so that it would not be treated as a line of symmetry by SAFIR.

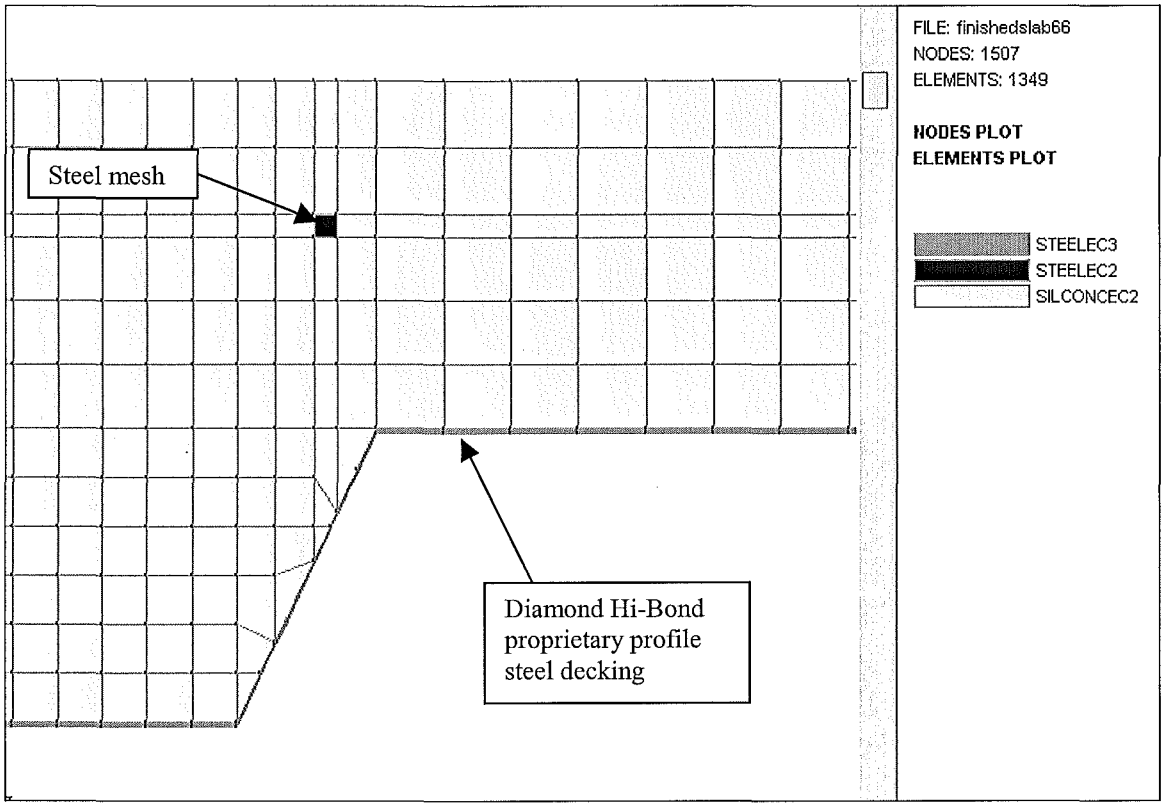

Figure 16) Detail of profiled concrete slab

The above detail (Figure 16) of the concrete slab shows how the steel mesh and the Diamond Hi-Bond proprietary profile steel decking was incorporated into the SAFIR analysis, the steel decking is used in construction as permanent form work for the concrete, and adds to the tensile strength at the bottom of the slab, particularly in cold conditions.

5.3 Structural Analysis

The steel beam, and composite beam cross-sections analysed using SAFIR as discussed earlier are used to make up structural beams and columns for the structural analysis. SAFIR assumes that the elements of the thermal analysis cross-section are extended out of plane to form long strings for the structural analysis. Each material's thermal degradation is calculated based on the temperature profile from the thermal analysis and the user defined ambient structural properties. These strings of elements make up the members of the beams and columns, which are in turn used to make up the supported beams and frames.

The support conditions used within this report are discussed below:

5.3.1 Supported beams

Both the steel beam and the composite beam will be analysed with the following support conditions. These support conditions are categorised as either axially restrained or axially unrestrained.

5.3.1.1 Axially restrained beams

Axially restrained beams are beams that are not able to move horizontally at the supports, hence axial expansions of the beam can not be accommodated by the supports.

- **Pin-pinned beam**

This structural system consists of a beam pinned at both ends (seeFigure 17). Because of the pinned connections at either end, rotation is possible at the ends allowing greater midspan deflections. A pin-pinned supported beam only requires one plastic hinge in order to form a mechanism. In cold conditions this plastic hinge will form at the midspan when the beam is loaded to its ultimate capacity, as is shown in Figure 18.

Figure 17) Schematic of a pin-pinned beam before failure

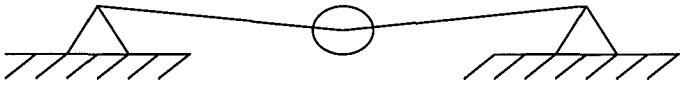

Figure 18) Schematic of pin-pinned beam at failure with a single plastic hinge at midspan

- **Fully-fixed beam**

This structural system consists of a beam fixed at both ends (Figure 19). The fixed connections at either end do not allow horizontal movement, vertical movement, or rotation. Midspan deflections are reduced compared to the pin-pin supported beam, as no rotation is possible at the supports.

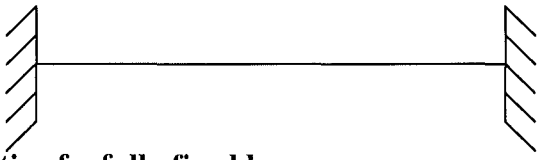

Figure 19) Schematic of a fully fixed beam

A fully-fixed beam requires three plastic hinges in order to form a mechanism, one at either support, and one at the midspan. In cold conditions the first plastic hinges will form at both supports simultaneously (see Figure 20). Bending moments are then able to redistribute so that loads are carried like a simply supported beam.

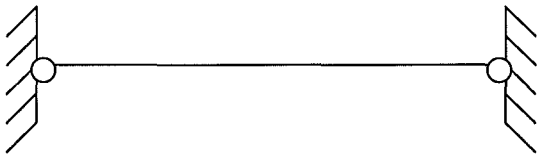

Figure 20) Schematic of a fully fixed beam after plastic hinges have formed at supports

The beam is stable until the third plastic hinge forms at the midspan, forming a mechanism at the ultimate capacity (Figure 21). Because three plastic hinges are required to form a mechanism, a fully-fixed beam will have a higher ultimate load capacity than the same beam with pinned supports at either end in cold conditions.

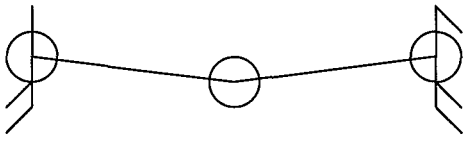

Figure 21) Schematic of a fully fixed beam after three plastic hinges have formed; the beam is now a mechanism

5.3.1.2 Axially unrestrained beams

Axially unrestrained beams are able to move horizontally at the supports, accommodating axial expansions.

- **Pin-roller beam**

This beam has a pinned connection at one end, and a pinned roller at the other, as shown in Figure 22. A pinned roller will resist vertical movement only, the beam is free to move axially and to rotate at the support.

Figure 22) Schematic of a pinned roller beam

Like a pin-pinned supported beam, a pin-roller supported beam only requires one plastic hinge in order to form a mechanism. In cold conditions this plastic hinge will form at the midspan when the beam is loaded to its ultimate capacity, this is shown in Figure 23.

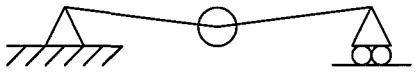

Figure 23) Schematic of a pin-roller beam with one plastic hinge

- **Fixed-slide beam**

This beam has a fixed connection at one end, and a sliding support at the other (Figure 24). Thus a slide support will resist vertical and rotational movement, while the beam is still free to move axially at the support. Because rotation is not permitted at either of the supports the beam is expected to behave similarly to the fully fixed beam, with the exception that elongation is accommodated at the supports.

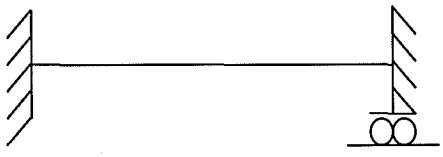

Figure 24) Schematic of the fixed slide beam

Like the fully fixed beam, the first plastic hinges will form at both supports simultaneously in cold conditions as shown in Figure 25. A mechanism forms when the third plastic hinge forms at the midspan at the ultimate load (Figure 26).

Figure 25) Schematic of the fixed slide beam with two plastic hinges

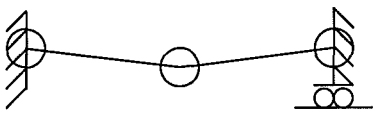

Figure 26) Schematic of the failed fixed slide beam with three plastic hinges

5.3.2 *Frames*

The frame analysed is similar to the fully-fixed beam discussed previously, but rather than the fixed connections completely resisting all vertical, horizontal, and rotational movement, varying degrees of movement are permitted. This movement is provided by the means of deflection of the columns to which the beam is rigidly connected at either end (see Figure 27). The movement of these columns supplies a support condition similar to an axial spring and rotational spring simultaneously. Increasing the stiffness of the columns is equivalent to increasing the stiffness of the springs. In all of the following frame scenarios, the columns are thermally protected against fire. Due to the thermal protection of the columns, the columns are assumed to be remain at ambient the temperature. This will give more realistic connections to the beams by allowing for frame action, without adding the variable of the fire resistance of the columns.

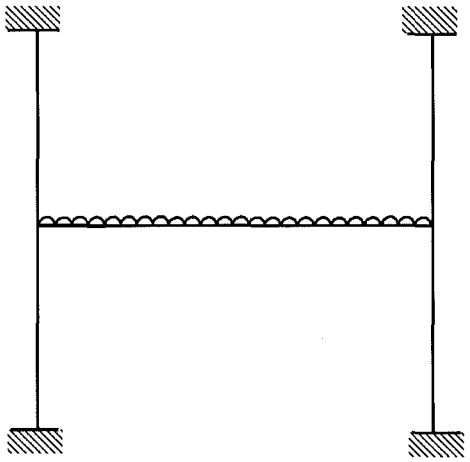

Figure 27) The frame consists of a beam, with uniformly distributed load, connected to two columns

5.3.2.1 Varying the column stiffness

Various scenarios of both the composite and the steel beam will be considered with different column stiffnesses. As described above, varying the column stiffness is equivalent to increasing the stiffness of an axial and rotational spring simultaneously. The purpose of this test is to investigate what role the frame action of the columns has on the fire resistance of the beam. Real fire tests at the Cardington test facility, and other structural fires such as the Broadgate fire, have shown that unprotected steel frames exposed to fire perform quite differently to the predicted performance of the isolated components.

5.3.2.2 Possible failure mechanisms of the frame

One of two possible failure mechanisms is likely to occur for the different scenario:

- **Beam mechanism**

Like the fully fixed beam, the first plastic hinges will form at both ends of the beam simultaneously (Figure 28).

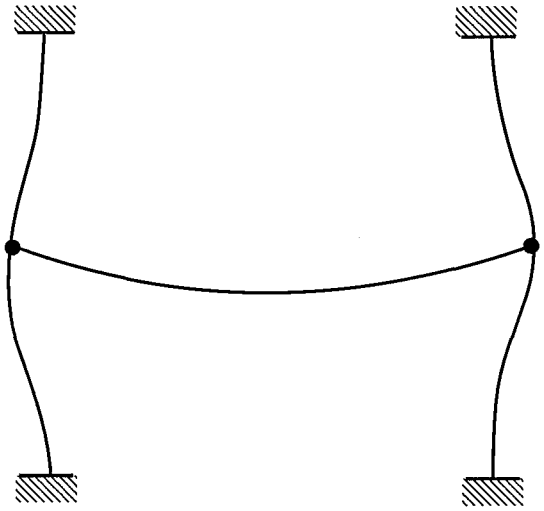

Figure 28) Plastic hinges form at both ends of the beam

A mechanism finally forms when the third plastic hinge forms at the beam's midspan (see Figure 29).

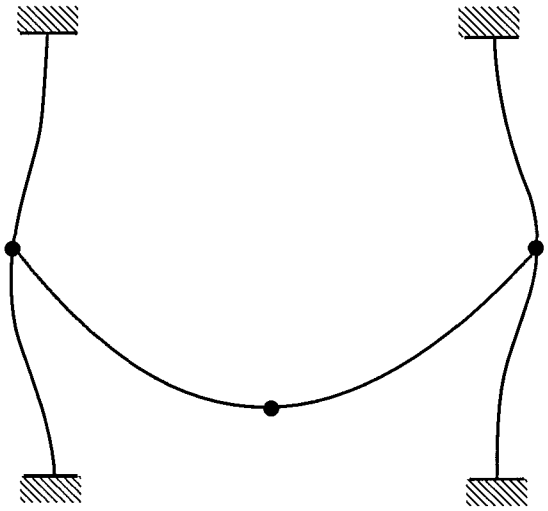

Figure 29) Formation of the third plastic hinge at the beam's midspan

- **Frame mechanism**

This mechanism starts when plastic hinges form at the top and bottom of each column (Figure 30), followed by a plastic hinge at each of the beam column joints (Figure 31). The hinges within the beam column joint may occur in either the beam, or the column. The frame mechanism is then completed when the sixth plastic hinge forms at the beam's midspan (Figure 32).

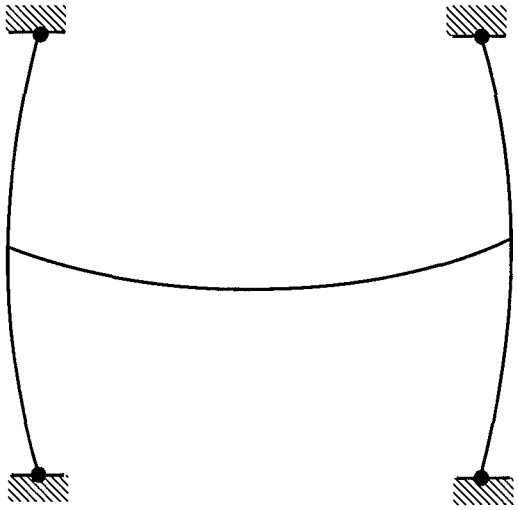

Figure 30) Plastic hinges form at the top and bottom of each column

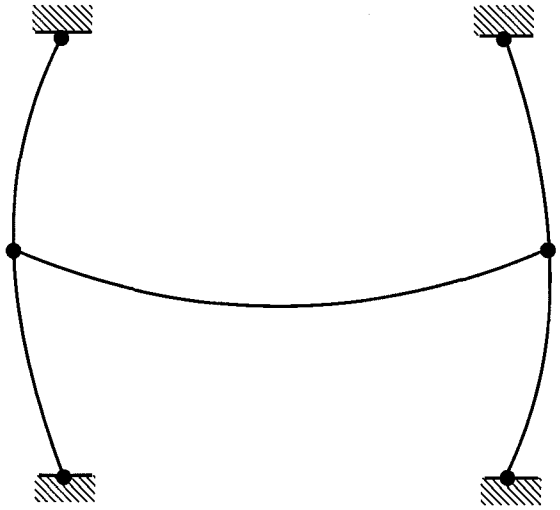

Figure 31) Next, a plastic hinge forms at each beam column joint.

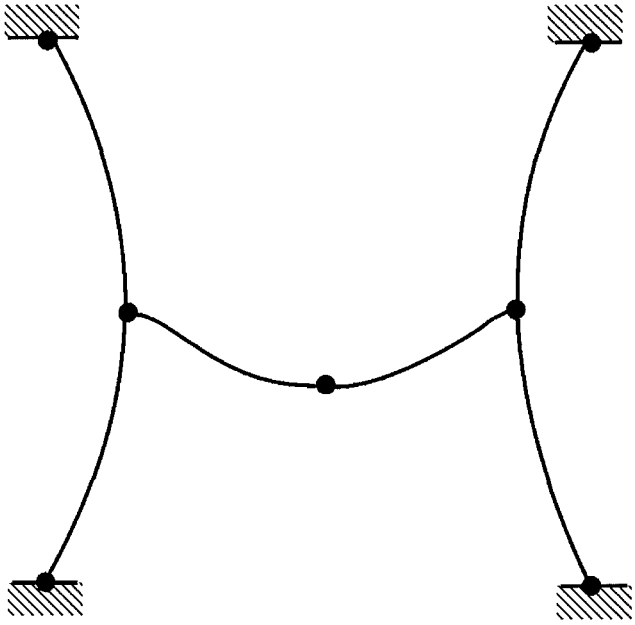

Figure 32) Finally, a seventh plastic hinge at the beam midspan completes the frame mechanism

6 Results of unprotected steel and composite steel beams exposed to the ISO fire

This chapter looks at the steel beam, and the composite beam with theoretical connection types exposed to the ISO fire. The theoretical connection types considered are divided into two categories: the axially restrained beams, and the axially unrestrained beams. The axially restrained beams consist of the pin-pinned beam and the fully-fixed beam as described in section 5.3.1.2. The axially restrained beams consist of the pin-roller beam and the fixed-slide beam as described in section 5.3.1.2. This analysis is the similar to earlier studies by Seputro (2001) for the steel beam, and Welsh (2001) for the composite beam with the exception of the fire exposure. Both Welsh (2001) and Septuro (2001) considered a relatively slow linear heating rate, as compared to the much faster ISO fire considered by the results within this chapter. Comparisons will be made between the behaviour of both the composite beam and the steel beam to the ISO fire and a slower linear heating rate as considered by Seputro (2001) and Welsh (2001).

6.1 Axially restrained steel beams

This section documents the results found by exposure of the steel beam and composite beam to the ISO fire when the beam is restrained axially at both ends.

6.1.1 *Pin-pin steel beam*

Table 7 below shows a summary of the sequence of events in the behaviour of the unprotected steel beam exposed to the ISO-fire.

Table 7) Behaviour of the pin-pinned steel beam exposed to the ISO-fire

Time of event (minutes)	**Description of event**	**Stress; Compression (C) or Tension (T)?**
$0 \rightarrow 3$ min	Beams thermal expansion restrained by axially fixed supports, causing high axial compressive stress.	C
3 min	Top flange reaches yield stress at midspan, Beam displacement increases releasing axial stress.	C
8.5 min	Bottom flange reaches proportional limit.	T
13 min	Top flange yield strength capacity begins to decrease due to thermal degradation, causing loads to be carried less by moment and more by axial tension	C
16.5 min	Web reaches proportional stress limit	T
18 min	Bottom flange yields	T
21 min	Web yields (plastic hinge forms at midspan)	T
23.5 min	Steel beam forms a catenary	T
31 min	Collapse of beam	

Each of these events well be explained in detail with reference to plots of the stresses in each half of the web (above and below the neutral axis), and each the flanges. Then these events will be further explained with reference to the beams axial forces, mid-span bending moment, and vertical deflection at the mid span.

Top Flange Stress

The stress of the top flange of the steel beam (Figure 33) increases rapidly from the onset of the fire until the compressive yield strength is reached after 3 minutes. This stress increase is due to the beam trying to expand as it heats, but is unable to expand axially due to the axial restraint of the pinned supports at either end of the beam. The yield stress limit of the top flange begins to decrease due to thermal degradation of the steel after 13 minutes; the stresses within the top flange must decrease accordingly. The stress of the top flange is maintained at the reducing compressive yield stress until the collapse of the beam at 31 minutes.

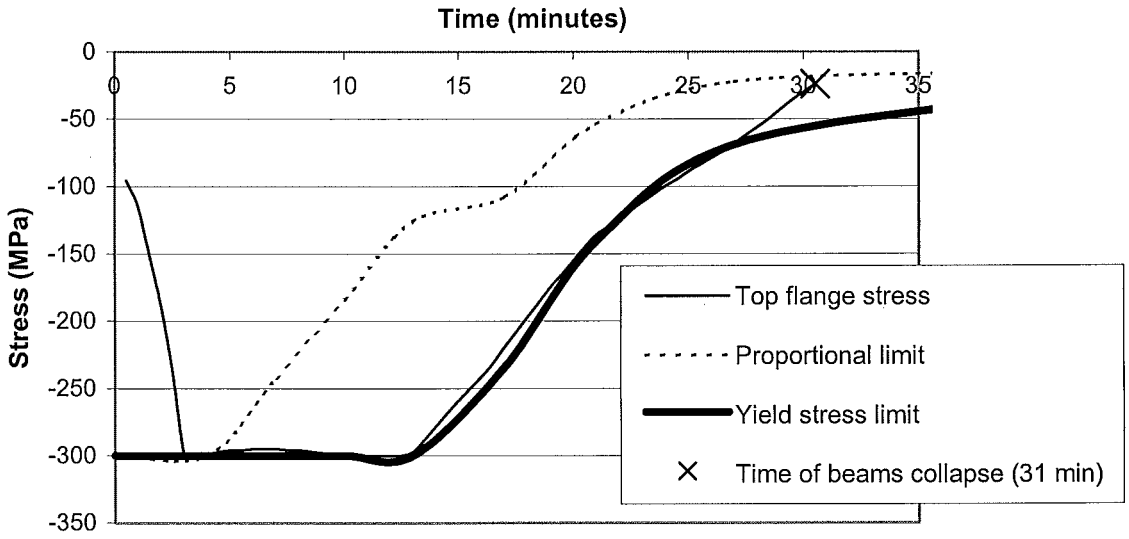

Figure 33) Top flange stress of pin-pin beam

Web stress

The stress of the top half of the web (Figure 34) follows a similar pattern to that of the top flange, reaching compressive yield after 3 minutes, then following the path of a steadily reducing yield strength until the beam collapses.

The bottom half of the web follows a similar path of increasing compressive stress as the beam heats up for the first 3 minutes. After the third minute the compressive stress starts to decrease, or tensile stress increases relative to the stress of the upper half of the web. The lower web reaches the reduced tensile yield strength of 60 MPa after 19.5 minutes, after which the path of the reduced tensile yield strength is followed until the beam collapses.

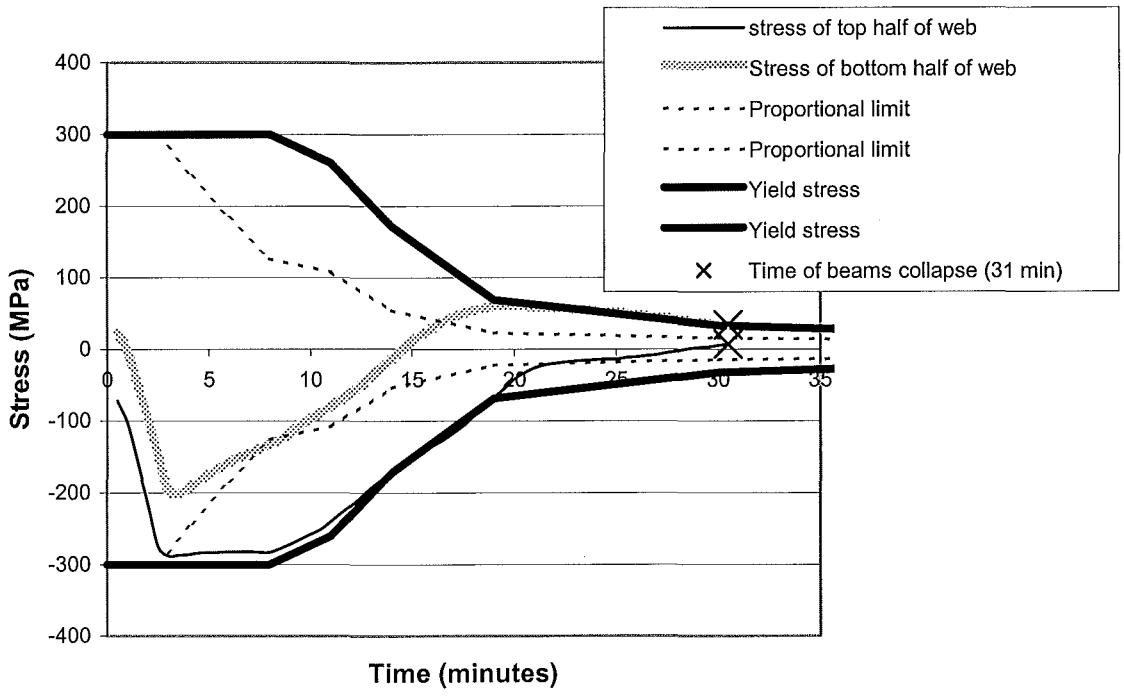

Figure 34) Web stress of pin-pin beam

Bottom flange stress

The bottom flange stress (Figure 35) is similar to the lower web, with increasing compressive stress as the beam heats up for the first 3 minutes, then the compressive stress starts to decrease, followed by a tensile stress increase. The lower flange reaches the reduced tensile yield strength of 100 MPa after 18 minutes, after which the path of the reduced tensile yield strength is followed until the beam collapses.

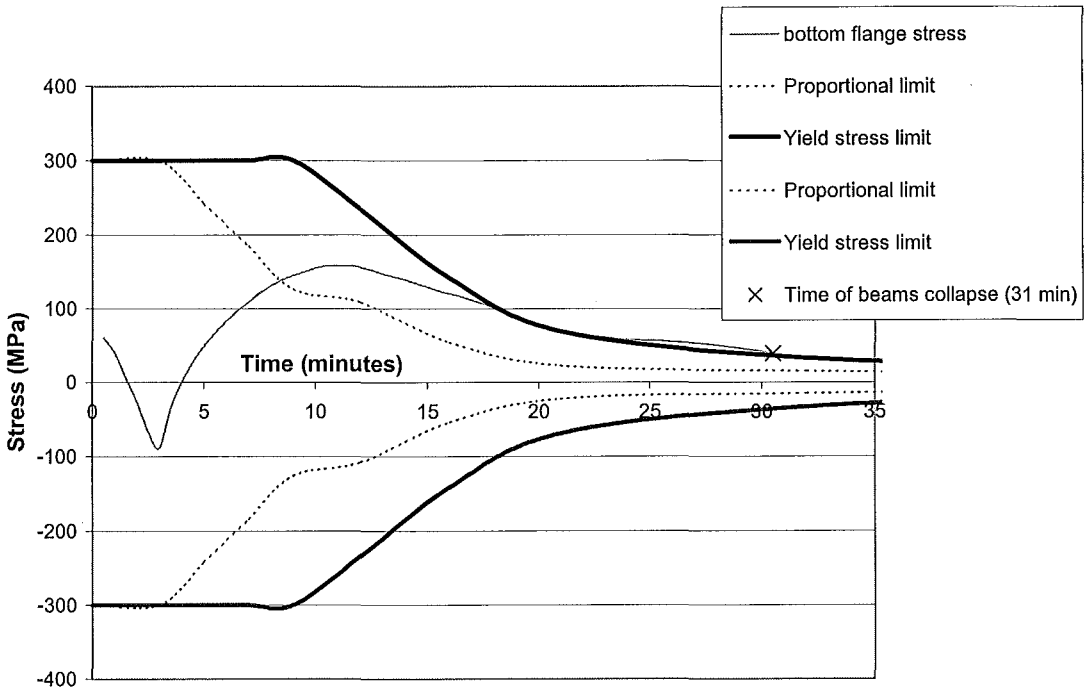

Figure 35) Bottom flange stress of pin-pin beam

Axial force

The beam's compressive axial force (Figure 36) increases rapidly (i.e. more negative) for the first 3 minutes of the fire's duration. This compressive force increase is due to the beam's expansion being restrained axially by the pinned supports at either end. As the steel beam is unable to expand, the thermal energy is transferred to compressive axial force instead. The peak axial force at 3 minutes corresponds to the compressive yielding of the top flange at the midspan. With the onset of yield, the beam starts to bow with rapidly increasing midspan deflection. This deflection relieves much of the axial force. As deflections increase, and moment capacity decreases with the gradual weakening of the beam, the beam eventually carries load primarily due to catenary action. Catenary action is where load is carried in tension only in the same manner as a draped cable held at either end supports it own weight.

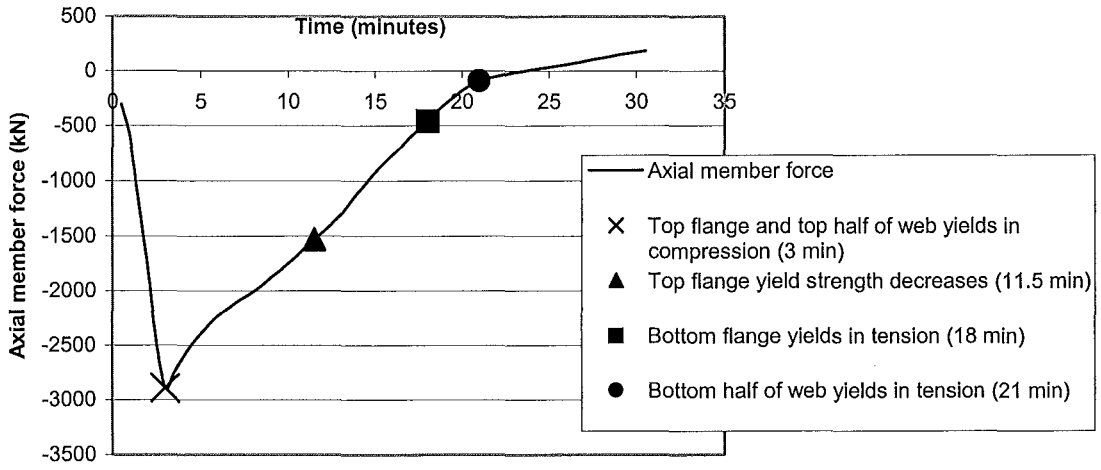

Figure 36) Pin-pin beam, axial force

Midspan moment

There are three points in time where the midspan moment is most worthy of notice from Figure 37:

1. *Time = 3 minutes.* At this time the top flange yields in compression causing the large deflections as discussed earlier. It can be noted that after the top flange yields the midspan moment rises rapidly despite the beam being subjected to a constant load, the reason for this is due to P-δ effects. The axial force times the increasing midspan deflection generates the P-δ effects.
2. *Time = 11 minutes.* Top flange yield strength starts to decrease. This decrease in yield strength means that the beams moment capacity begins to decrease, and loads begin to be carried by axial tension (catenary action) as well as bending.
3. *Time = 21 minutes.* Both bottom flange and bottom half of the web have yielded in tension. From this point on the mid span moment decreases less rapidly as the tensile capacity of the bottom flange and bottom half of the web gradually reduce until failure of the beam.

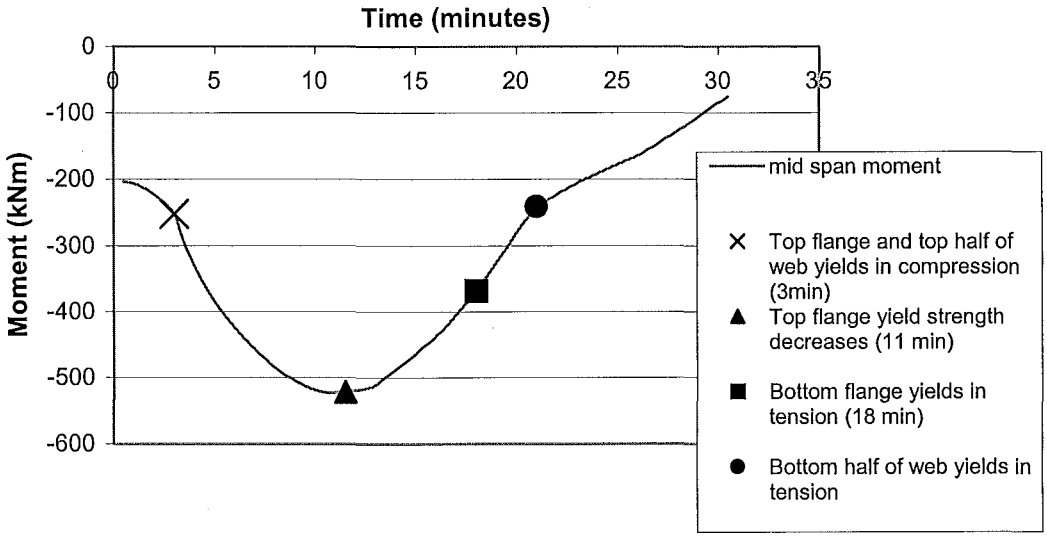

Figure 37) Pin-pin beam midspan moment

Midspan deflection

Midspan deflections are small until the yield of the top flange and top half of the web. After this point the beam stiffness reduces rapidly with the sequential yield and reductions to yield stresses that follow, as noted in Figure 38. The beam stiffness reduces more rapidly until the eventual collapse of the beam.

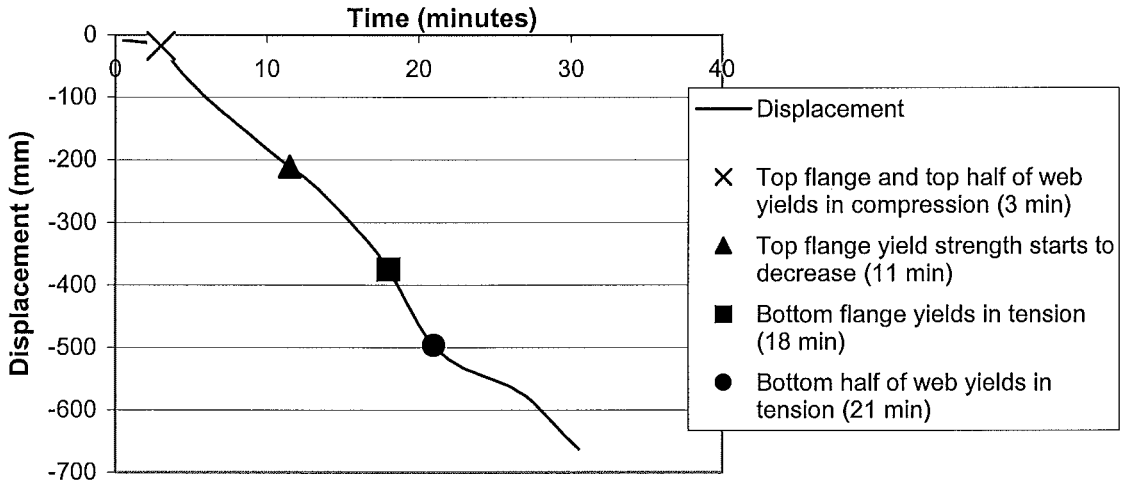

Figure 38) Pin-pin beam midspan displacement

6.1.2 *Fixed-fixed steel beam*

The following table summarises the main events of the exposure of the fixed-fixed connected steel beam to the ISO-fire.

Table 8) Behaviour of the fixed-fixed steel beam exposed to the ISO-fire

Time of event (minutes)	Description of event	Stress; Compression (C) or Tension (T)?
0 → 3 minutes	Compressive axial stress increases in fully restrained beam	C
3 minutes	Bottom flange reaches proportional limit at supports	C
	Bottom web reaches proportional limit at supports	C
	Bottom web reaches proportional limit at midspan	C
3.5 minutes	Top web reaches proportional limit at midspan	C
4.5 minutes	Top flange reaches proportional limit at midspan	C
9.5 minutes	Bottom flange yields at supports	C
13.5 minutes	Top web reaches yield at midspan	C
20 minutes	Top flange reaches yield at midspan	C
23 minutes	Bottom web reaches yield supports	C
27 minutes	Bottom flange reaches yield at midspan (First plastic hinge formed at mid span)	T
30.5 minutes	Top flange reaches yield at supports (second and third plastic hinges form at both supports)	T
	Bottom web reaches proportional limit at midspan	T
	Beam fails (Catenary never forms)	

Each of these events will be discussed in further detail within the following sections.

Bottom flange stress

The bottom flange at the supports (Figure 39) is the first part of the beam to reach the proportional limit as the compressive stress builds up. This stress results from restraint of the fixed beam as it tries to expand with heating. After the proportional limit is reached, the stresses within the beam are reduced as the beam is freer to rotate at the supports. The midspan bottom flange also initially builds up high compressive stresses for the same reason as at the supports. When the axial stresses are released by the support bottom flange reaching the proportional limit, the beam goes into tension. This tensile force reaches yield at a time of 26 minutes.

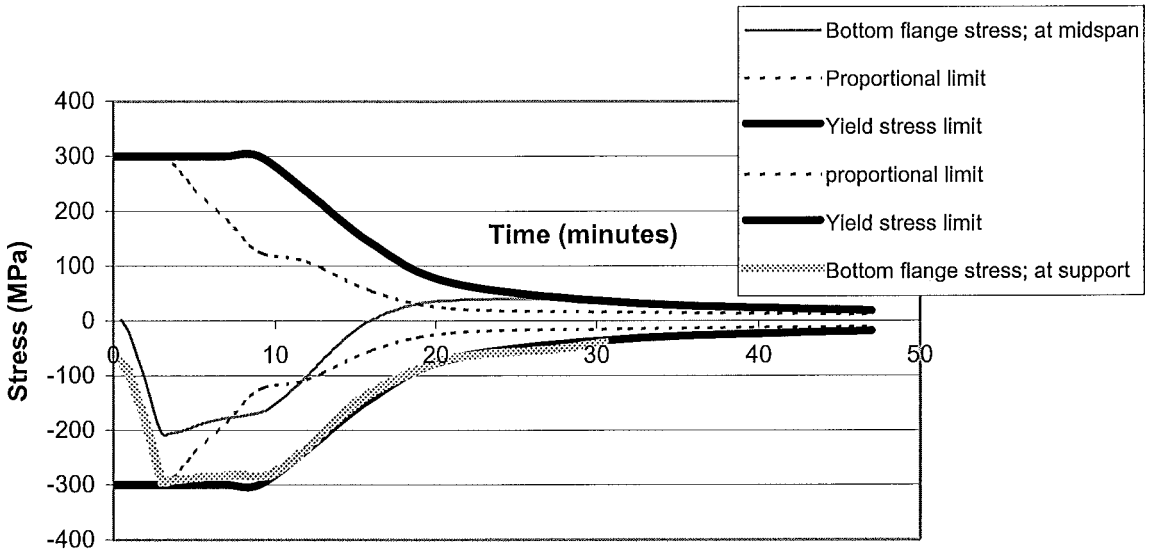

Figure 39) Bottom flange for fully fixed steel beam

Top flange stress

The top flange at the midspan also builds up a high compressive stress (Figure 40), but does not reach yield until 20 minutes into the fire duration. The top flange at supports gradually goes into tension when the support bottom flange reaches the proportional limit, releasing axial compressive force. The support top flange then yields at 30.5 minutes of fire time; leading to the collapse of the beam.

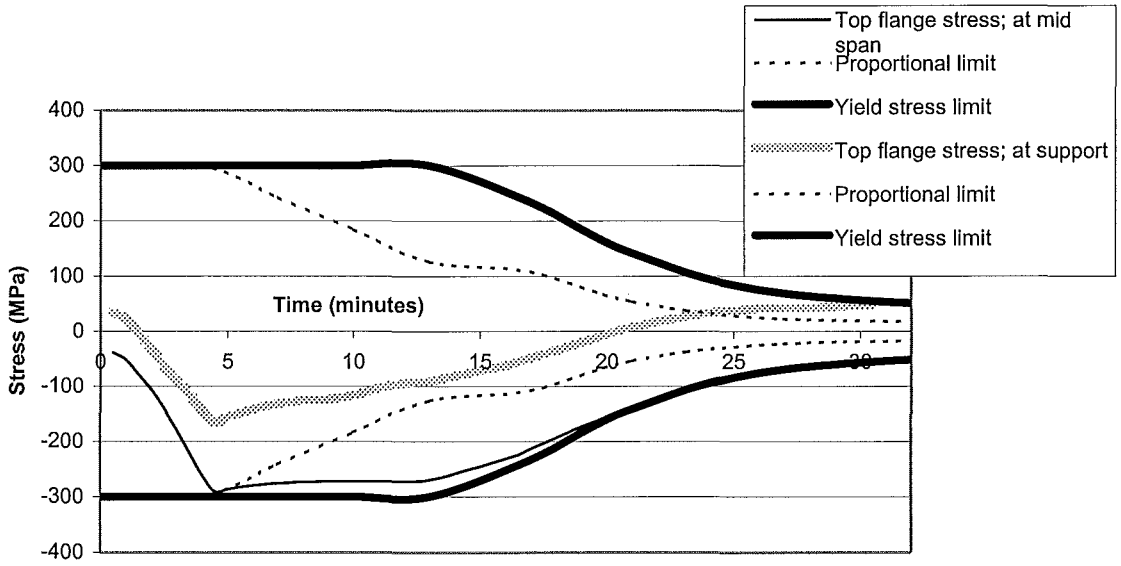

Figure 40) Top flange stress for fully fixed steel beam

Web stresses

The web stresses follow a very similar path as their respective top and bottom flange at both the midspan and the supports (see Figure 41).

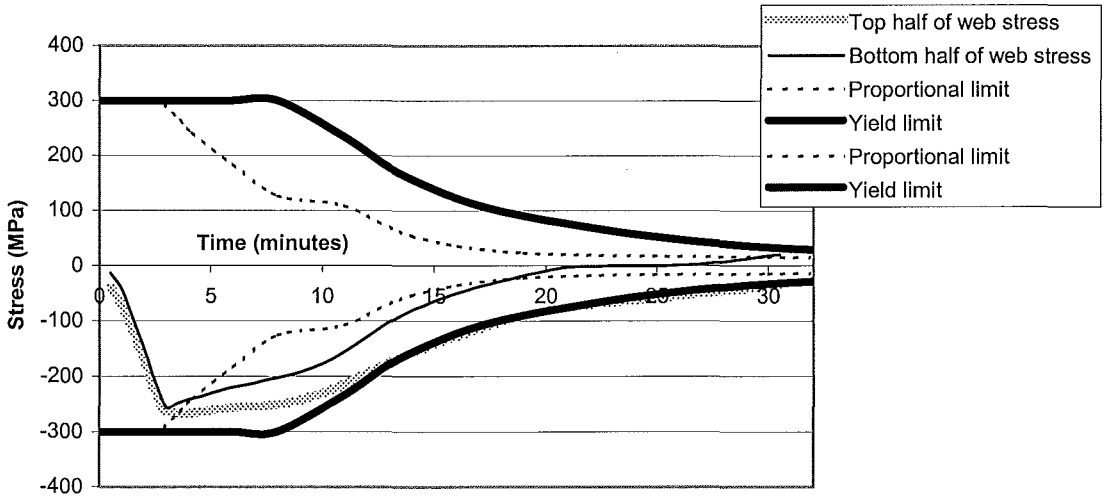

Figure 41) Stresses of the web of the fully fixed steel beam

Axial force

Figure 42 shows how the axial compressive force within the beam builds up to a peak when the bottom flanges at the supports reach the proportional limit. Also of importance is the fact that the beam never develops a net tensile force as did the pin-pin supported steel beam. The beam fails when all three plastic hinges form, without the beam continuing to carry loads as a catenary as the pin-pinned steel beam did.

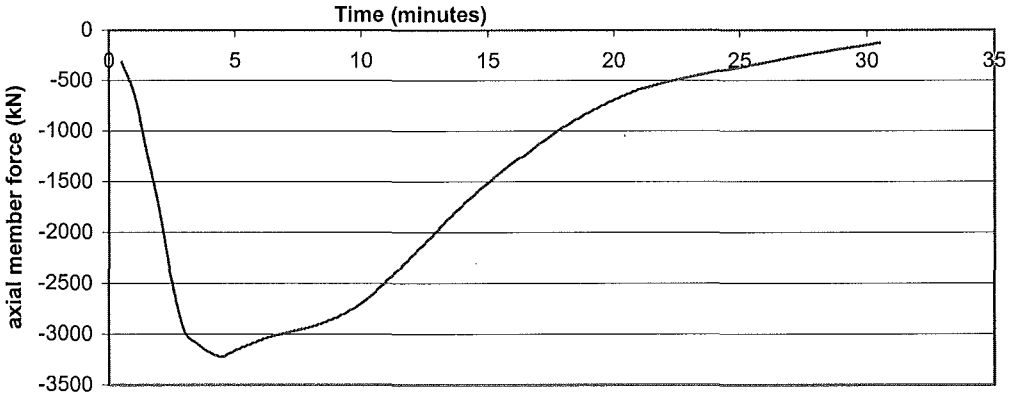

Figure 42) Beam axial force of fully fixed steel beam

Moments

The ratio of the bending moment magnitudes within the beam at the supports compared with the midspan prior to the fire is $WL^2/12 : WL^2/24$, (or 1:2). This ratio is generally maintained throughout the fire's duration.

The actual magnitude of the bending moment at each location varied with the following main changes caused by the heating of the beam. These are highlighted on the following bending moment plot (Figure 43):

1. **From 0 to 3 minutes fire time:** The initial increase in the bending moment arises from the restrained thermal expansion developing an increasing net compressive force leading to increasing P-δ effects.
2. **Bottom flange reaches the proportional limit at the supports:** The start of non-linear deformations at the fixed supports begins to allow more rotation adjacent to the supports, resulting in greater midspan deflection, decreasing the P-δ moment at supports. The moment at the midspan drops also as it is affected by compression in the bottom flange.
3. **Top flange reaches the proportional limit at midspan:** The support moment increases more rapidly while moment redistribution causes the supports to take proportionally more moment than the midspan.
4. **Bottom flange yield at supports:** moment reduces as axial force reduces with the start of formation of plastic hinges while midspan deflection continues to increase.
5. **Top half of flange yields at midspan:** Midspan moment reduces while moment redistribution causes the supports to take proportionally more moment.

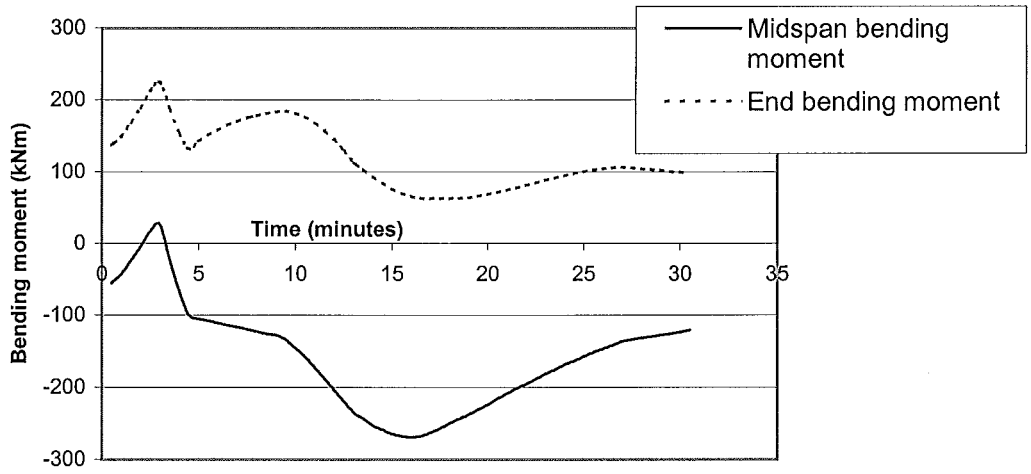

Figure 43) Bending moments for fully fixed steel beam

Midspan deflection

The most notable trend that is revealed by this plot (see Figure 44) is that the midspan deflection is very small until the bottom flanges reach the proportional limit at the supports (3 minutes). Also it is important to note that despite this initial yielding of part of the section the beam has far from failed.

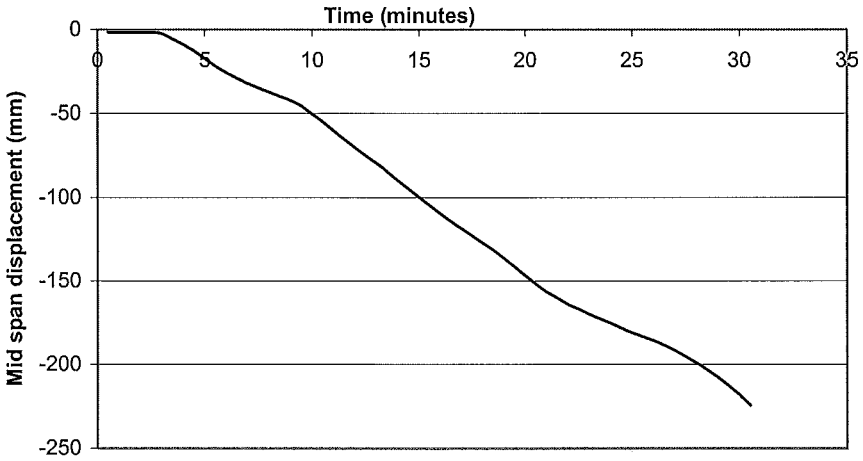

Figure 44) Midspan vertical displacement of fully fixed steel beam

6.2 Axially restrained composite beams

This section documents the results found by exposure of the steel beam and composite beam to the ISO fire when the beam is not restrained axially at one end.

6.2.1 Pinned-pinned composite beam

The following table summarises the main events of the exposure of the pinned-pinned connected composite steel beam to the ISO-fire.

Table 9) Behaviour of the pin-pinned composite steel beam exposed to the ISO-fire

Time of event (minutes)	Description of event	Stress; Compression (C) or Tension (T)?
4.5 minutes	Top flange reaches compressive proportional limit at midspan	C
5 minutes	Bottom flange reaches tensile proportional limit at midspan	T
5.5 minutes	Rate of increase of axial compression reduced due to deflection of weakened beam.	C
13 minutes	Bottom flange yields at midspan (start of plastic hinge at midspan)	T
16 minutes	Web reaches tensile proportional limit	T
16.5 minutes	Bottom of slab cracks in tension	T
18.5 minutes	Sagging beam starts to carry load predominantly as a catenary	T
20 minutes	Top flange of beam reaches steel tensile proportional limit at midspan	T
27.5 minutes	Top of slab cracks in tension	T
38 minutes	Top flange reaches tensile yield limit at midspan (plastic hinge forms at midspan)	T
	Beam fails, no longer able to carry loads as a catenary	

Each of these events will be discussed in further detail within the following sections.

Midspan bottom flange stress

As the steel beam heats it expands but since the concrete slab does not heat or expand as quickly, the beam bows down at the midspan, closer to the fire. This is called thermal bowing and causes the build up in tensile stress of the bottom flange as seen in Figure 45 in the initial stages of the fire. When the bottom flange reaches the proportional limit the axial stresses are relieved to some extent due to an increase in the midspan deflection. The stress of the bottom flange remains almost constant until the yield strength of the beam drops due to higher temperatures of the steel. When the steel of the bottom flange yields, the stress within the beam must decrease as the thermally reducing yield strength of the steel drops. The tensile yield of the bottom flange is associated with a sharp increase in the midspan deflection. This should be expected with substantial loss of stiffness of the beam.

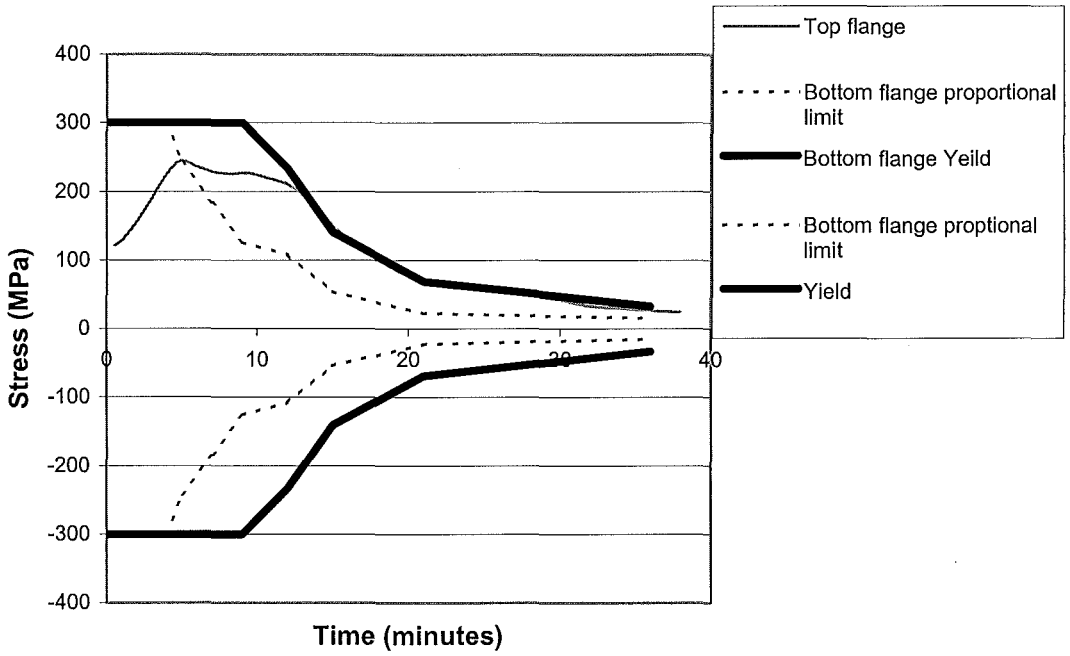

Figure 45) Bottom flange stress of pin-pin connected composite beam

Top flange stress

The top flange initially experiences high compressive stress resulting from both axial restraint of the thermally expanding beam, and p-δ moments from the induced axial force, as shown in Figure 46. After 5 minutes of fire duration the top flange reaches the proportional limit, however it never reaches yield in compression. As the bottom flange yields in tension the beam sags rapidly with little increase in axial tension, reducing midspan moment and hence top flange stress. As the deflection of the beam's midspan increases the bending moments decrease and axial force of the beam goes into tension. As this axial force increases the stress of the top flange also becomes tensile. At a time of 38 minutes the top flange yields in tension, marking the onset of the plastic hinge at the midspan. This single plastic hinge completes a mechanism where the beam fails.

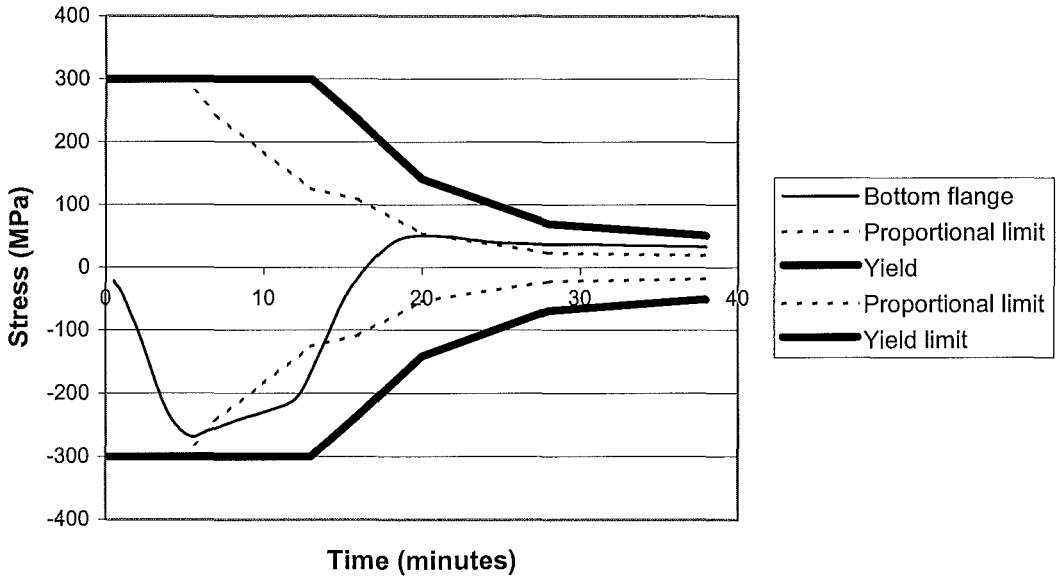

Figure 46) Top flange stress for pin-pin connected composite beam

Web stresses

The web stress, as shown by Figure 47, follows a similar path to the top flange. The two main differences between the web and top flange is that the web stresses follow a similar trend but are lower in magnitude, and yield occurs sooner for the web than for the top flange. The stresses are generally lower, especially when the sections are in the compressive region, because the top flange is further from the neutral axis. The web yields before the top flange, even though the tensile stress is higher in the flange than the web at the time that the web yields. This is because the web heats up faster being

heated from both sides, and having less thermal mass than the flange.

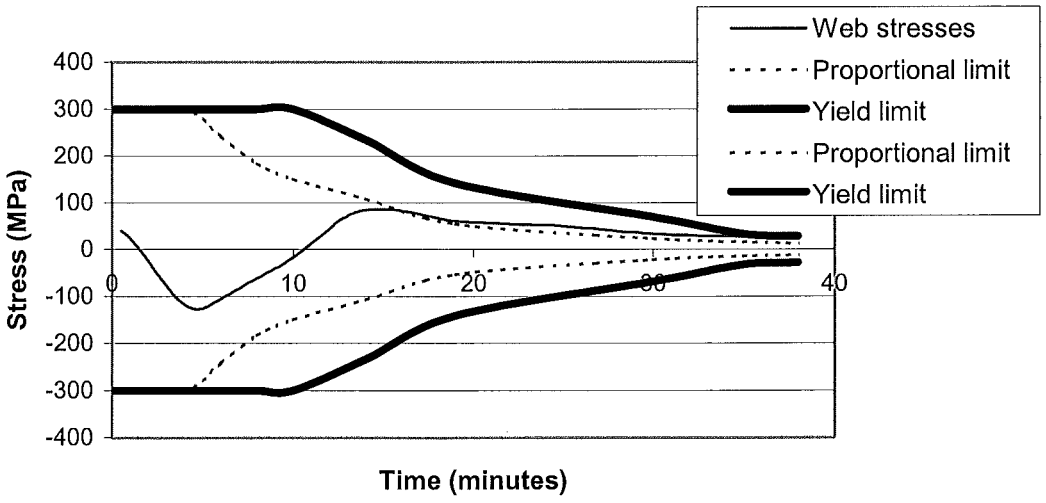

Figure 47) Stress of steel web of the pin-pin connected composite beam

Stresses within the concrete slab

Stresses within the slab increase in compression until the bottom flange approaches tensile yield (13 minutes) when the beam sags rapidly relieving much of the axial compression. This is shown in Figure 48.

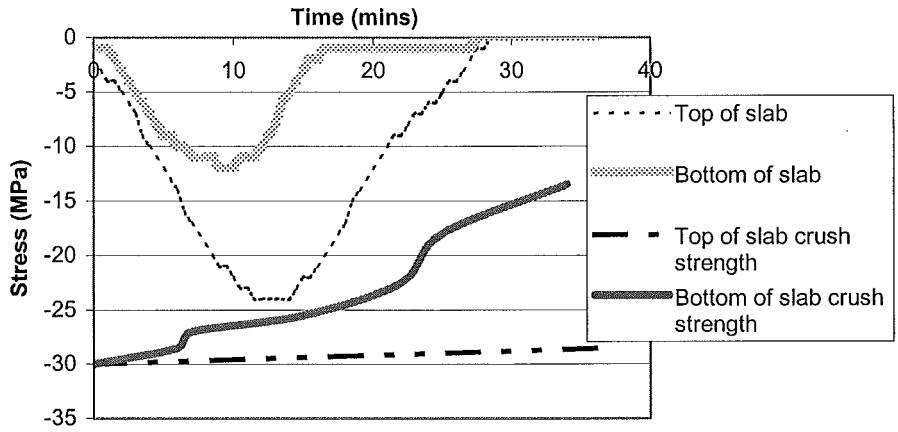

Figure 48) Slab stresses for pin-pin connected composite beam

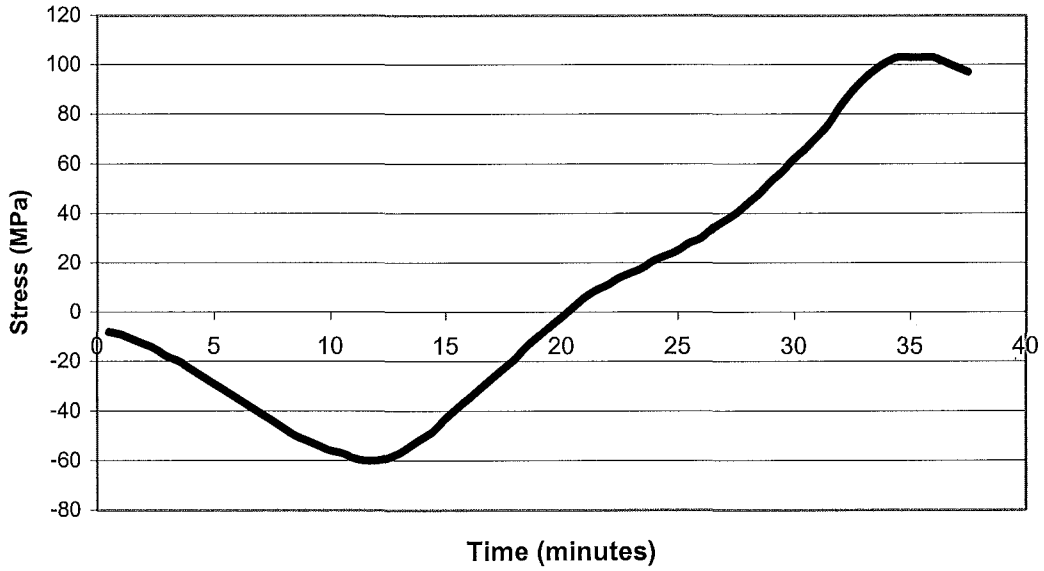

Figure 49) Steel mesh stresses for pin-pinned composite beam

Note: the lines representing the yield and proportional limiting stresses have both been omitted from Figure 49 for clarity. These limiting stresses are of a much larger scale than the actual stresses that occur within the slab, hence the mesh does not approach these limits.

The stresses of the steel mesh follow a similar path to the top of the slab, with the exception that tensile forces maybe carried within the steel mesh, but not the concrete slab.

Axial force

As previously discussed the axial compressive force within the beam builds up rapidly as the beam is restricted against axial expansion. After the bottom flange reaches the tensile proportional limit at a time of 5 minutes the vertical midspan deflection increases rapidly, and hence relieves much of the axial compression within the beam. At 18.5 minutes the sagging beam starts to carry loads dominantly by catenary action, hence the beam has a net tensile axial force as shown in Figure 50.

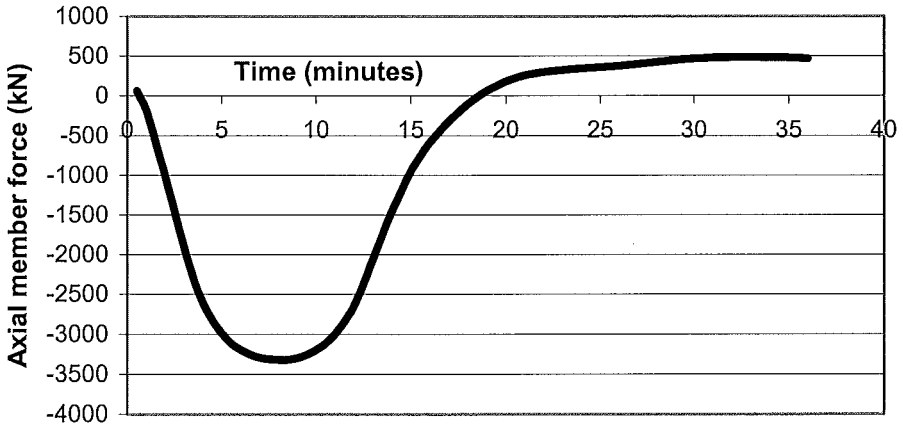

Figure 50) Axial force for pin-pin connected composite beam

Midspan moments

As shown in Figure 51, bending moments increase rapidly for the first 13.5 minutes of the fire as the axial force builds up faster than the midspan deflection. As the bottom flange approaches tensile yield at 13 minutes the beam sags rapidly with little increase in axial force, reducing midspan moment.

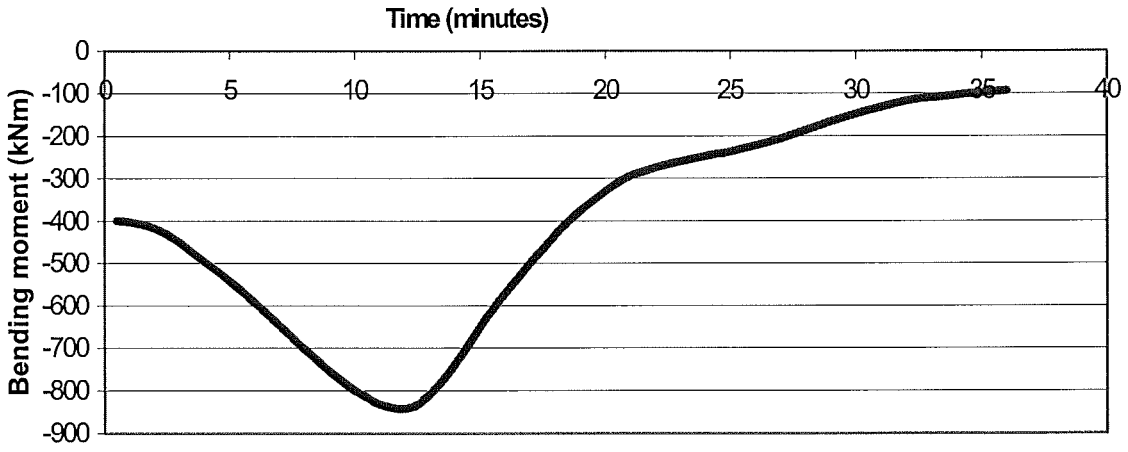

Figure 51) Midspan moment of pin-pin connected composite beam

Midspan deflection

The midspan deflection (Figure 52) is relatively small for the first 5 minutes, until the bottom flange reaches the tensile proportional limit, after which the deflections increase very rapidly. The midspan has a total midspan deflection of 640mm at the time of beam failure.

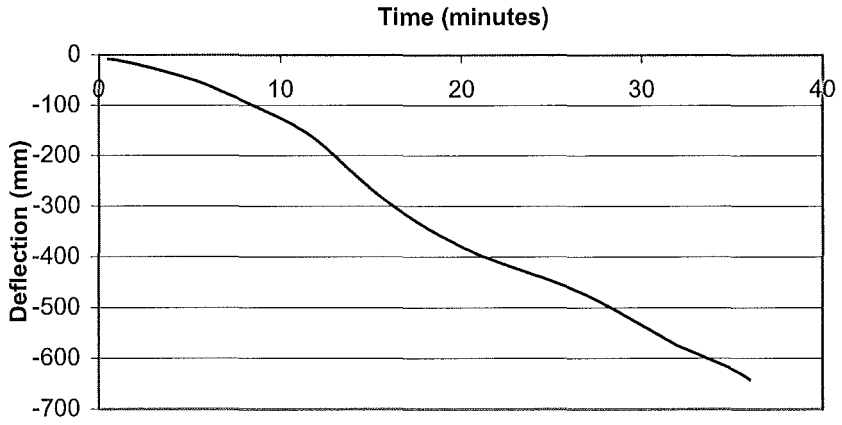

Figure 52) Midspan vertical deflection of pin-pin connected composite beam

6.2.2 *Fixed-fixed composite beam*

The following table summarises the main events of the exposure of the fixed-fixed connected composite steel beam to the ISO-fire.

Table 10) Behaviour of the fixed-fixed composite steel beam exposed to the ISO-fire

Time of event (minutes)	Description of event	Stress; Compression (C) or Tension (T)?
0 minutes	Tension cracking at top of slab at supports	T
3 minutes	Bottom flange at fixed supports reaches yield	C
4 minutes	Top flanges at both midspan and supports reach proportional limit	C
9 minutes	Web at fixed supports reaches yield	C
11 minutes	Top flange at fixed supports reach yield	C
18.5 minutes	Bottom flange and web at midspan both reach yield	T
	Midspan concrete crushes at the top of slab	C
21 minutes	Beam starts to carry loads by catenary action	T
	Bottom of slab cracks at supports	T
25 minutes	Sufficient loss of stiffness and strength of the beam causes failure. The beam is no longer capable of catenary action.	T

Each of these events will be discussed in further detail within the following sections.

Bottom flange stress

As can be seen Figure 53, compressive stresses build up rapidly within the bottom flange of the fully fixed composite beam when heated. This increase in compressive stress is due to the beams thermal expansion being greatly restricted by the fixed supports of the beam. This compressive stress builds up, yielding the bottom flange at the supports. This yielding reduces the beam's stiffness, increasing midspan deflection and allowing the compressive stress in the flanges to remain constant until 11 minutes of fire duration. The compressive stress of the midspan bottom flange does not rise as rapidly as at the supports as some vertical deflection of the beam is possible before any section yielding. This helps relieve some of this compressive force. At 9 minutes it can be seen that the tensile stress of the bottom flange at the midspan and the supports increase. This is due to further loss of beam stiffness as the heated steel yield strength drops. As the beam's deflection increases, loads are increasingly carried by axial tension until failure.

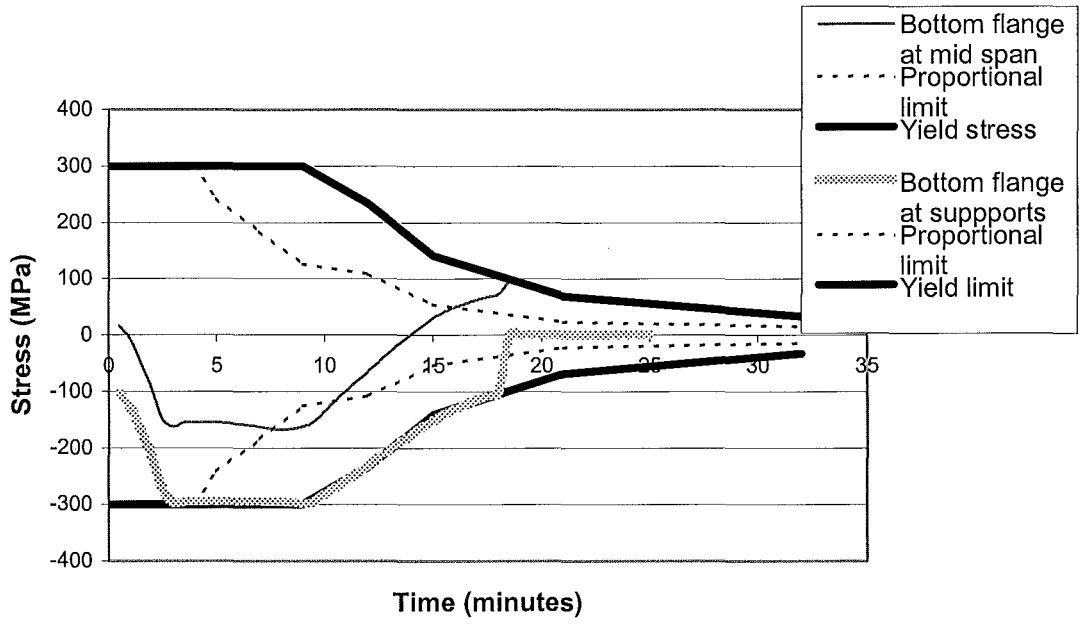

Figure 53) Bottom flange stress for composite beam with fixed-fixed support conditions

Top flange stress

The top flange stresses (refer Figure 54), like the bottom flange stresses build up initially, but are then released with the yielding of the bottom flange as explained above. The increased beam deflections associated with the yield of the bottom flange at

the supports allows the steel beam more axial expansion without further increase due to axial compressive stress. For the top flange this can be seen by a steady compressive stress after five minutes for both midspan and supports. Despite the flange stresses not increasing, the top flanges reach compressive yield as the yield stress limit decreases with thermal degradation. As the concrete crushes the top flanges both rapidly go into tension as the beam deflects. Shortly after this, at 21 minutes, the beam forms a catenary, where the loads are carried almost exclusively in axial tension.

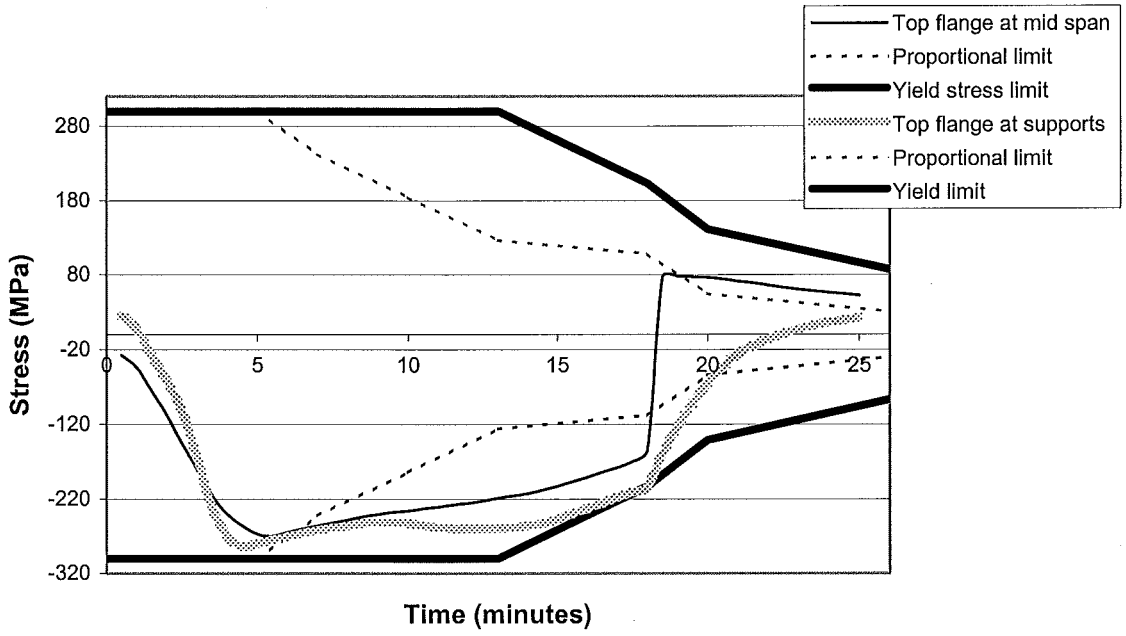

Figure 54) Top flange stress for composite beam with fixed-fixed support conditions

Web stresses

The web stresses behaviour, as shown in Figure 55, is similar to the top flange, increasing in compression until yield of the bottom flange at the supports occurs. Like the top flange, the web at the supports reaches the compressive yield as the steel yield strength decreases with heating. The midspan web does not yield in compression, but gradually increases in tensile stress (or decreases in compressive stress) before the top of the concrete slab begins crushing at midspan. The slab crushing causes the tensile stress of the webs to increase rapidly until yield of the midspan web at 18 minutes; at which time the beam begins to act as a catenary until failure.

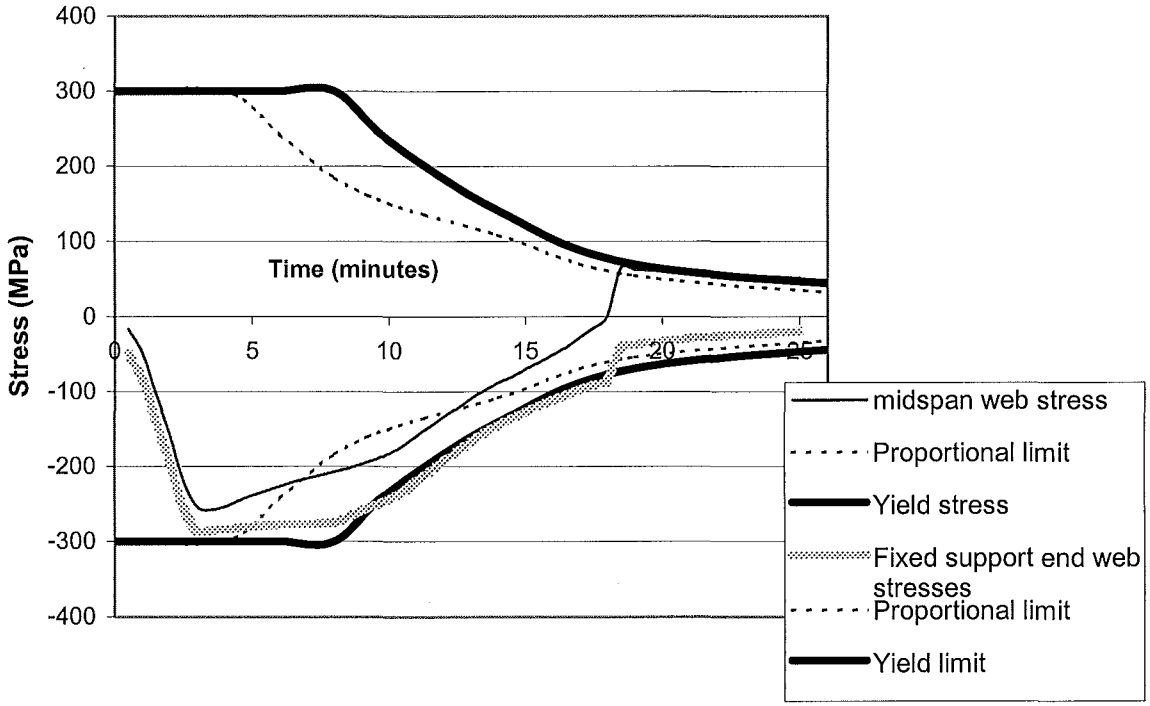

Figure 55) Steel beam web stresses for composite beam with fixed-fixed support conditions

Axial force

Figure 56 shows how axial compressive stress increases very rapidly causing the web and bottom flange to yield at the supports. This axial stress is reduced as the weakened beam is now able to deflect vertically at the midspan. Note also the other points where the crushing of concrete and the tensile yielding of the midspan bottom flange reduce axial compressive stress. The beam forms a catenary after 21 minutes where the axial force in the beam changes from a net compressive force to a net tensile force.

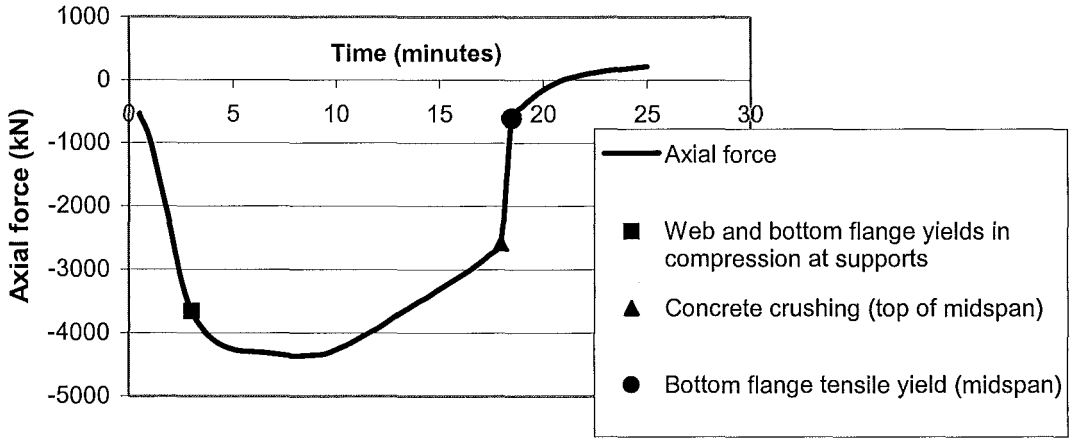

Figure 56) Axial force for composite beam with fixed-fixed support conditions

Midspan moments

The moments of both the beam's midpoint and end supports, plotted in Figure 57, reflect changes to the way loads are carried after the three main events as labelled in the following:

- *Web and bottom flange yield in compression at supports (3 minutes):*

This is the time where axial stress within the beam is released, reducing bending moments. The P-δ effects of the beams axial force within the deflected beam cause this bending moment. The knee of the bending moment curves at the time of 9.5 minutes is due to the reduction of the yield strength of the steel beam as it heats.

- *Concrete crushes at the top of the slab at midspan (18 minutes)*

The composite beam loses a substantial amount of the compressive stress capacity as the concrete slab begins to reach its crushing strength. After the concrete crushes loads are carried more by catenary action (axial tension in the beam) than by flexure; this occurs from 18 minutes onwards.

- *Bottom flange yields in tension at the midspan (18.5 minutes)*

This has the effect of further loss of moment carrying capacity, and hence another transition to more load carrying by catenary action.

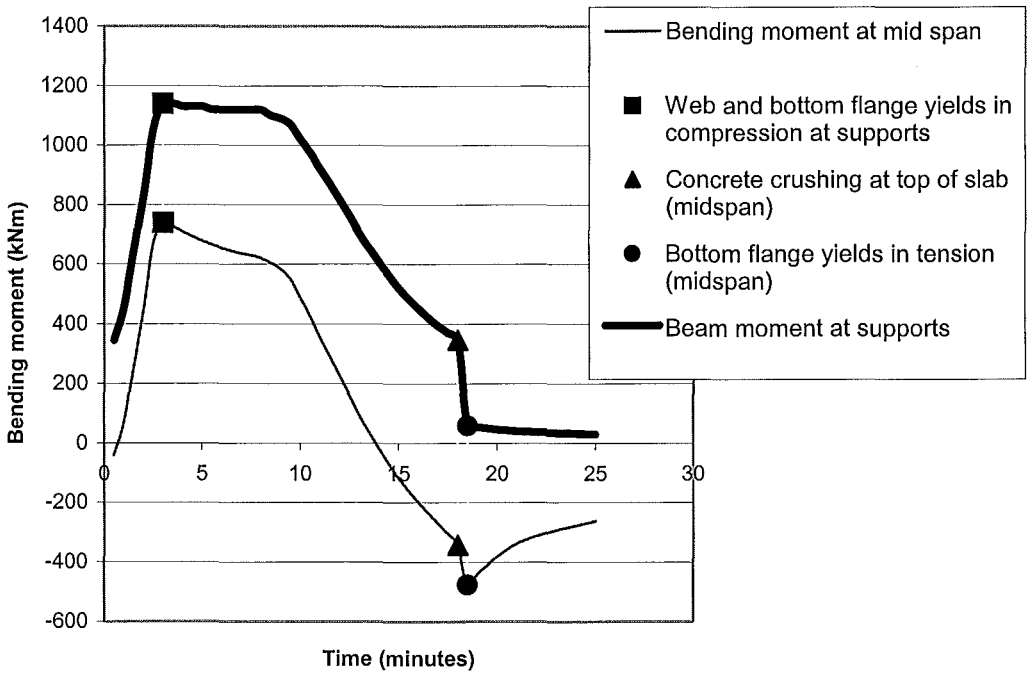

Figure 57) Bending moment for composite beam with fixed-fixed support conditions

Midspan deflection

In Figure 58 it can be seen that there is relatively little vertical deflection of the midspan before yielding of the bottom flanges at the supports. After this, the beam is sufficiently weakened to allow a rapid increase in deflection. The two other points of interest as noted in Figure 58 show how the beams deflection rapidly increases further as more of the section's strength is lost. Note how the midspan deflection becomes very large as loads are increasingly carried by catenary action of the beam rather than flexure. The beam has a total midspan deflection of 400mm at the time of collapse.

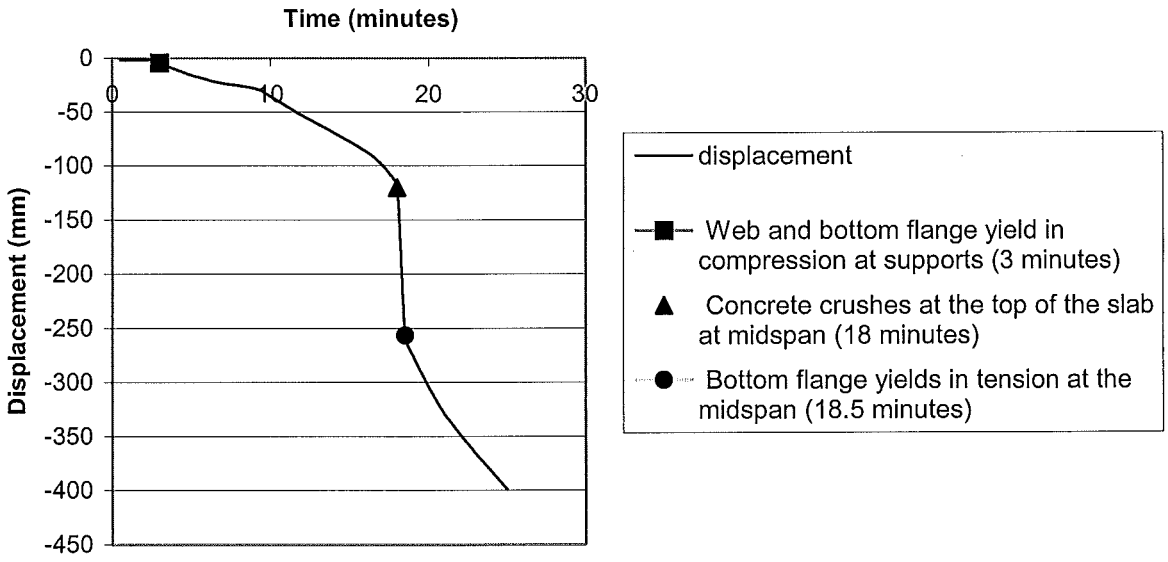

Figure 58) Vertical midspan displacement for composite beam with fixed-fixed support conditions

6.3 Summary of restrained steel and steel composite beams

The fire resistance of the pin-pinned and fix-fixed beams differed from one another for both the composite and the steel beam scenarios. The pin-pin beam lasted 31 minutes for the steel beam, and 38 minutes for the composite beam, while the fix-fixed beam lasted 30.5 minutes for the steel beam, and only 25 minutes for the composite beam. As has already been demonstrated by Seputro (2001), Welsh (2001) and Usmani & Rotter (2000) with slow linear temperature increases, the pin-pinned case allows rotation at the supports, reducing axial stresses while increasing midspan deflections within the beam. Hence the pin-pin scenario will outlast the fully fixed supported beam for most fire scenarios. As demonstrated here for the steel beam exposed to the rapidly heating ISO fire, the time difference of beam failure between the fix-fix and pin-pin cases becomes very small as the rate of heating increases. Therefore with a rapidly heated beam the ability to use catenary action quickly diminishes for the steel beam. The composite beam however shows similar results to the earlier findings of Welsh (2001) for the slow linear temperature increases. This is due to the greater heat sink effects of the composite beam, which helps to cool the top flange and mesh, giving a more noticeable period of catenary action to the pin-pinned beam.

Other noticeable trends that were observed with faster fires was the sequence that parts of the section yielded. Often the web would yield before the flanges, even though the stresses were higher in the flanges. Because the web is much thinner, it heats up more rapidly and therefore the proportional and yield stress limits reduce earlier in the fire.

With the fully fixed scenario for both the steel and the composite beam the failure mode has been the formation of three plastic hinges. With both cases the first plastic hinge formed at the centre of the beam. In cold conditions it is normal to expect the plastic hinges to form at the supports before the midspan as the bending moments are greater at the supports. The order of plastic hinge formation can be accounted for by looking at the time of tensile yield in each location. As the beam is initially under high compressive axial loads, compressive failure marks the initiation of plastic hinge formation at both the midspan and the supports. As the beam begins to sag the tensile

stresses within the beam increase. It is noted that the first plastic hinge forms at the midspan as the bottom flange reaches tensile yield first, even though the stresses are higher at the supports. The next two plastic hinges form at the supports with the top flanges yielding in tension. The reason the midspan bottom flange yields before the top flange at the supports is that the yield limit stress is much less in the bottom flange than it is in the top flange, due to the thermal effects. At the midspan it is the bottom flange that yields to form the plastic hinge, as compared to the top flange of the supports. The bottom flange heats up faster than the top flange (which is only heated from below and both sides). Hence with a fast growing fire such as the ISO-fire, the thermal reduction of yield stress of different parts of the section can determine the order of plastic hinge formation.

6.4 Axially Unrestrained steel beams

This section documents the results found by exposure of the steel beam and composite beam to the ISO fire when the beam is not restrained axially at one end.

6.4.1 Fix-slide supported steel beam

The fixed-slide supported beam was able to slide axially at one end, eliminating axial force in the beam arising from restrained thermal expansion.

The following table summarises the main events of the exposure of the fixed-slide connected steel beam to the ISO-fire.

Table 11) Behaviour of the fixed-slide steel beam exposed to the ISO-fire

Time of event (minutes)	**Description of event**	**Stress; Compression (C) or Tension (T)?**
0 → 26 minutes	Beam has a net expansion, axially displacing the sliding support	
5 minutes	Top flange at supports reaches proportional limit	T
6.5 minutes	Bottom half of web at supports reaches proportional limit	C
7.5 minutes	Bottom flange at supports reaches proportional limit	C
14 minutes	Top half of web at midspan reaches the proportional limit	C
17.5 minutes	Bottom flange at midspan reaches the proportional limit	T
21 minutes	Bottom half at web of midspan reaches the proportional limit	T
	Top half of web at supports reaches proportional limit	T
22 minutes	Bottom flange and bottom half of web at supports reaches yield	C

22.5 minutes	Top flange at midspan reaches proportional limit	C
25.5 minutes	Top flange at supports reaches yield; completing plastic hinge at both supports.	C
26 minutes	Beam starts to contract, retracting at the sliding support	
27.5 minutes	Bottom flange at midspan reaches yield	T
29.5 minutes	Top flange at midspan reaches yield	C
30 minutes	Bottom web at midspan reaches yield; completing plastic hinge at midspan. Due to the slide connection no catenary action is possible; hence beam fails.	T

Each of these events will be discussed in further detail within the following sections.

Bottom flange stress

The bottom flange heats up faster than the top so this tends to induce axial stress through the section particularly in the earlier time steps where these temperature differences are more pronounced. Compressive stresses build up at the supports where the bottom flange is more axially restrained against thermal expansion. Meanwhile, as the beam midspan deflects downward with thermal expansion, the bottom flange stress slightly increases in tension. These thermal bowing effects reduce as the temperature becomes more even through the steel cross section. This is shown in Figure 59, below:

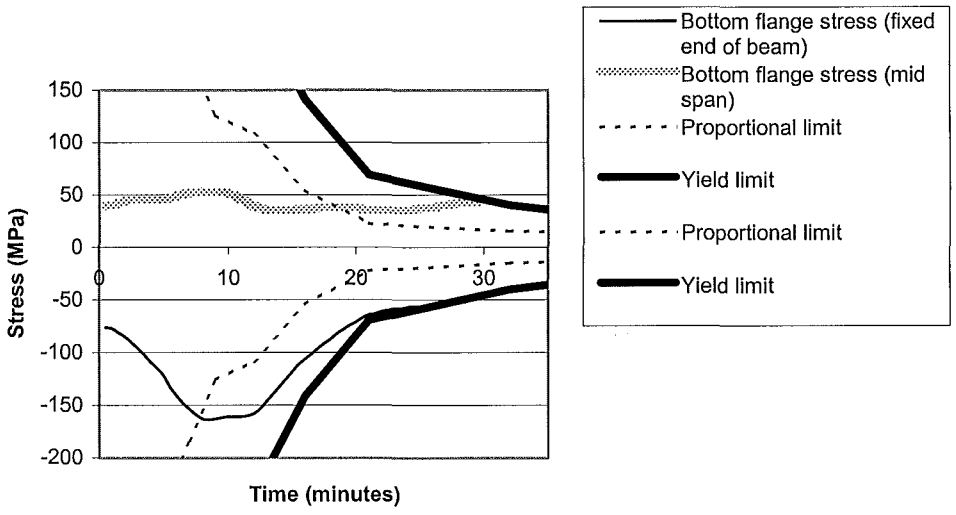

Figure 59) Bottom flange stress of fixed slide steel beam

Top flange stress

Figure 60 shows the top flange at the fixed support being forced into tension due to the thermal bowing, as the ends are restrained against rotation. Meanwhile the midspan top flange goes into tension as the expanding bottom flange pulls it out, and latter back into compression when these thermal effects reduce.

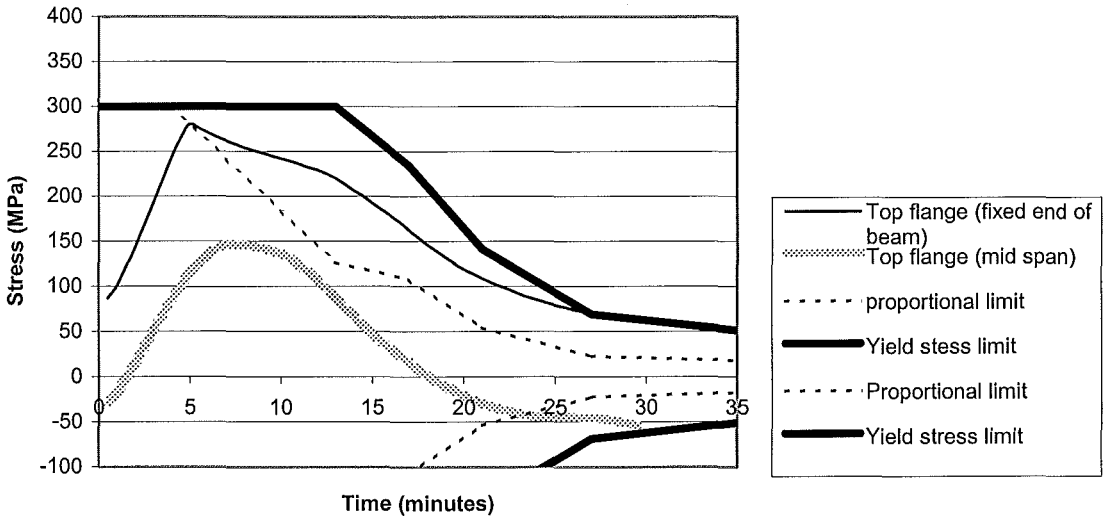

Figure 60) Top flange stresses of steel beam with fixed-slide support conditions

Axial force

There is no net axial force possible within the beam as the end slide support is free to move longitudinally.

Web stress

As shown by Figure 61 and Figure 62, the stresses in the top and bottom halves of the web at both mid and end of span follow a similar trend to the respective top and bottom flanges.

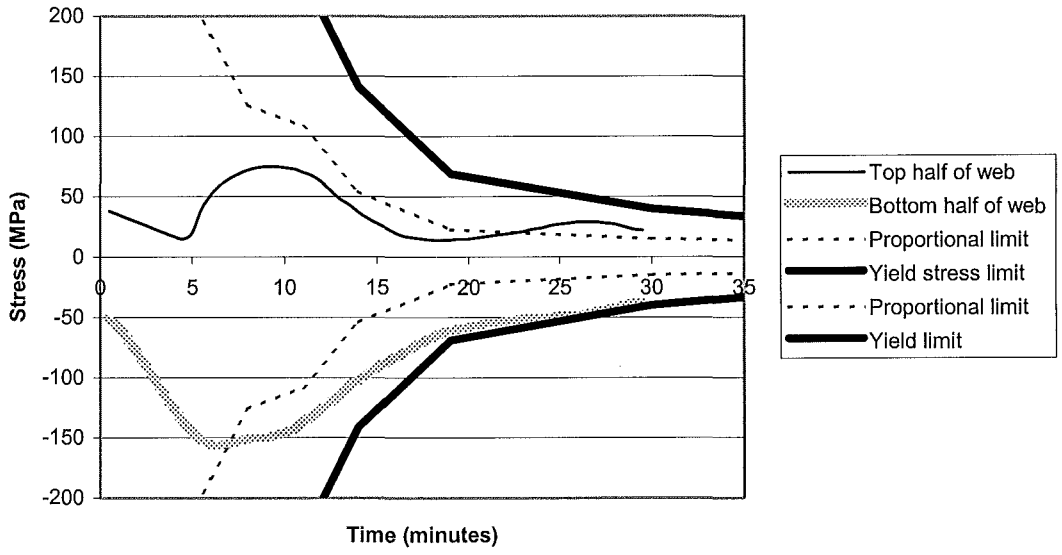

Figure 61) Web stresses at fixed ends of steel beam with fixed slide supports

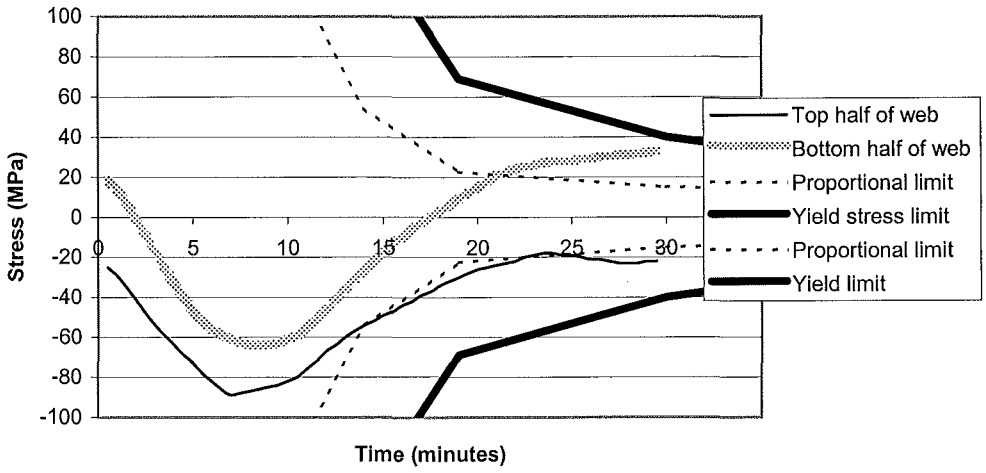

Figure 62) Midspan web stresses of steel beam with fixed slide supports

Moments

The moment increases at the fixed support as a result of the thermal bowing, the midspan moment changes accordingly (see Figure 63). This effect is reduced as the temperature becomes more uniform.

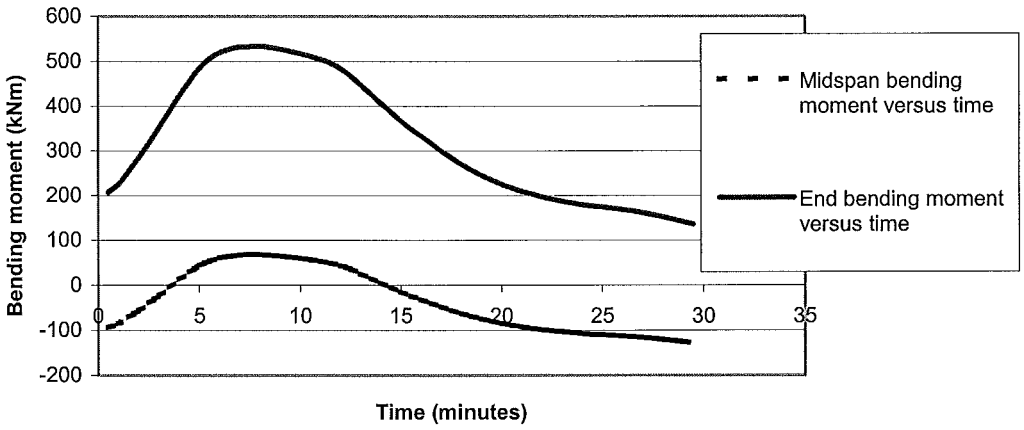

Figure 63) Bending moment versus time of steel beam with fixed slide supports

Midspan deflection

The midspan vertical deflection of Figure 64 is relatively small in the early stages of the fire as the beam does not need to deflect vertically to relieve axial stress due to the slide support. After the first plastic hinges form at the supports and the end slide support starts to move back, the midspan deflection increases rapidly. This is the start of the run-away deflection that leads to the failure of the beam.

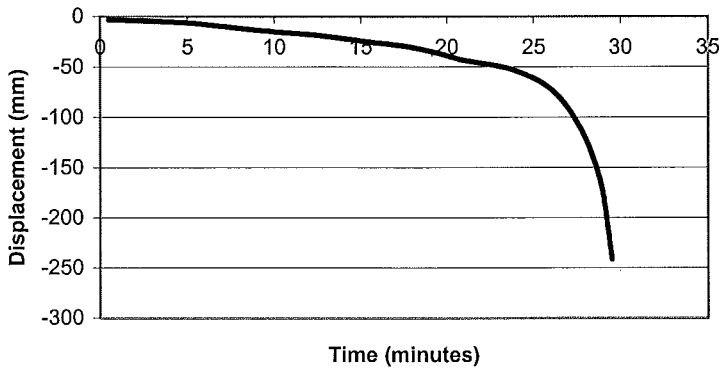

Figure 64) Midspan displacement of steel beam with fixed slide supports

Horizontal displacement of slide support connection

Figure 65 shows the horizontal displacement of the slide support. An expansion in the beam shows as an increasing displacement, while a beam contraction shows as a decreasing displacement.

The roller axial displacement is positive (beam elongating) for the first 25 minutes of fire duration as the beam expands. With the formation of plastic hinges at the supports the beam deflects downward at the midspan, pulling the slide support back in. The steep negative slope of the slide support displacement curve after plastic hinges form at the end supports (25.5 minutes) indicates that the slide support is pulled back in very quickly until the beam fails, with the formation of another plastic hinge at the midspan.

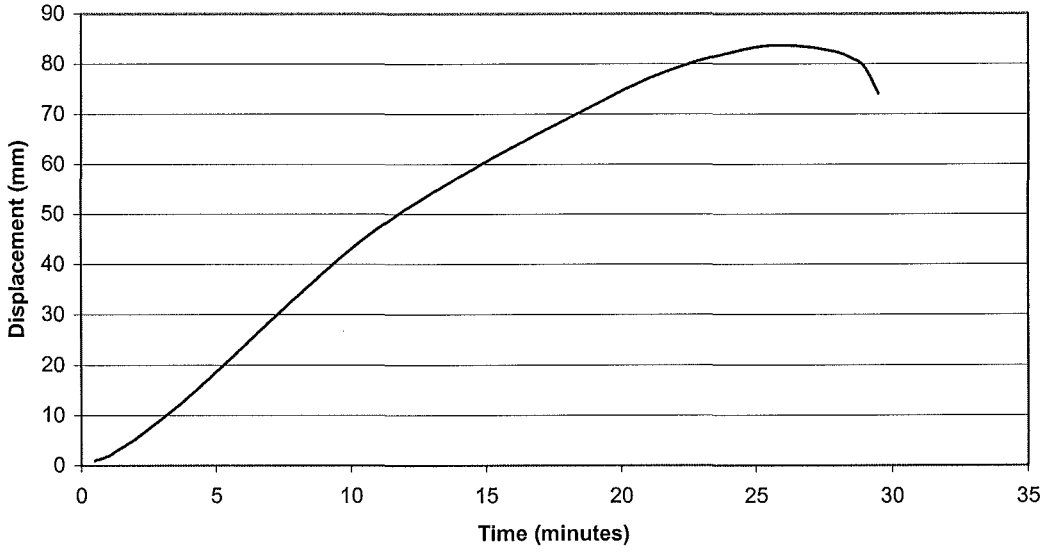

Figure 65) Horizontal displacement of slide support

6.4.2 Pin-roller connected steel beam.

The following table summarises the main events of the exposure of the pin-roller connected steel beam to the ISO-fire.

Table 12) Behaviour of the pin-roller steel beam exposed to the ISO-fire

Time of event (minutes)	**Description of event**	**Stress; Compression (C) or Tension (T)?**
7. 5 minutes	Bottom flange reaches proportional stress limit	T
	Top half of web reaches proportional stress limit	C
15 minutes	Bottom half of web reaches proportional stress limit	T
18. 5 minutes	Top flange reaches proportional stress limit	C
21.5 minutes	Bottom half of web and bottom flange both reach yield stress limit	T
23.5 minutes	Top flange reaches yield stress limit, leading to failure mechanism of beam.	C
24 minutes	Run-away failure of beam	

Each of these events will be discussed in further detail within the following sections.

Bottom flange stress

Bottom flange stresses (see Figure 66) increase initially due to thermal bowing, where the proportional limit is reached. The thermal bowing occurs because the bottom flange heats faster than the top flange, causing the beam to deflect downward, toward the fire. This stress is then reduced again due to the temperature profile dispersing more evenly throughout the beam at a time of 7.5 minutes.

As the pin-roller connected beam can only carry loads in bending, the failure mode of this system occurs with the formation of one plastic hinge, weakening the beam, causing run-away failure. This plastic hinge forms at centre span, starting with the bottom flange and bottom half of the web yielding in tension simultaneously at 21.5 minutes.

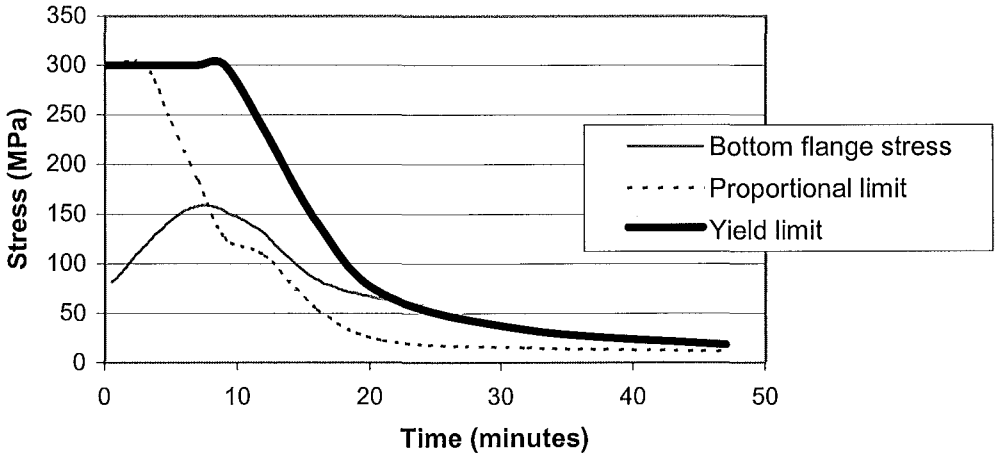

Figure 66) Bottom flange stress of pin-roller supported steel beam

Top flange stress

The top flange stress (Figure 67) follows a similar path to that of the lower flange (Figure 66), with initial increases in stress due to thermal bowing, which reduce as the beam's temperature becomes more uniform. The top flange yields in compression 2 minutes later than the bottom flange yielded in tension at a time of 23.5 minutes. This completes the midspan plastic hinge. This plastic hinge weakens the beam as moment capacity can no longer be maintained, this causes the beam to rapidly sag causing the run-away failure.

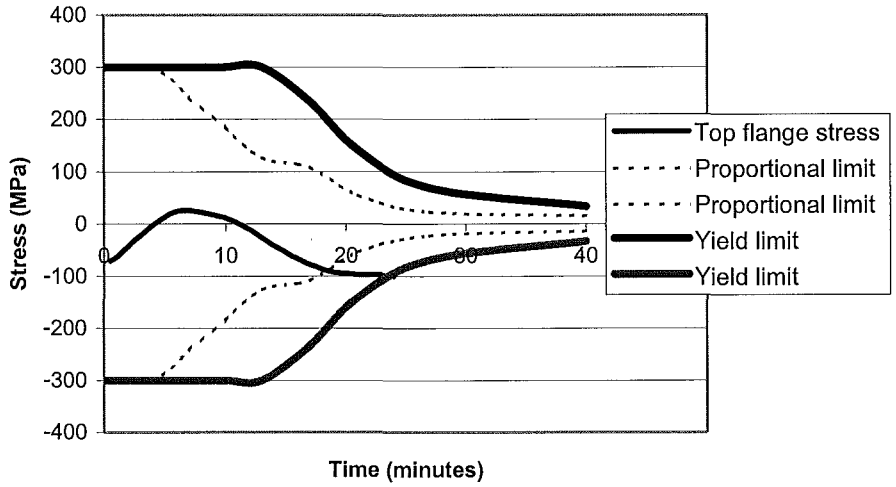

Figure 67) Top flange stress of pin-roller supported steel beam

Web stresses

Top and bottom halves of the web follow very similar trends to their respective flanges as can be seen in Figure 68:

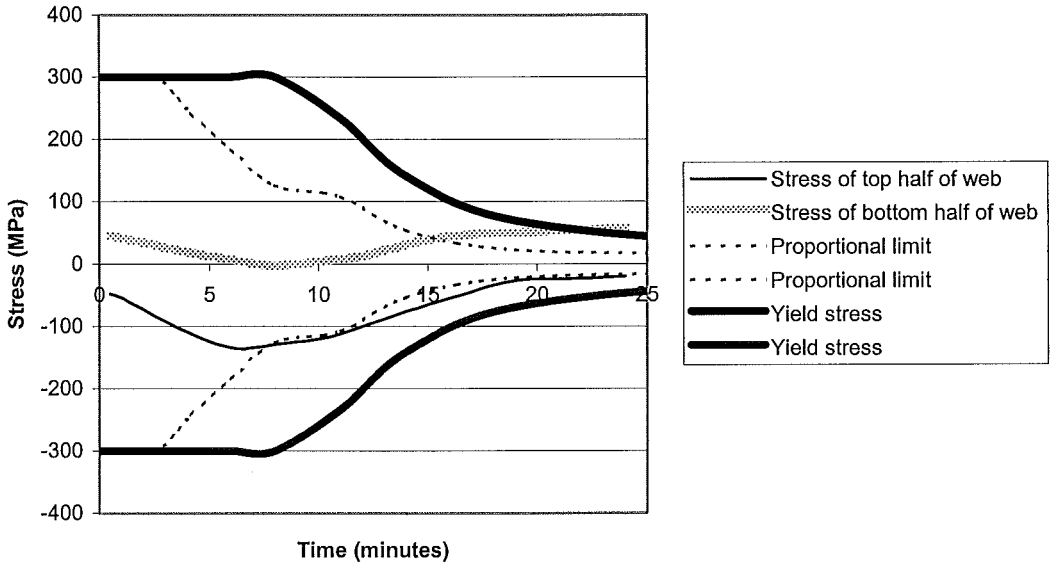

Figure 68) Web stresses of pin-roller supported steel beam

Axial force

As there is no horizontal restraint offered by the roller connection, the overall axial forces are zero throughout this simulation.

Midspan moments

Figure 69 shows that the midspan moment remains constant throughout this simulation. The bending moment can not be increased due to P-δ effects as the axial forces can not be induced in a beam with a roller connection. Nor can the midspan bending moment be reduced due to catenary action within the beam as this action also relies upon an axial force within the beam. The beam forms a single plastic hinge at midspan at a time of 23.5 minutes. 30 seconds later (time = 24 minutes) a rapid run-away failure results from the weakened beam pulling the roller connection back. Unlike the case of the pin-pin supported beam there is no horizontal resistance to form a catenary at the roller support.

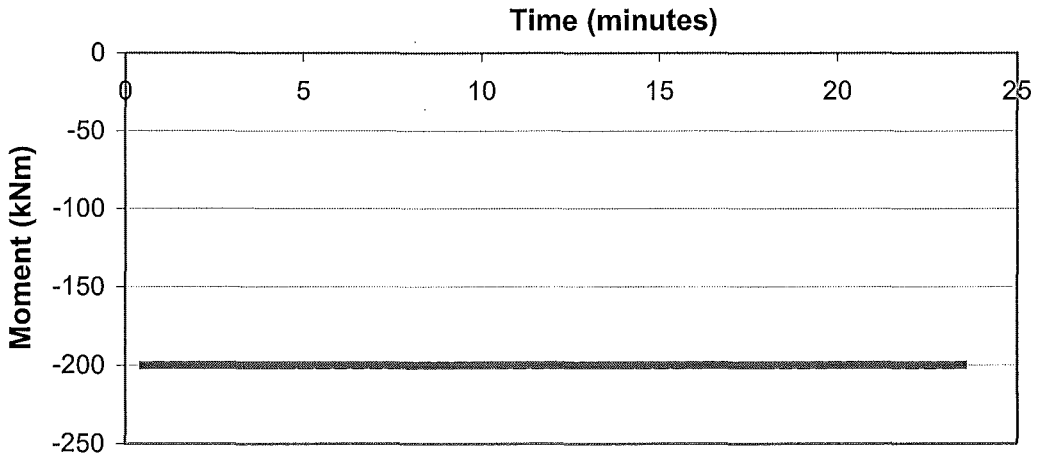

Figure 69) Midspan moment of pin-roller supported steel beam

Roller displacement

Figure 70 shows the horizontal displacement of the roller at the beam support. An expansion in the beam shows as an increasing displacement while a beam contraction shows as a decreasing displacement.

It can be seen that the roller allowed for the beam's expansion for the first 21.5 minutes, just as the section began to yield. Then the beam midspan deflections increased with decreasing beam stiffness, causing the beam to pull back in on the roller, this causes a run-away failure. As expected, the runaway mechanism occurred shortly after the yield of the section at midspan, unlike the pin-pin supported steel beam catenary action was impossible with the roller connection.

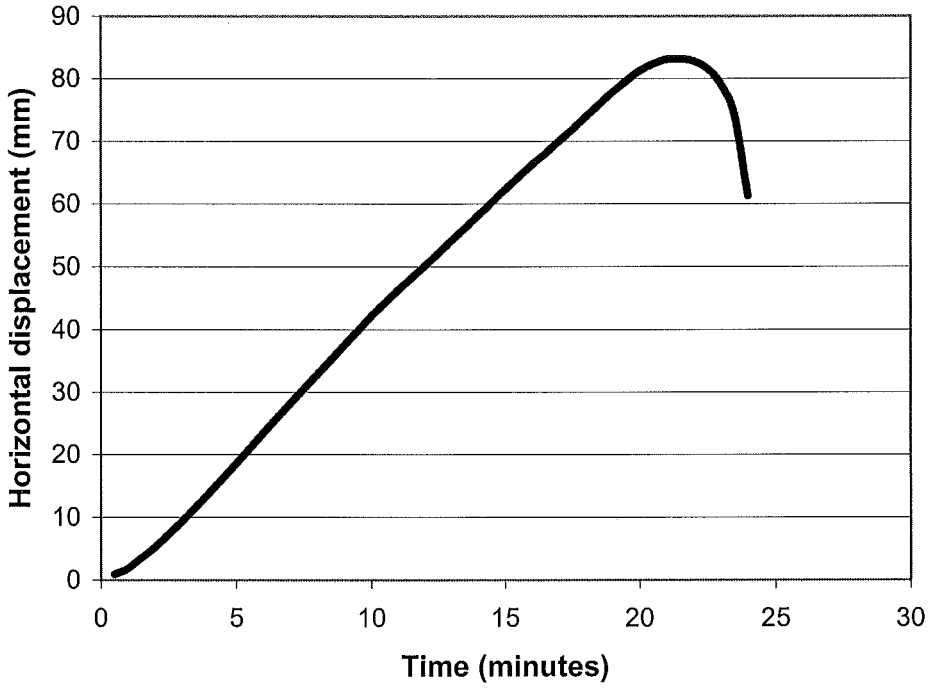

Figure 70) Horizontal roller displacement

Midspan deflection

The midspan deflection of the pin-roller connected steel beam, as seen in Figure 71, is very small for the first 21.5 seconds compared with the pin-pin supported beam. After this time however this deflection increases rapidly as the run-away failure mechanism develops.

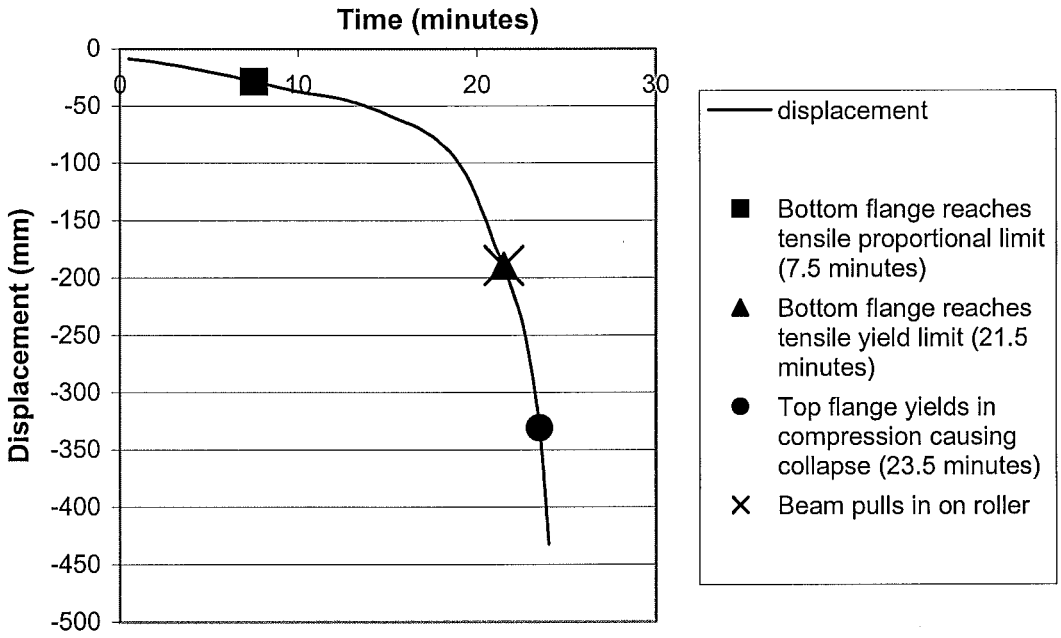

Figure 71) Midspan displacement of pin-roller supported steel beam

6.5 Axially Unrestrained composite steel beams

6.5.1 Fixed-slide composite beam

The following table summarises the main events of the exposure of the fixed-roller connected composite steel beam to the ISO-fire.

Table 13) Behaviour of the fixed-side composite steel beam exposed to the ISO-fire

Time of event (minutes)	**Description of event**	**Stress; Compression (C) or Tension (T)?**
1.5 minutes	Compressive stresses at the top slab reduce to zero	C
5 minutes	Top flange at fixed end support reaches the proportional limit stress	T
5.5 minutes	Bottom flange at fixed end support reaches the proportional limit stress	C
13.5 minutes	Bottom flange at midspan reaches the tensile proportional limit	T
14.5 minutes	Bottom flange at fixed end support reaches yield	C
18 minutes	Roller at maximum horizontal displacement. Sagging beam begins pulling slide support back in	
18.5 minutes	Top flange at midspan reaches compressive proportional limit	C
19.5	Bottom of slab goes in to compression	C
20 minutes	Bottom flange at midspan reaches tensile yield stress limit	T
	Run-away failure of weakened beam occurs as catenary action is impossible with a sliding connection	

Each of these events will be discussed in further detail within the following sections.

Bottom flange stresses

As this beam is not axially restrained, net compressive forces due to the expansion of the beam do not occur as the beam is heated (see Figure 72). As the beam is heated it is free to expand axially with the free movement of the roller connection. However stresses do change in the beam due to the thermal bowing of the section. As the bottom flange heats more rapidly than the top flange it tries to expand more. At the supports where rotation is not possible, the bottom flange's thermal expansion is restrained. At the midspan the bottom flange stresses remain relatively constant.

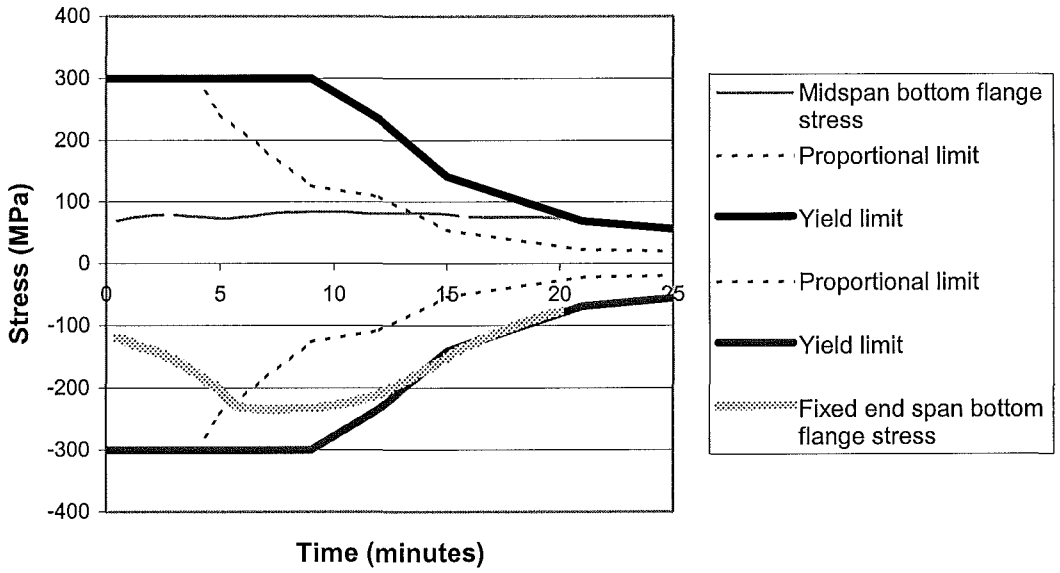

Figure 72) Bottom flange of fixed-slide supported composite beam

Top flange stresses

The top flange at the supports (see Figure 73) is rapidly forced in to tension by the restrained bottom flange as it tries to expand. As the support bottom flange reaches the compressive proportional stress limit (see Figure 72) and the top flange reaches the proportional tensile limit the beam loses stiffness allowing some rotation close to the fixed support. This relieves the stress to some extent at the support, so stresses do not build up further.

At the midspan the expanding bottom flange, which is not restrained axially due to the sliding support pulls the top flange and slab along with it, hence the mid span top flange also goes into tension. After 6 minutes the thermal gradient through the steel section become more uniform, and therefore these thermal-bowing effects diminish. The top flanges do not reach their yield stress as do the bottom flanges because the top flanges

do not get hot enough to reduce the yield stress sufficiently before a run-away failure occurs in the beam.

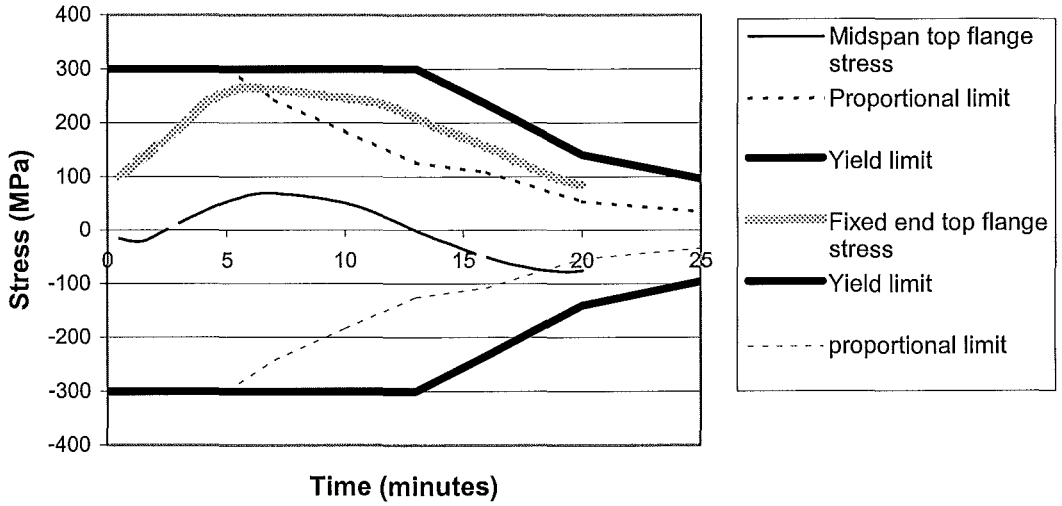

Figure 73) Top flange stress of fixed-slide supported composite beam

Web stresses

The web at both the fixed support and the midspan experience increasing compressive stresses due to thermal bowing, these effects diminish as the steel section temperatures become more uniform (Figure 74).

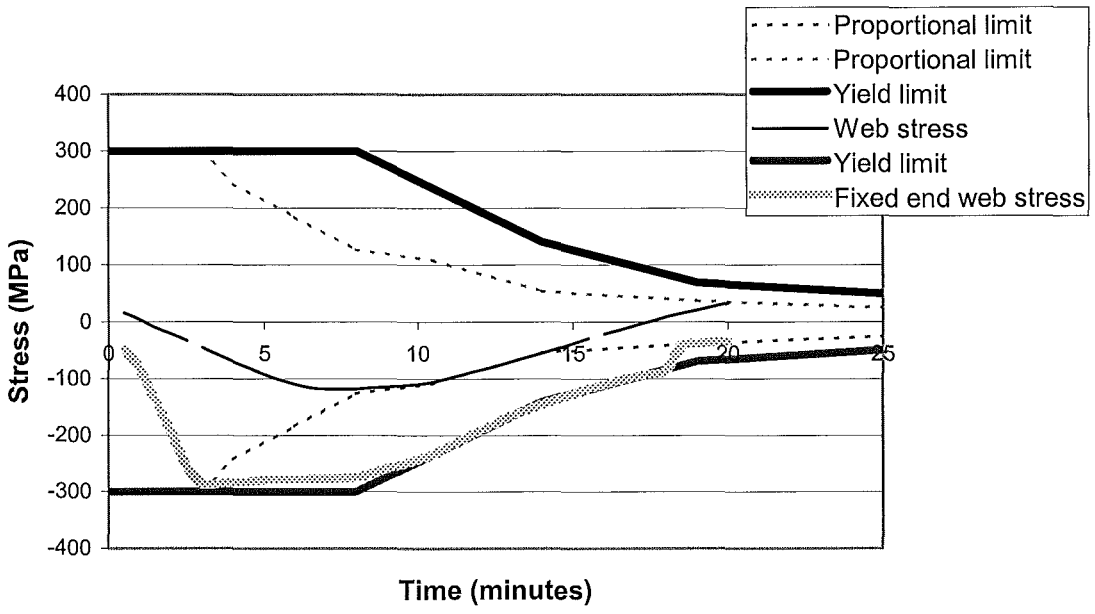

Figure 74) Web stresses of fixed-slide supported composite beam

Axial force

There is no net axial force with the sliding connection, hence this plot has not been included.

Bending moments

The moment increases at the fixed support as a result of the thermal bowing, the midspan moment changes accordingly. This effect is reduced as the temperature becomes more uniform (see Figure 75).

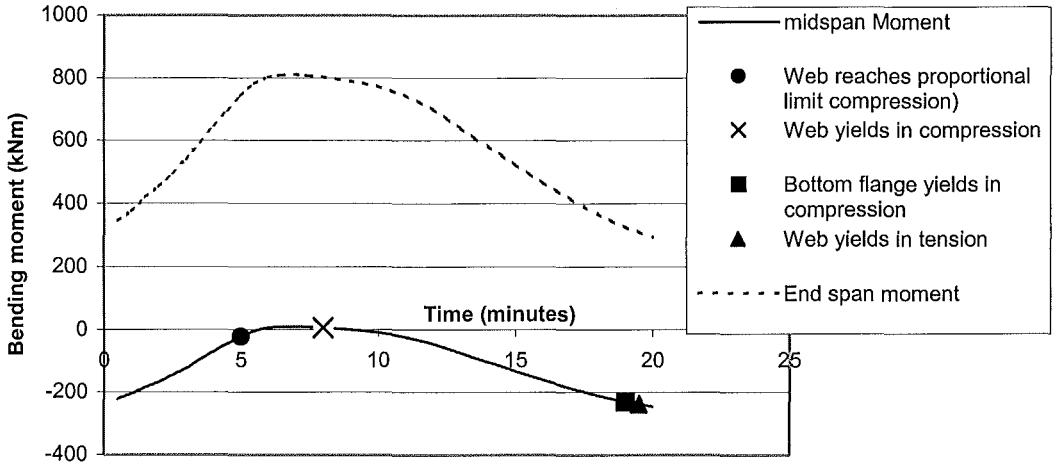

Figure 75) Mid-span bending moment of fixed-slide supported composite beam

Midspan deflection

The midspan vertical deflection (Figure 76) is relatively small for the first 5 minutes of the fire as the beam is expanding, pushing the sliding support out. It is not until the first part of the beam reaches yield that non-linear behaviour causes midspan vertical deflections to increase rapidly. At 20 minutes, when the beam fails, the slope of the vertical midspan deflection versus time is almost vertical. This vertical slope signifies that the beam is experiencing a run-away deflection, and is structurally very unstable.

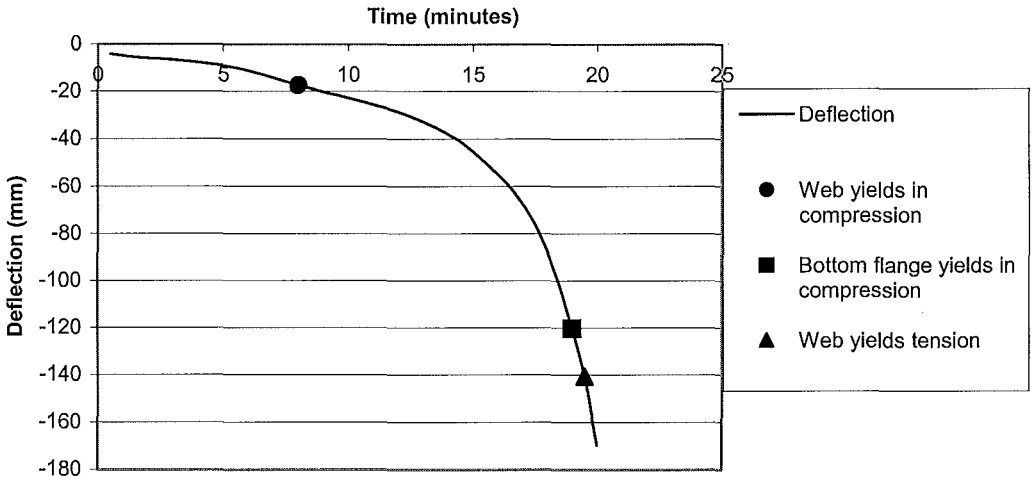

Figure 76) Mid-span deflection of fixed-slide supported composite beam

End sliding support displacement

Figure 77 shows how the sliding support is displaced horizontally as the beam expands up until a time of 18 minutes. After this time the beam has lost much of its stiffness, and the midspan vertical displacement is pulling in on the beam supports with more force than the net expansion. This marks the start of the run-away failure of the beam.

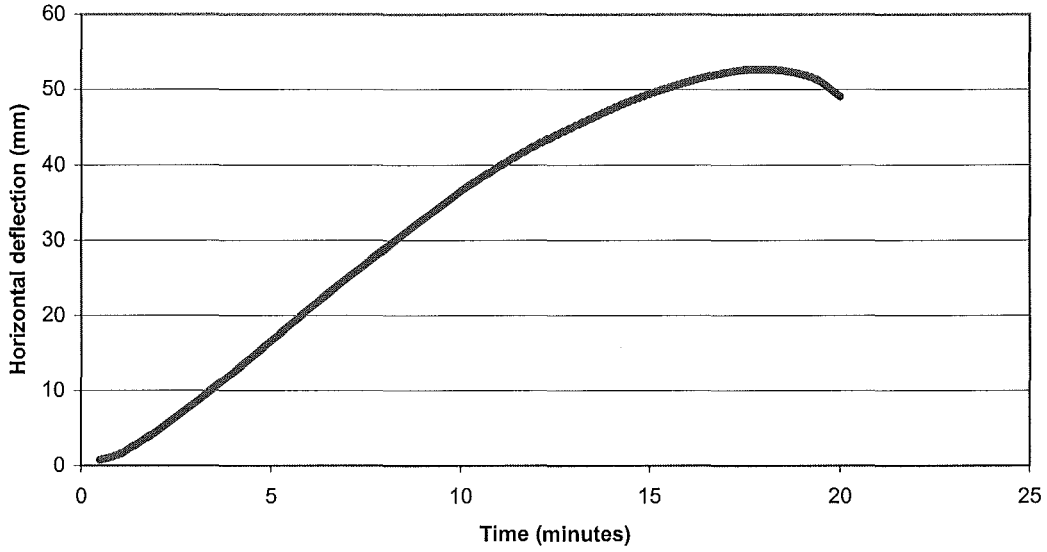

Figure 77) Horizontal deflection at sliding support of composite beam

6.5.2 *Pinned-roller composite beam*

The following table summarises the main events of the exposure of the pinned-roller connected composite steel beam to the ISO-fire.

Table 14) Behaviour of the pinned-roller composite steel beam exposed to the ISO-fire

Time of event (minutes)	Description of event	Stress; Compression (C) or Tension (T)?
2.5 minutes	Slab compressive stress reduces to zero as roller moves to accommodate axial beam expansion	C
5.5 minutes	Bottom flange at midspan reaches tensile proportional limit	T
13.5 minutes	Top flange at midspan reaches compressive proportional limit	C
15 minutes	Bottom flange at midspan reaches yield in tension	T
16.5 minutes	Top of slab goes into compression	C
19 minutes	Top flange at midspan reaches tensile proportional limit	T
21 minutes	Top of slab crushes	C
21.5 minutes	Top flange at midspan reaches yield in tension, forming one plastic hinge.	T
	Failure of the beam	

Each of these events will be discussed in further detail within the following sections.

Bottom flange stress

Figure 78 shows that the bottom flange quickly goes into tension due to thermal bowing. The bottom flange heats up much faster than the top flange because of the heat sink effects of the slab, hence the bottom flange tries to expand sooner. This expansion leads to the bottom flange bowing downwards, causing increasing tension. After the steel has been exposed to the fire for a longer duration the temperature is more uniform throughout the section. Therefore thermal bowing effects reduce, with a noticeable drop in the bottom flange tensile stress after 6 minutes.

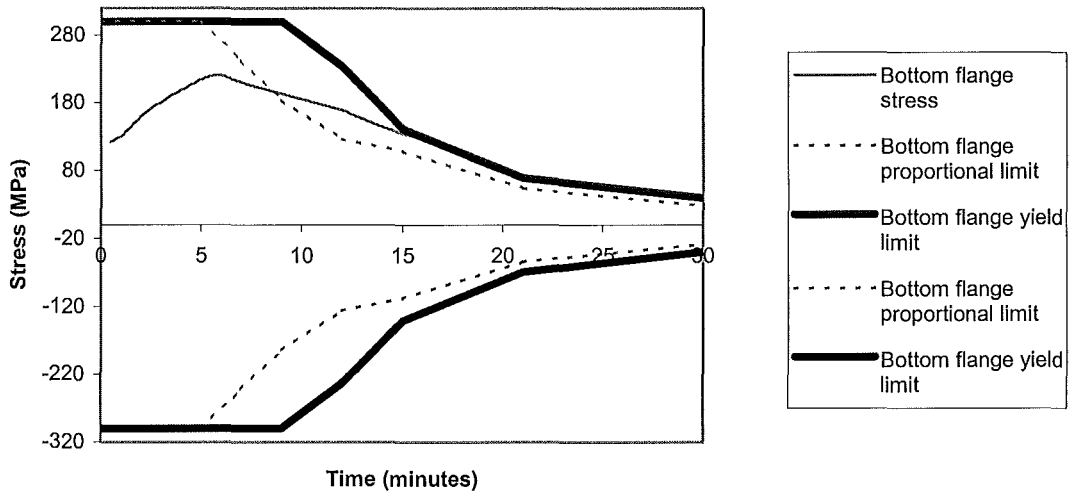

Figure 78) Beam bottom flange stress at midspan for pin-roller supported composite beam

Top flange stress

The top flange increases slightly in compressive stress (Figure 79) due to the effects of thermal bowing as described above for the bottom flange. After the bottom flange reaches it's tensile proportional stress limit as explained above, the beam has lost a substantial amount of its stiffness and midspan deflections increase quickly due to the partial formation of a plastic hinge. This causes the top flange to now take on tensile stresses as the beam carries loads more by catenary action rather than flexure.

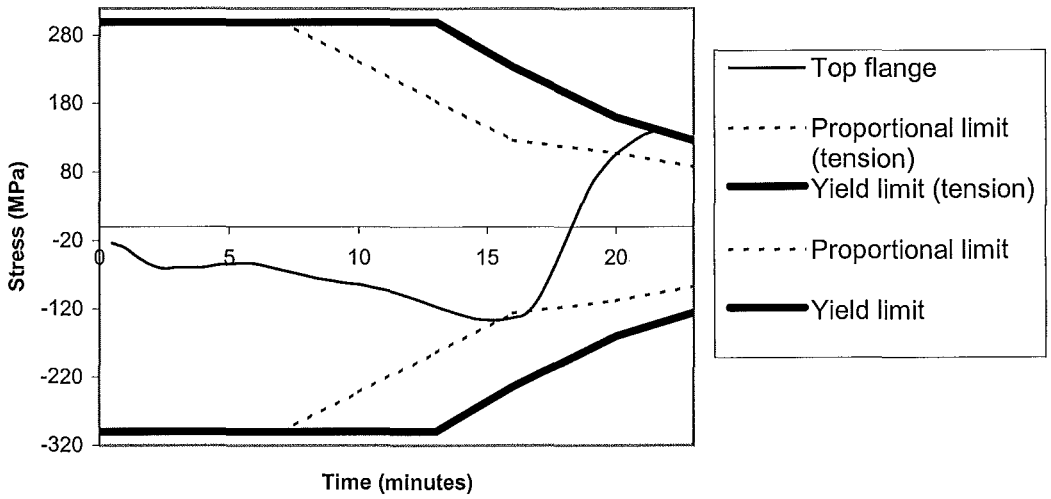

Figure 79) Beam top flange stress for pin-roller supported composite beam

Web stresses

The web stresses of Figure 80 follow a very similar trend to the top flange, as seen below:

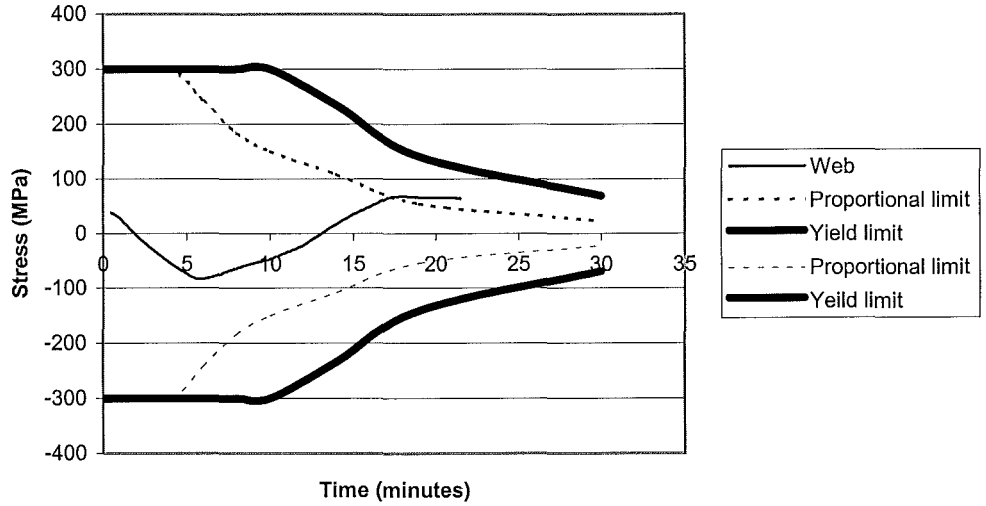

Figure 80) Beam web stress for pin-roller supported composite beam

Axial force

As there is no horizontal restraint offered by the roller connection, therefore the overall axial forces are zero throughout this simulation.

Midspan moments

The midspan moment shown in Figure 81, remains constant throughout this simulation as the bending moment can not be increased due to P-δ effects. This is because axial forces can not be induced in a beam with a roller connection, nor can the midspan bending moment be reduced due to catenary action, as this also relies upon an axial force within the beam.

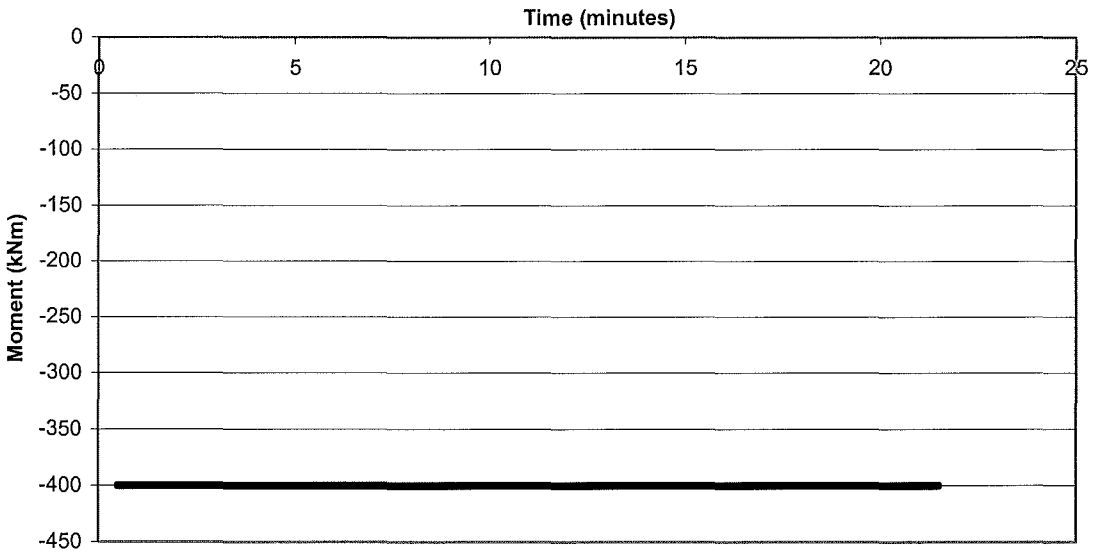

Figure 81) Bending moment for pin-roller supported composite beam

Midspan deflection

The midspan deflection of the pin-roller connected steel composite beam is very small for the first 15 seconds compared with the pin-pinned supported beam (see Figure 82). After this time however the deflection increases rapidly as the run-away failure mechanism develops and the roller support is pulled in.

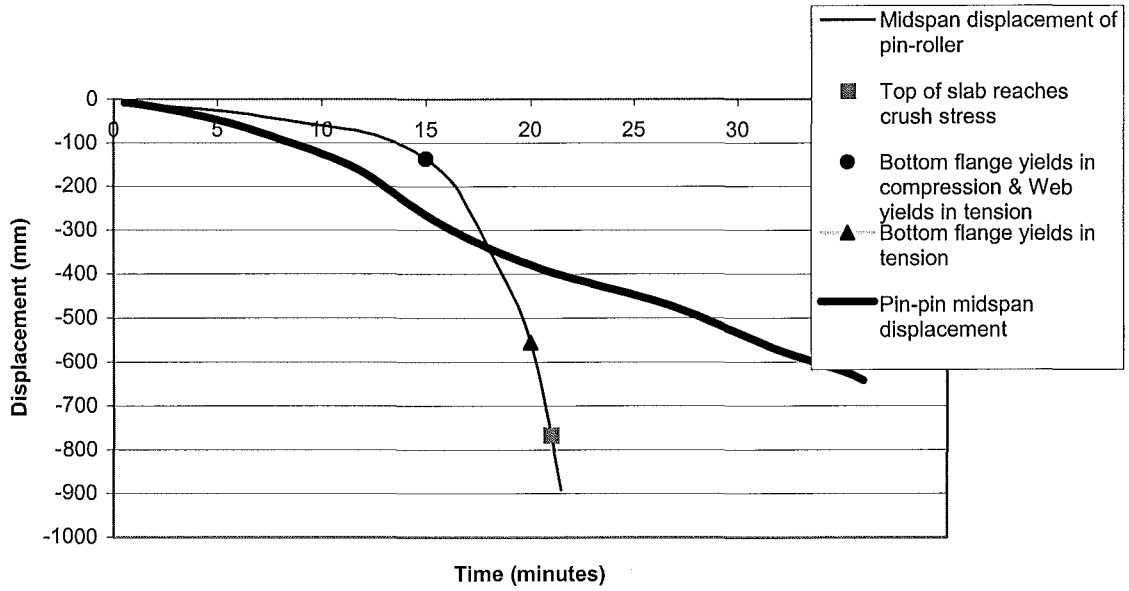

Figure 82) Midspan displacement for pin-roller supported composite beam

End roller support horizontal displacement

Figure 83, below shows the horizontal displacement of the roller at the beam's support, an expansion in the beam shows as an increasing positive displacement, while a beam contraction shows as a decreasing displacement.

It can be seen below that the roller allowed for the beams expansion for the first 17 minutes, just after the bottom flange has yielded in tension at the midspan. As the beam pulled back in on the roller as midspan vertical displacement increased with decreased beam stiffness a run away failure began to occur. It seems that this runaway mechanism occurred shortly after the yield of the bottom flange at midspan, unlike the pin-pin supported steel beam, since catenary action was impossible with the roller connection.

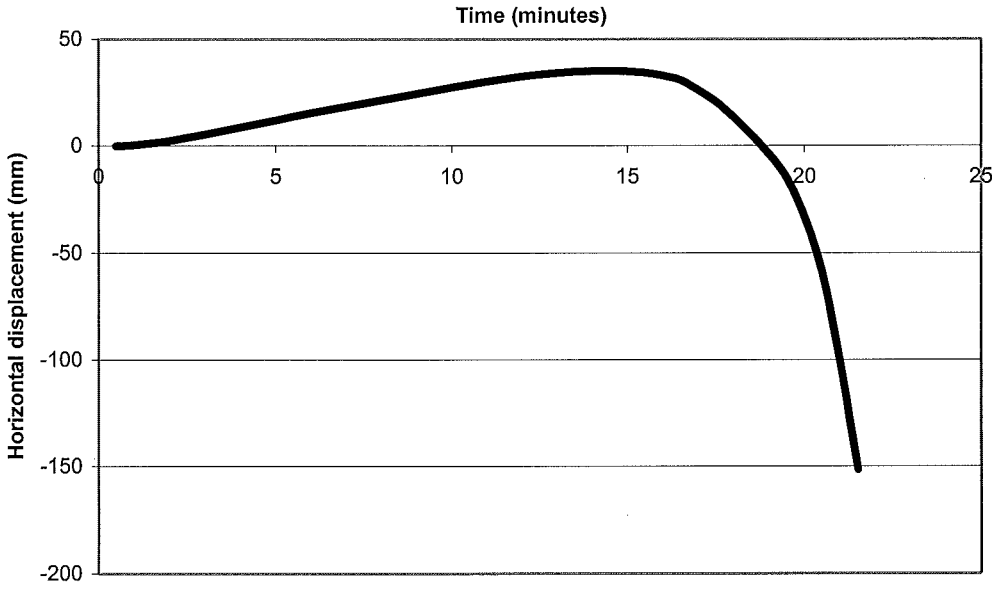

Figure 83) Horizontal roller displacement for pin-roller supported composite beam

6.6 Summary of unrestrained steel and steel composite beams

These beams were free to elongate as they expanded with increasing temperature, hence they experienced no net axial force within the beam for either the composite or the steel beam. Stresses within the beams did however change with heating, particularly in the earlier stages of the fire. These stresses arise from thermal bowing of the beam; this is the result of differential heating, and hence differential rates of expansion through the cross-section.

Midspan deflections of the unrestrained beams were noted to steadily increase due to loss of strength of the steel with increasing temperature. When enough plastic hinges had formed for the failure mechanism, i.e. three plastic hinges in the case of the fixed-slide, or one in the case of the pinned-roller; the beam experienced a runaway failure. This is where the roller, or sliding support is pulled back in as the midspan deflects down rapidly. With the restrained beams discussed earlier, the beam may have had some more capacity left due to tensile catenary action. This is not possible with either the roller or sliding support. These findings are consistent with the findings of Seputro (2001), Welsh (2001) and Usmani & Rotter (2000) who looked at slower linear temperature increases.

7 Results from simulations of frames with varied column stiffness exposed to the ISO fire.

7.1 Introduction

This chapter looks at the effect of fire on unprotected steel beams, and unprotected composite beams with the addition of frame action. This is achieved by the addition of columns of varied stiffness which replace the supports of the beams analysed within chapter 6. The beam is connected to the columns with ridged moment resisting beam-column joints. The columns are fixed to rigid supports at the top and bottom. The beam's end flexibility is therefore supplied only by the columns' flexibility. The columns are assumed to have full thermal protection against the fire, and hence remain at ambient temperatures. As the columns remain at ambient temperature, the steel within the columns will maintain it's constant yield stress. The steel of the beam will by contrast, be exposed to the ISO fire from both sides, and below, and hence will have a decreasing yield and proportional stress limit due to thermal degradation.

7.1.1 Column details

Within this chapter the flanges of the columns will be referred to either as being on the inside or the outside of the frame, as shown in Figure 84. The columns are each 8m long between supports, and are connected to the beam at mid-height as shown in Figure 84. The cross-section of the column is the same as the cross-section of the steel beam for the frames with both the composite and the steel beam. Varying Young's Modulus, while the cross-sectional area and second moment of area remain constant alters the stiffness of the columns. The stiffness of the columns is quoted as a percentage of the steel beam stiffness, i.e. when the columns are quoted as being at 100% beam stiffness, the Young's Modulus of the beam and column are the same. For the steel beam, this means that the beam and column stiffness is identical. The composite beam however, has a flexural stiffness ratio of approximately 2.49 to the column because the second moment of area is different each section (I_{xx} composite beam / I_{xx} steel column = 1.8930E+9 mm^4 / 7.610E+6 mm^4).

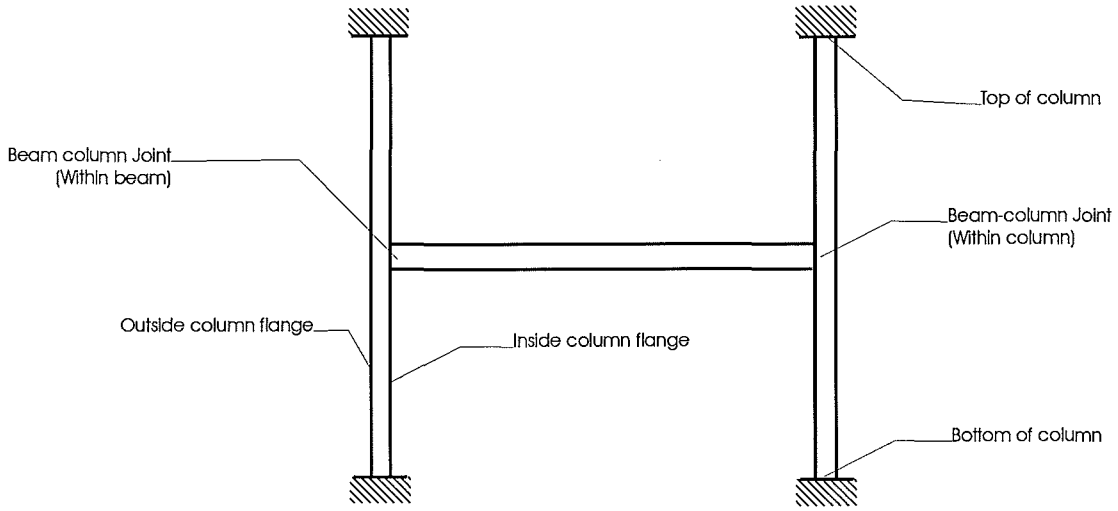

Figure 84) Locations within columns where stresses are considered

7.2 Steel beam

This section considers frames with protected columns supporting the steel beam. The column stiffness will be varied by changing the columns modulus of elasticity (see section 7.1.1), and quoted as a percentage of the steel beam stiffness.

Beam axial force

Axial forces within the unprotected steel beam vary quite markedly for different column stiffness as shown by Figure 85. When the columns are stiffer than the beam, the axial force within the beam builds up very rapidly, reaching a peak compressive force. The peak of the initial compressive force becomes sharper as the column stiffness increases. This peak axial force is associated with yielding at the top and bottom of both columns. After yielding of the columns the steel beam can expand more freely as it is heated, relieving axial strain increases after 3 minutes for the very stiff columns.

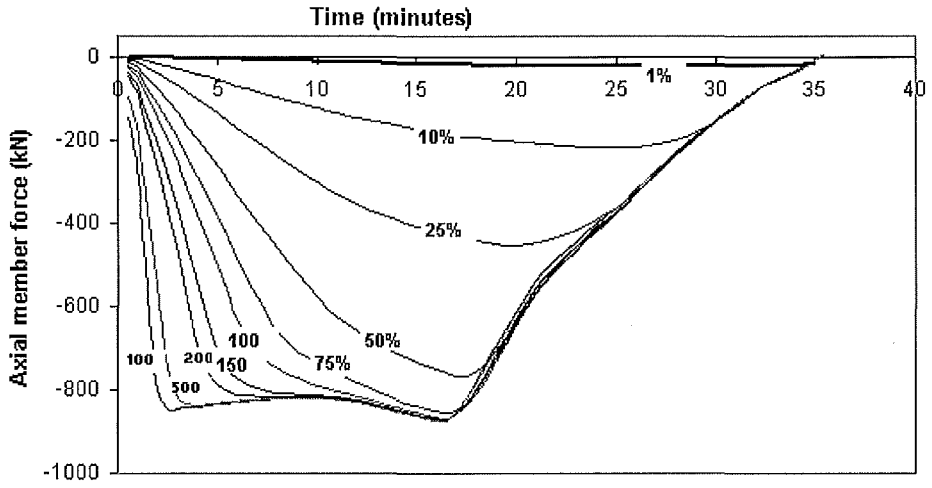

Figure 85) Axial force within steel beam of frame

After yield within the columns, the axial force within the beam remains relatively constant until about 17 minutes for the very stiff columns, or 23 minutes for those less stiff. At this time the axial force within the beam is reduced rapidly with the yielding of the bottom flange at either end of the beam. This is similar to the axial force reducing action that occurs within the fully fixed beam. In the fully fixed beam the bottom flange at either end of the beam reaching the proportional limit relieves the axial force. There is one major difference between the fully fixed beam and the beam with columns. The

steel beam with columns has some flexibility at the supports where the fully fixed beam does not. This extra flexibility at the ends of the beam with columns means that the bottom flange reaching the proportional limit has much less overall effect on the axial force of the beam. It is not until the bottom flange at the beam-column joint actually yields that a significant difference is made to the beam's axial force. The axial force within the beam with very flexible columns, i.e. 1% of the beam stiffness, is very low throughout the duration. This is because the beam is very free to expand and contract. It is as if the ends were supported with roller connections with very soft springs. This behaviour is similar to that noted by Seputro (2001) for the steel beam with very soft axial springs[1] on rollers with the exception of duration before collapse in the fire.

Midspan displacement

The midspan displacement plots of Figure 86 have been divided into two groups, the first group being the frames with the beam stiffer than the column (see Figure 87), and the second being those where the column is stiffer than the beam (see Figure 88). The midspan deflections of both groups of steel beams with columns have been compared with the steel beam with pin-roller supports and with fully-fixed supports as analysed in chapter 6 of this report. These two groups appear to show behaviour distinct from one another as is detailed in the following:

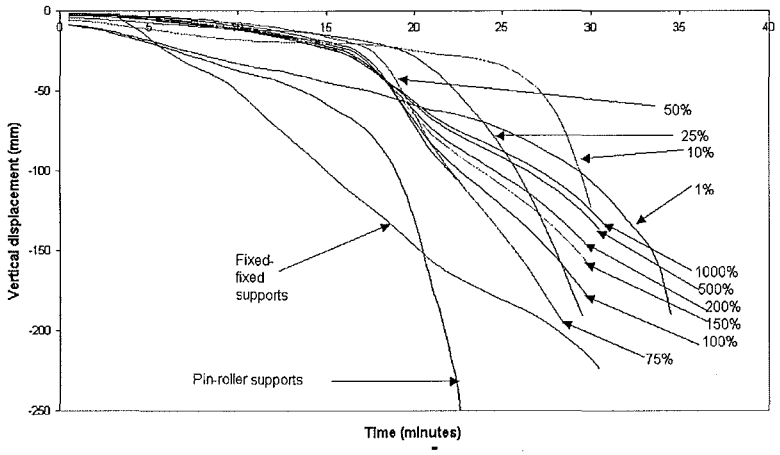

Figure 86) Vertical displacement at midspan

[1] Seputro (2001) looked at very soft axial springs with a spring stiffness within the range of 0 to 0.1

- *Beam stiffer than the column*

In the scenario of the beam stiffer than the column, the midspan deflections appeared to converge upon a scenario nearest in behaviour to the steel beam with pin-roller supports (see Figure 87). The beam connected to columns with only 1% of the beam's stiffness very closely resembles the pin-roller supported beam initially. It is reasonable to expect this; because as the column stiffness is reduced the beam column joint allows less rotational and axial restraint to the beam. This is similar to the behaviour of the roller connection.

There was, however, considerable difference between midspan deflection of the steel beam with 1% column stiffness and pin-roller supports; most noticeably in the latter stages of the fire. This is due to the columns being able to offer some tensile axial resistance to the beam. The beam with a roller connection is able to move to allow for the expansions of the beam, but as soon as the beam forms one plastic hinge; the roller connection is unable to offer any tensile axial resistance. This causes the run-away failure observed in section 6.4.2 of this report. It is clear from the plot below that even with a very modest amount of tensile axial restraint, as offered by the column with 1% of the beam's stiffness; the beam can avoid an early run-away failure.

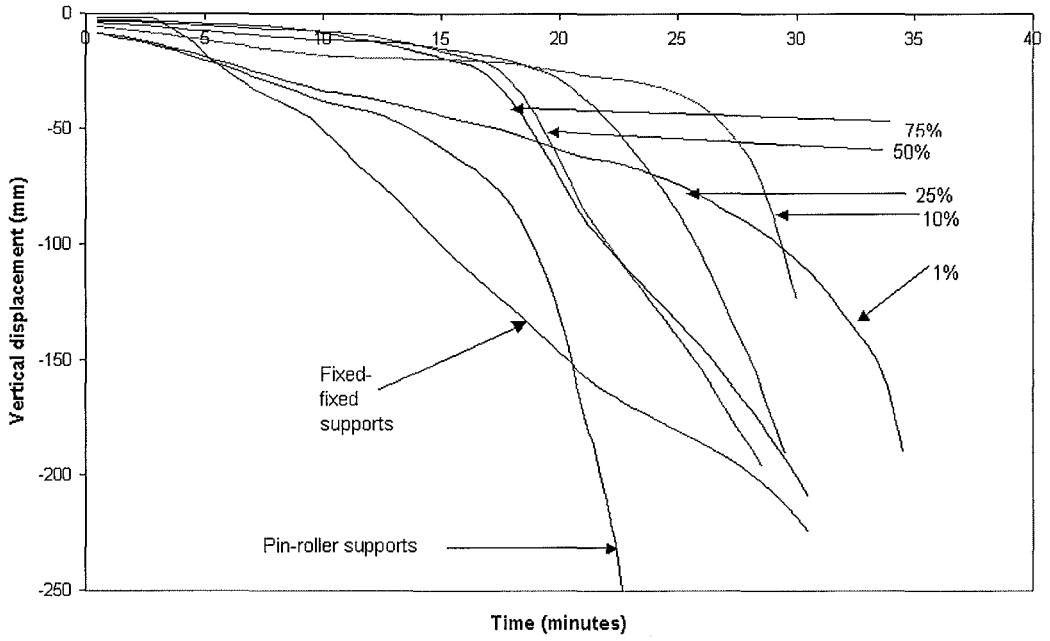

Figure 87) Midspan displacement of frame with steel beam stiffer than columns

- *Column stiffer than the beam*

As the column stiffness increases, the beam's midspan deflection changes progressively toward a more linear displacement versus time plot as shown by Figure 88. This is similar to the initial behaviour of the fully fixed beam as analysed in section 6.1.2. The first difference between the beam with stiff columns and the fully fixed beam is observed at a time of 3 minutes. At this time the fully-fixed beam reaches the compressive proportional limit in the lower flange at the supports. This does not occur in the same beam supported by stiff columns. The increasing axial force within the beam with stiff columns is relieved by the formation of plastic hinges at the top and bottom of each column. This results in considerably lower midspan deflection for most of the duration. The midspan deflection again increases rapidly for the beam with stiff columns at a time of approximately 17 minutes. This corresponds to the bottom flange stresses of the beam at the beam column joint reaching the yield stress limit.

The less stiff the columns, the more the rapidly the midspan deflections increase after yield of the bottom flange at the beam column joint. This is because the columns are more flexible and offer less axial resistance too the weakened beam. After the yield of the bottom flange at the beam column joints the columns act similarly to axial springs of varying stiffness.

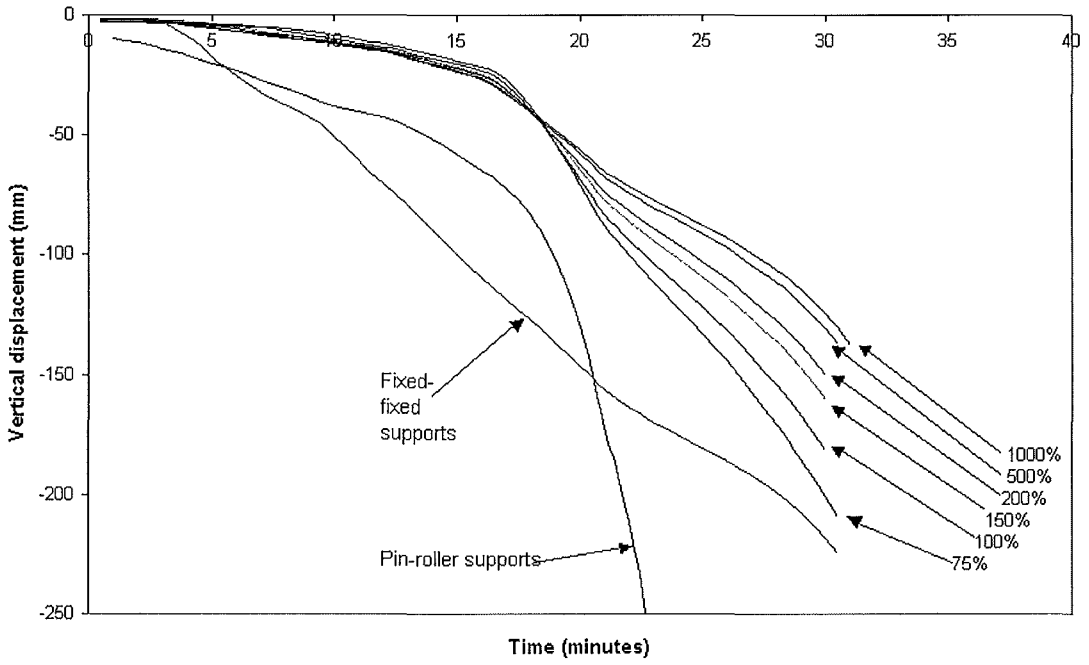

Figure 88) Midspan displacement of frame with columns stiffer than steel beam

- *Midspan displacement comparison with the fully fixed beam*

The previous midspan deflection plot of beams with varying column stiffness (see Figure 88) appears to show that even as the column stiffness increases, the midspan beam deflection behaviour does not appear to converge upon that of the fully-fixed beam. Possible reasons for this behaviour could be that the column is either providing sufficient rotation, or horizontal movement at the beam column joint. If this occurs even a very stiff column is somewhat different than the fully-fixed support conditions. Both the horizontal movement, and the rotation at the beam-column joint's contribution to midspan deflection have been considered independently, as well as together. The results can be seen in Figure 89 below:

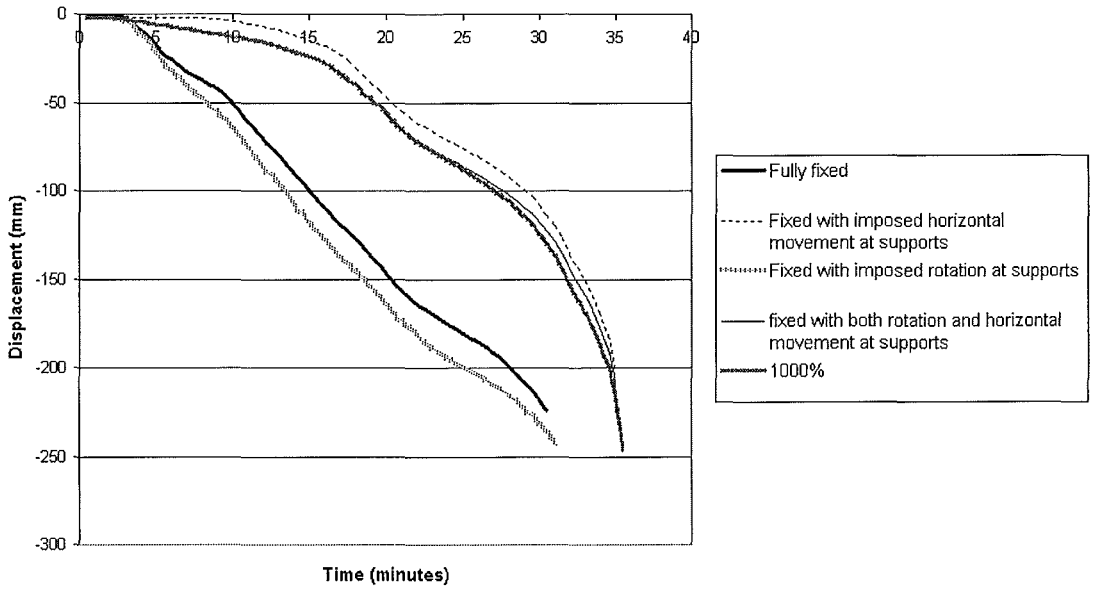

Figure 89) Comparison of fully-fixed steel beam midspan deflection with 1000% column stiffness

The above plot shows the results of modification of the support conditions of the fully-fixed steel beam analysed in section 6.1.2. The horizontal movement at the column joint for the stiffest column analysed , i.e. 1000% of the beam stiffness, was recorded. This same horizontal movement was imposed upon both the supports of the fully-fixed beam. That is, the supports were fixed rotationally, and vertically, but the beam had horizontal movement only, as if columns were in place. A similar scenario was considered where only the rotation of the beam column joint was included. The supports were fixed for horizontal and vertical movement, but the rotation at the

supports was as if columns were in place. Finally both the horizontal and rotation at the support were considered simultaneously.

When the rotation of the beam-column joint only is considered, the midspan deflections are similar, but slightly increased over what is observed for the fully-fixed beam. The restricted rotation at the supports does not prevent the very small initial deflections, which is followed by rapidly increasing deflection after the bottom flange reaches the proportional limit at supports. This is characteristic behaviour of the fully-fixed beam, as discussed in section 6.1.2. The slight increase of midspan deflection of the beam with imposed joint rotation over the fully-fixed beam is a result of the joint rotation giving more flexibility to the supports. The beam is able to deflect further once axial forces are relieved.

When the supports have the beam-column joint horizontal movement only, the behaviour becomes very similar to the steel beam of the frame with 1000% column stiffness. This small amount of horizontal movement at the ends of the beam prevents the support bottom flanges reaching the compressive proportional limit at the same time as the fully-fixed beam.

Finally, both the horizontal support movement, and rotation of the 1000% beam-column joint are imposed on the fixed beam simultaneously. As expected, the behaviour of the supported beam is now identical to the beam within the frame. The slight differences observed are due to an approximation of the support movements as a step wise function with time, using 30 second time steps.

These results show that even with the very small horizontal column movement axial force relief is offered to the beam. The result is the beam midspan deflection behaviour appears quite different to that of the fully fixed beam and smaller, almost linear deflections with time are observed.

Horizontal deflection at the beam column joint

The trends observed for the horizontal movement at the beam column joint (see Figure 90) can be divided into two main categories. First, where the beam is stiffer than the column, and second, where the column is stiffer than the beam.

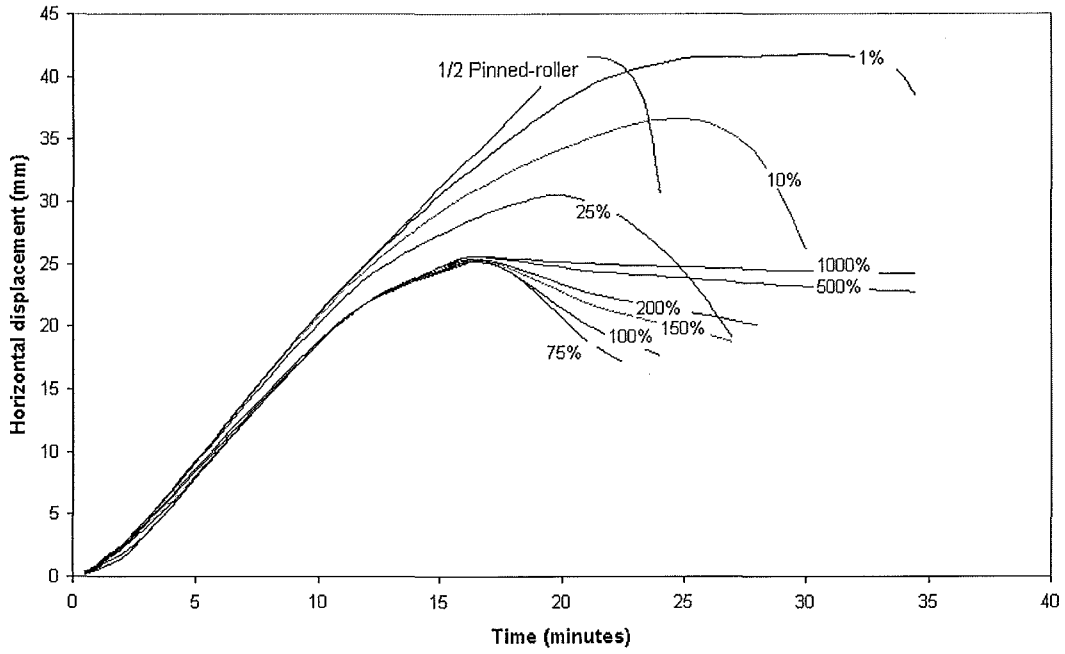

Figure 90) Horizontal movement of beam column connection

- *Beam stiffer than the column*

As the column stiffness drops, the beam-column joint's movement can be likened to the movement noted for the pinned roller support of the same beam without columns considered in section 6.4.2. Note in Figure 90, the pinned-roller's horizontal displacement is divided by 2. This is to allow for the fact that the pinned-roller supported beam is only able to expand axially at one end, compared to both ends of the beam supported within a frame.

The reason that the frame behaviour with flexible columns is similar to the pinned-roller supported beam is because as the column stiffness is reduced, more rotation and horizontal movement is possible at the beam-column joint.

When the column stiffness has dropped to 1% of the steel beam stiffness the beam end horizontal displacement is almost identical for the first 15 minutes. The most noticeable difference between the frame with 1% column stiffness and the pinned-roller is that the

frame does not experience the same run-away failure as the pinned roller. This is because the columns are able to offer some tensile resistance to the collapsing beam.

- *Column stiffer than the beam*

As the column stiffness is increased beyond 75% there is very little noticeable variation in the beam-column joint horizontal displacement for the first 17 minutes (see Figure 90). The stiffest frame analysed, however, does not compare well with the fully fixed beam, which will not have any horizontal displacement at all. This indicates that even with very stiff columns the axial force imposed by the expanding beam is likely to cause some support movement with real connections. After 17 minutes, the bottom flange of the beam yields at the supports. The beams with stiffest columns are then pulled back in to a lesser extent. The explanation for this is that the stiffer columns can offer more horizontal resistance to the beam. Typically where the columns are stiffer than the beams the frame does not last as long when exposed to the ISO fire. This is because after the yield of the bottom flange at the beam column joints, the stiffer columns typically offer less horizontal restraint to the beam because of the plastic hinges at the column ends. These plastic hinges are not present in the column ends of frames with columns more flexible than the beam.

Bending moments

Throughout the fire duration it is noticeable that the ratio of the magnitude of bending moments at the supports (Figure 91) compared with the midspan (Figure 92) are typically of the order of 2:1. This is similar to what is observed for the fully-fixed beam (Figure 43), and is what is expected of fixed frame bending moments at cold conditions. As the beam is heated the bending moments at the beam column joints increase due to the P-δ effects of the beam's axial force. The midspan bending moments also change, maintaining the support to midspan beam bending moment of 2:1. After the bottom flange yields at the beam column joints, this axial force is substantially reduced, and the bending moments drop accordingly at both the ends and the midspan of the beam. The beam-column joint bending moments of the beam with 1% column stiffness is very small throughout the fire's duration. This is because the columns are so flexible that sufficient rotation at the supports occurs that the beam behaves similarly to the pin-pinned beam. The bending moments of the beam with 1%

column stiffness also lacks the distinctive peak of the stiffer columned frames. This is because the columns deflect before large axial forces build-up within the beam. Because of the lower axial forces, the bottom flange at the beam column joint does not yield in compression as occurs in the frames with stiffer columns.

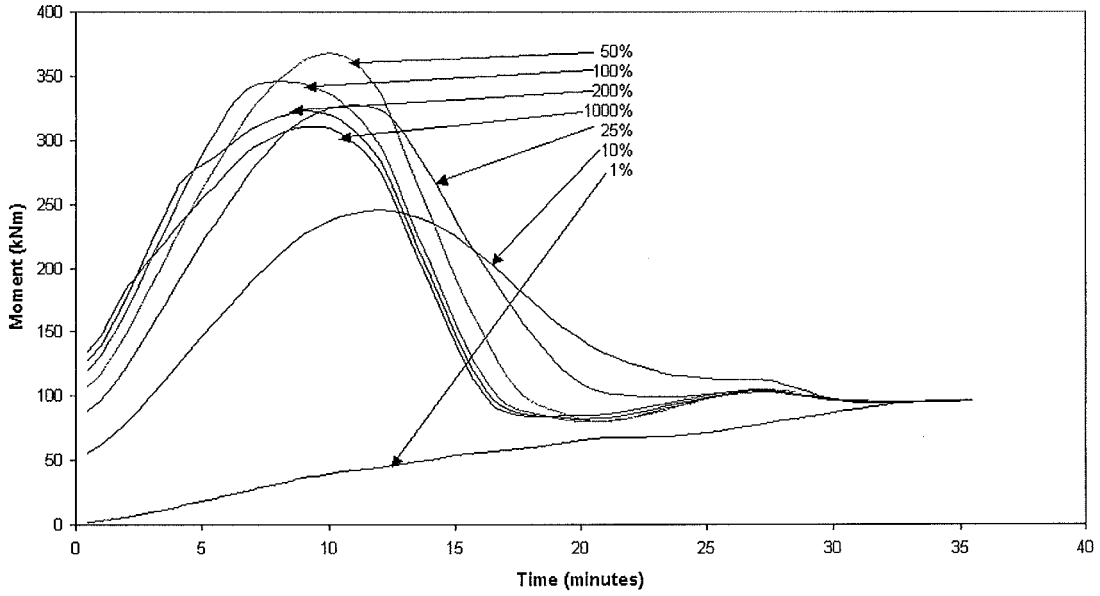

Figure 91) Moments within beam at the beam-column joint

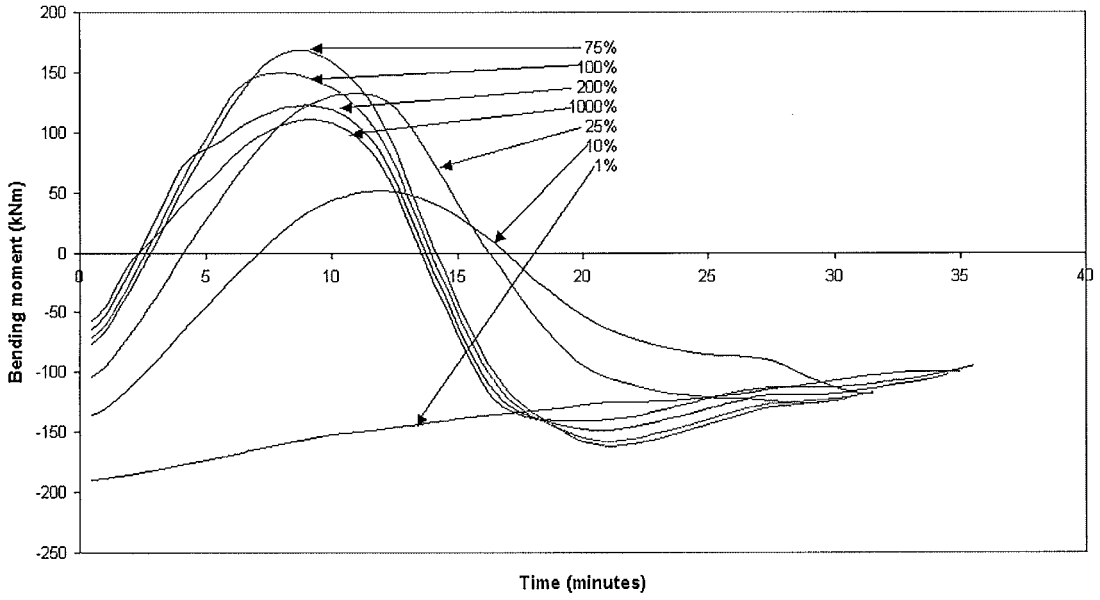

Figure 92) Beam midspan bending moments

Stresses in columns

The inner and outer column flanges, and locations within columns, as stated within this section are defined by paragraph 7.1.1, and Figure 84.

- *Bottom of column flange stresses*

It can be seen in Figure 93, and Figure 94, that the bottom of the column has very large stresses due to column bending moments from the expanding beam. As the inside flange of the column is in tension and the outside flange is in compression we can tell that the column is bowing out with the expanding beam. The flanges of the column bottom yield sooner for the stiffer columns that the less stiff columns. This is because the less stiff columns are able to deflect further in the elastic range before yield. The stiffer the columns, the less they are able to deflect elastically with column expansion, and hence the higher their bending moments and associated stresses.

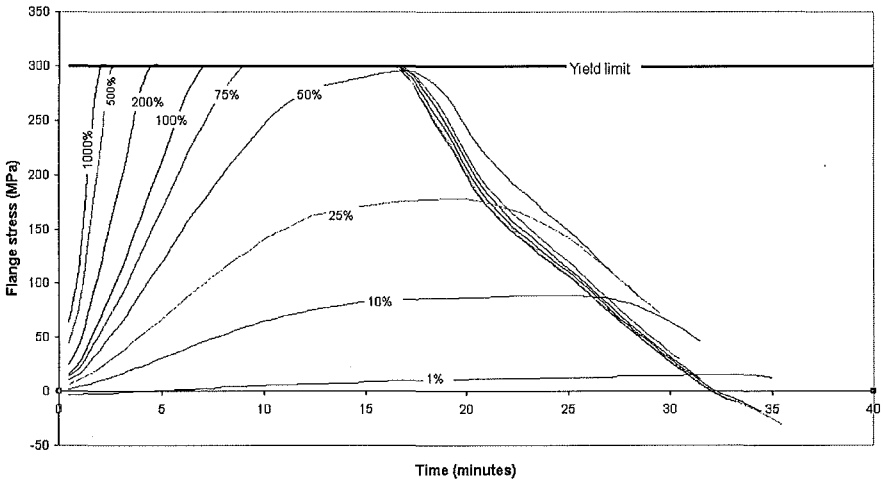

Figure 93) Bottom end of column; flange stress at inside of frame

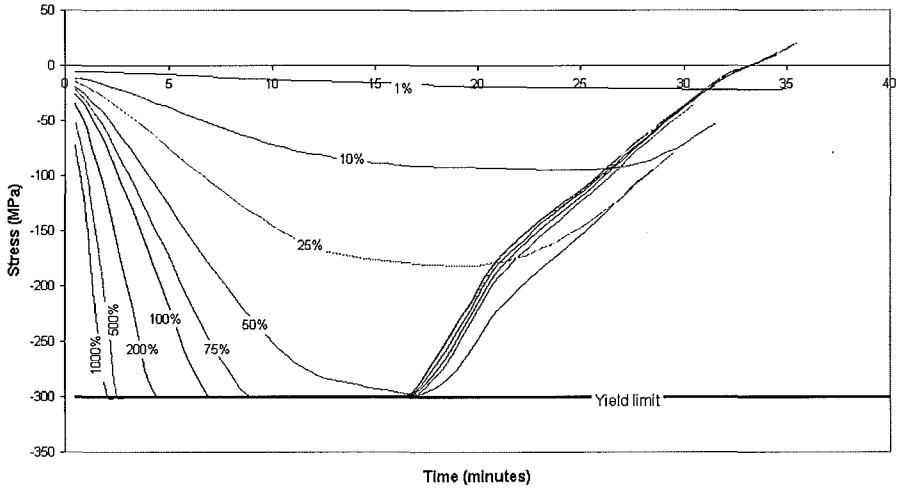

Figure 94) Bottom end of column; flange stress at outside of frame

- *Top of column flange stresses*

The Stresses of the top of the column's flanges (see Figure 95 and Figure 96) are similar to the stresses in the bottom of the column's flanges (see Figure 93, and Figure 94) with the main difference being that the bottom of the column is in higher compression from supporting the beam. Again it can be seen that the tension of the inside flange and the compression of the outside flange indicate that the column is bowing out with the expanding beam. Note also that the flanges of the top of the column yields sooner for the stiffer columns that the less stiff column as was the case of the column base due to thermal expansion of the beam.

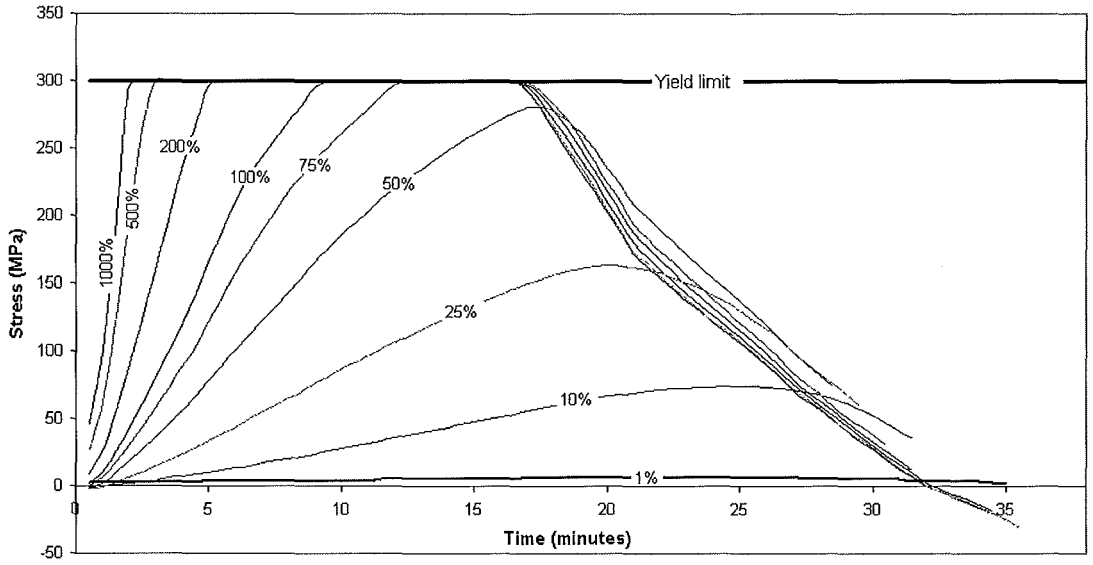

Figure 95) Top end of column; flange stress at inside of frame

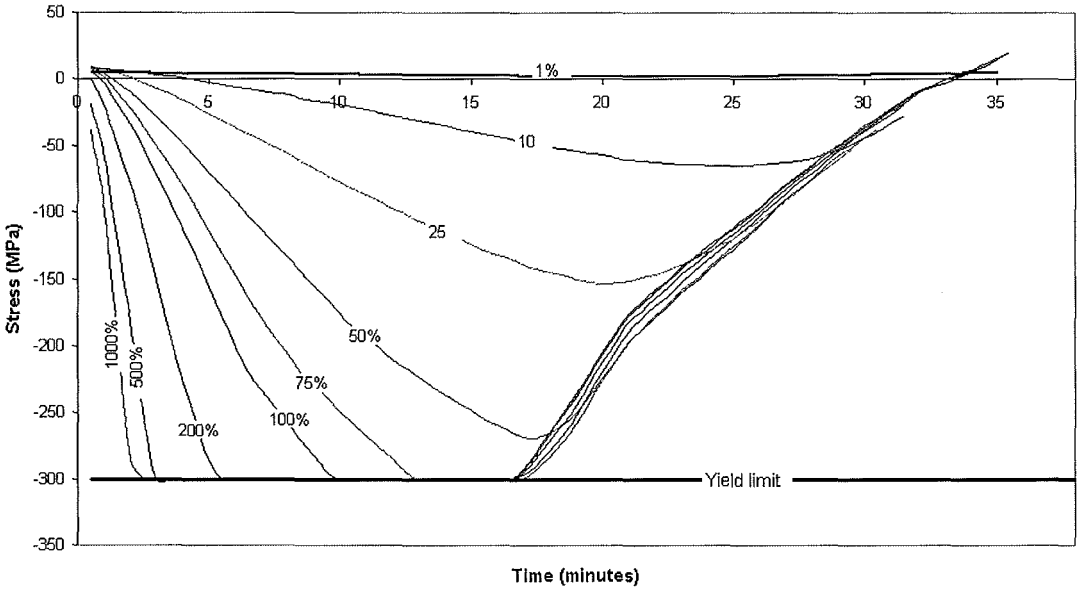

Figure 96) Top end of column; flange stress at outside of frame

- *Column stresses at the beam-column joint*

The stresses within the beam column joint, as shown in Figure 97, and Figure 98, also increase rapidly for the stiff columns, in the same way as did the top and bottom of the columns. These stresses do not reach yield however, as the stresses are relieved by the yielding at the column ends. The stresses increase again as the beam continues to expand, but then these stresses are rapidly decreased as yield occurs in the bottom flange of the beam.

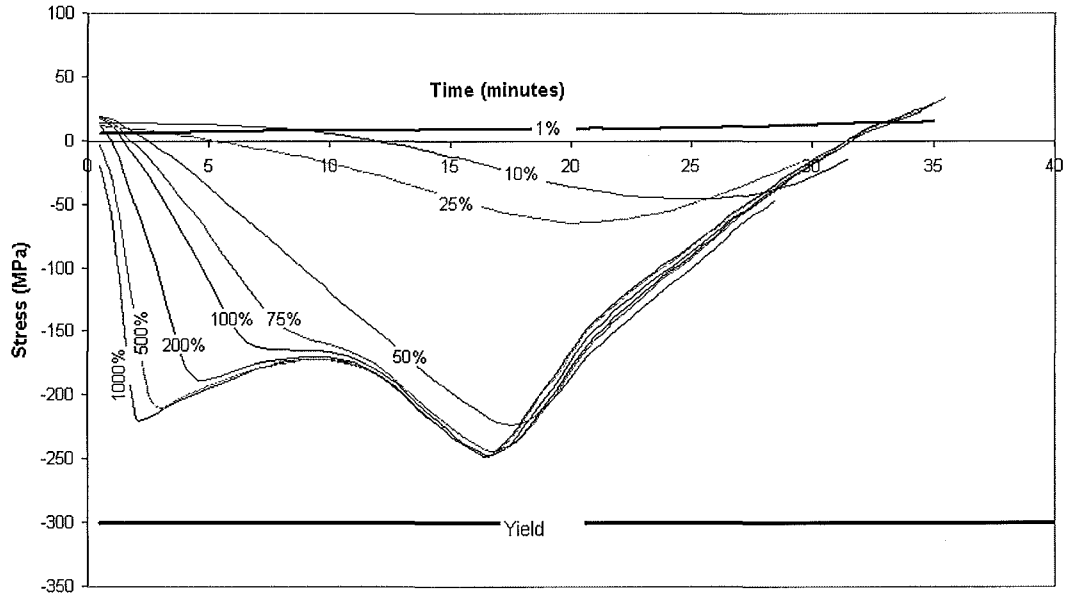

Figure 97) Inside flange stresses of column at the beam column joint

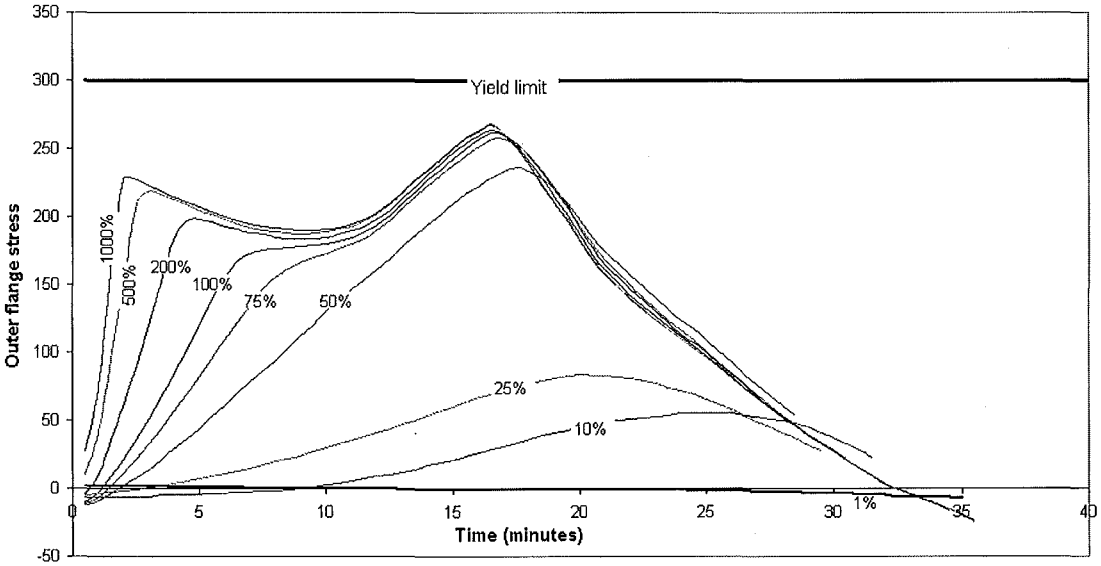

Figure 98) Outside flange stresses of column at the beam column joint

Stresses in beam

- *Beam flange stresses at the beam-column joint*

The beams connected to stiff columns initially increase in compressive stress within the bottom flange, and increase in tensile stress within the top flange at the beam column joints (see Figure 99, and Figure 100). This indicates that the beams with stiff columns have large induced moments resulting from the beam's thermal expansions. These compressive stresses of the bottom flanges are relieved by the yield at the top and bottom of the columns. As these compressive stresses again build up due to the continued beam expansion, some relief is found after reaching the proportional limit, but the stresses are notably reduced by the yield of the bottom flange. The beams connected to less stiff columns, by contrast, tend to carry loads by both the flanges in higher tension than the stiffer columns. This indicates that the bending moments of the beam with less stiff columns are more like the pin-pinned supported beam than the fully fixed beam. This is due to the relative ease with which rotation is able to occur at the beam-column joints.

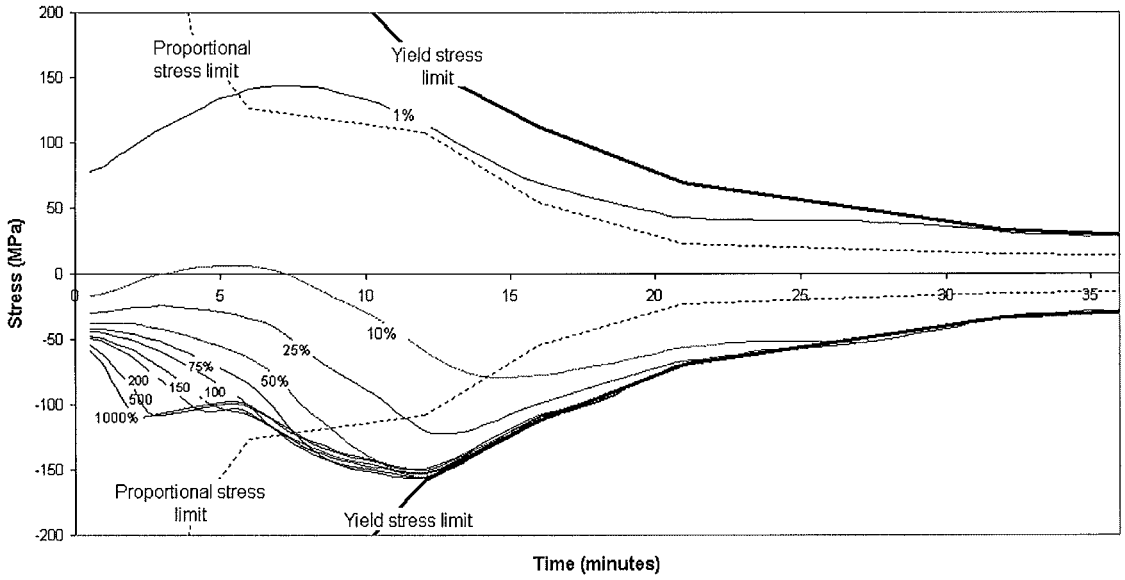

Figure 99) Beam bottom flange stresses at beam-column joint

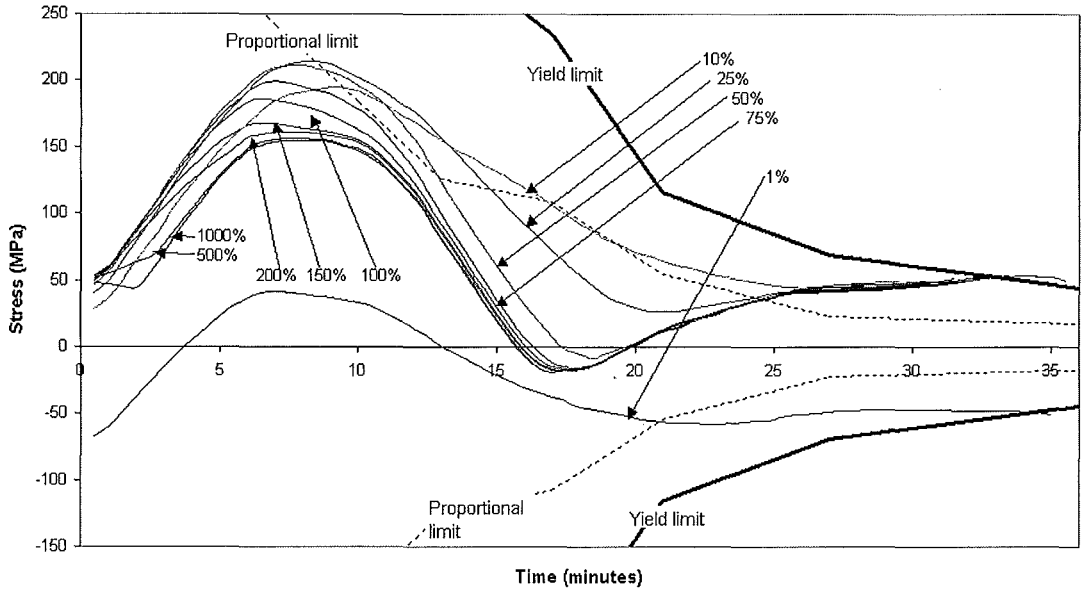

Figure 100) Beam top flange stresses at beam-column joint

- *Beam flange stresses at the midspan*

The bottom flange (Figure 101), from cold, starts out in tension and the top flange in compression (Figure 102) as is expected. The bottom flange increases in compressive stress as the beam's thermal expansions are initially restrained when the beams are connected to stiff columns. These compressive stresses are reduced when the columns yield at the top and bottom, and then again when yield occurs in the bottom flange of the beam at the beam-column joints. The failure of the frame finally occurs when the beam yields at the midspan.

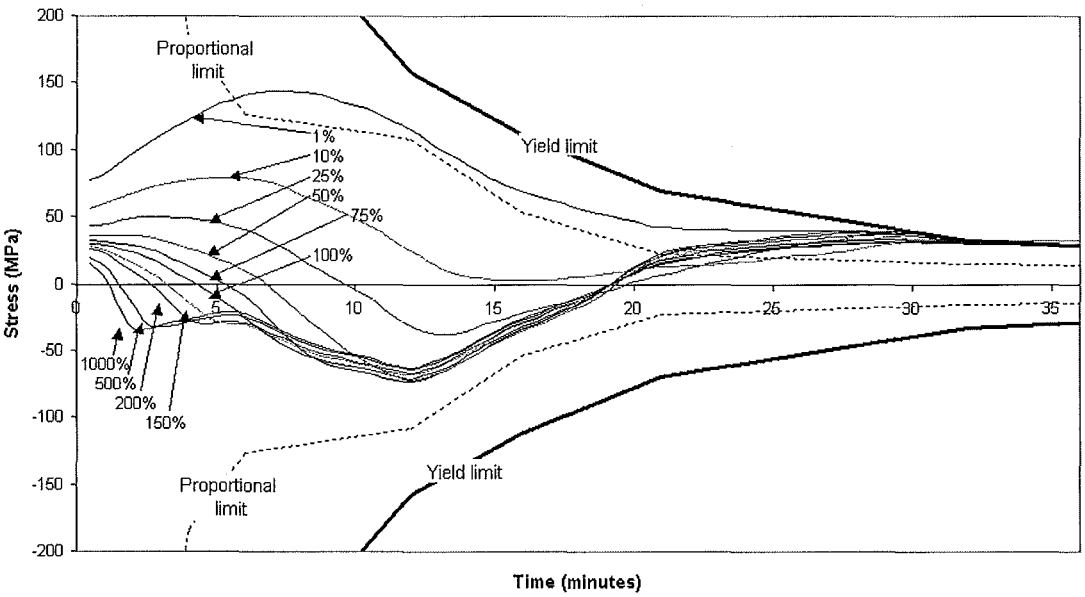

Figure 101) Beam bottom flange stresses at midspan

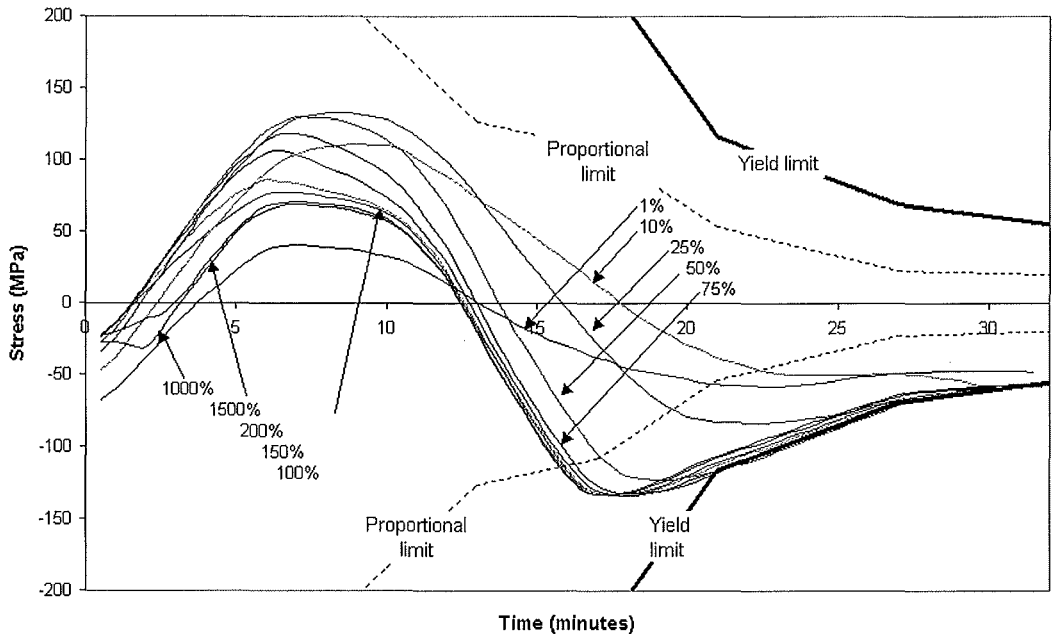

Figure 102) Beam top flange stress at midspan

7.3 Composite beam

This section considers frames with protected columns supporting the composite beam. The column stiffness will be varied, and quoted as a percentage of the steel beams stiffness (see section 7.1.1).

Beam axial force

Like the steel beam, axial forces within the unprotected composite beam vary quite markedly for frames with different column stiffness, as is shown by Figure 103. When the columns are stiffer than the beam, the axial force within the beam builds up very rapidly, reaching a peak compressive force. The peak of the initial compressive force becomes sharper as the column stiffness increases. This peak axial force is associated with yielding at the top and bottom of the columns. This gives more flexibility to the frame, allowing the beam to expand more freely as it is heated, relieving the axial strain.

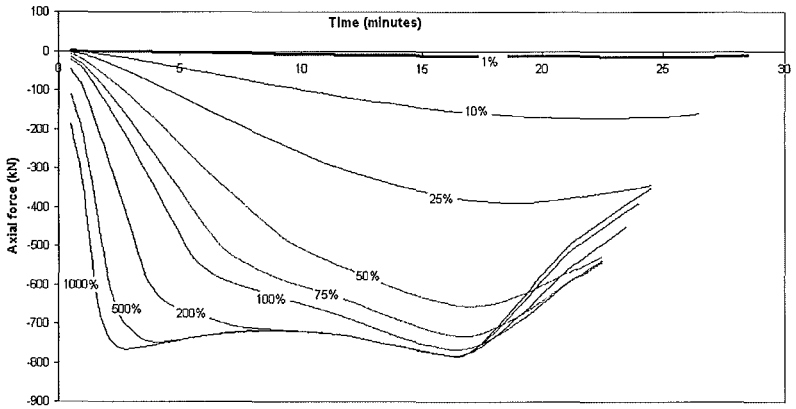

Figure 103) Axial within the composite beam with varied column stiffness

- *Axial force of frames with columns stiffer than beams*

After yield within the columns, the axial force within the beam remains relatively constant until about 17 minutes for the stiff columns (see Figure 103). At this time the axial force within the beam is reduced rapidly with the yielding of the bottom flange at either end of the beam. This is similar to the axial force reducing action that occurs within the fully fixed composite beam where the beam axial force is relieved by the bottom flange at either end of the beam reaching the proportional limit. This behaviour is also very similar to that noted for the steel beam with varied column stiffness, as documented within the previous section of this report.

- *Axial force of frames with beams stiffer than columns*

The axial force within the beam for very flexible columns, i.e. 1% of the beam stiffness, is very low throughout the duration (see Figure 103). This is because the beam is very free to expand and contract, as if the ends were supported with roller connections with very soft springs. This behaviour is similar to the steel beam with columns described within the previous section. This is trend is also documented by Welsh (2001) for the composite beam with very soft axial springs[2] on rollers but with the exception of duration before collapse. Welsh (2001) found that the very soft spring lasted for a time of up to 158 minutes, compared to 24 minutes as seen above for the same beam, but with columns. It should again be noted that Welsh (2001) was considering exposure to a fire with a slower linear heating rate, as opposed to the much faster ISO fire considered here.

Midspan displacement

The midspan displacement plots have been divided into two groups, as was done for the previous section. The first group are the frames with a beam stiffer than the columns, and the second, where the column is stiffer than the beam. The midspan deflections of both groups of composite beams with columns have been compared with the composite beam with pin-roller supports and with fully-fixed supports as analysed in chapter 6. As with the steel beam, these two groups appear to show behaviour distinct from each other, as is detailed in the following.

[2] Welsh (2001) looked at very soft axial springs with a spring stiffness within the range of 0 to 6

- *Beam stiffer than the column*

In the scenario of the beam stiffer than column the midspan deflections (see Figure 104) appeared to progressively converge upon the pin-roller scenario of section 6.5.2. Like the frame with a steel beam, the composite beam connected to columns with only 1% of the beam's stiffness initially resembles the pin-roller supported beam. It seems that the 1% column stiffness allows less rotational and axial restraint to the beam for the composite beam. This was also noted for the steel beam with 1% column stiffness. It is also clear from the plot that for the composite beam, even with a very modest amount of tensile axial restraint, as offered by the column with 1% of the beam's stiffness the beam can avoid an early run-away failure.

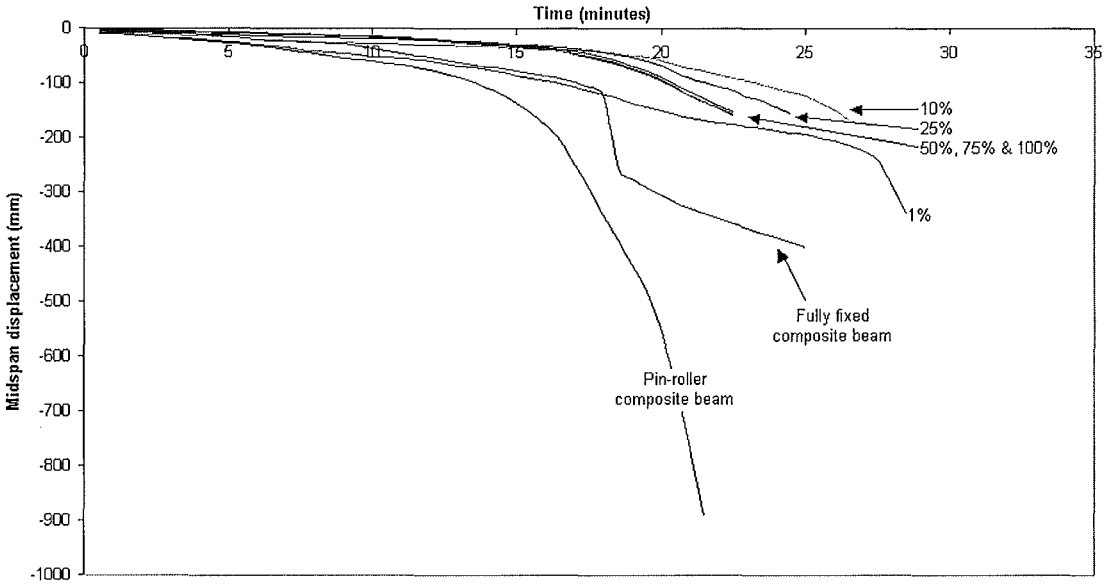

Figure 104) Composite frame midspan displacement; beams stiffer than columns

- *Column stiffer than the beam*

With the stiff columns of Figure 105, the midspan deflection compares well with the fully-fixed composite beam from section 6.2.2 only for the first 3 minutes. At this time the fully-fixed beam yields in the bottom flange at the supports. This does not occur with the frame scenarios, even with the very stiff columns. This is consistent with the finding for the steel beam with columns from the previous section. The main difference between the frames with a composite beam and with a steel beam was that with the composite beam plastic hinges formed at the beam-column joint within the columns as well as at the bottom and top. This can be accounted for by considering that the composite beam of this section is a lot stiffer than the steel beam from the previous section. This increased axial stiffness of the beam, relative to the columns, means less flexure is possible within the beam. Hence when the stiff columns will not deflect to allow for the expanding beam, three plastic hinges form within each column, rather than just the two as occurred in steel beam frame.

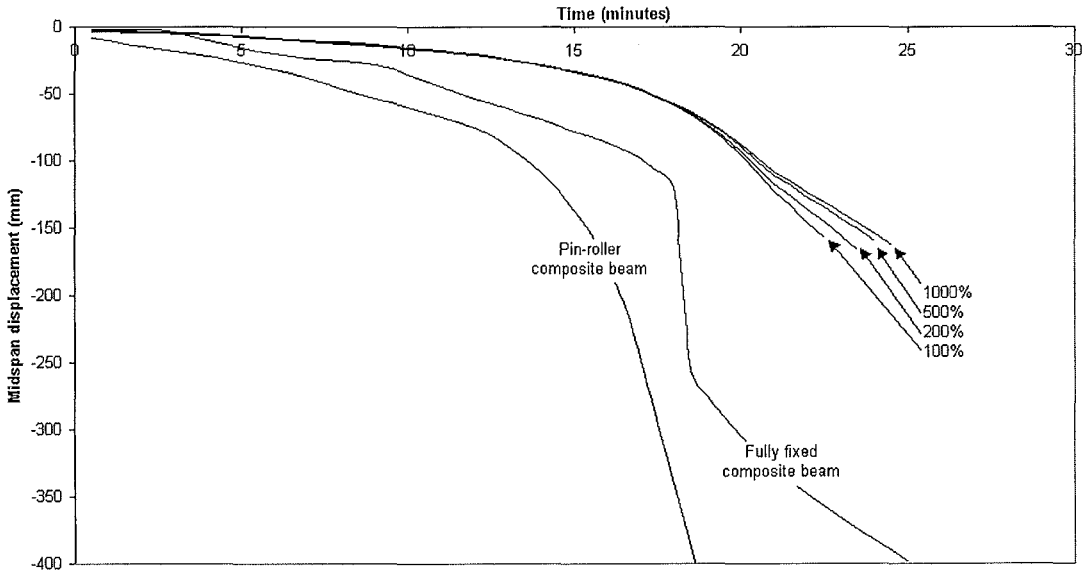

Figure 105) Composite frame midspan displacement; columns stiffer than beams

- *Comparison with the fully fixed beam*

Even with the very stiff columns it was found that the midspan displacement did not closely approach the behaviour of the fully-fixed composite beam in Figure 105. This was also the case for the steel beam from the previous section. As done previously for the steel beam with columns, the end rotations and displacements from the framed composite beam were each imposed separately on the beam without columns (see Figure 106). The reason for this was to check the consistency of the models, and to confirm whether it is the horizontal or the rotational movement at the beam-column joints that cause this result.

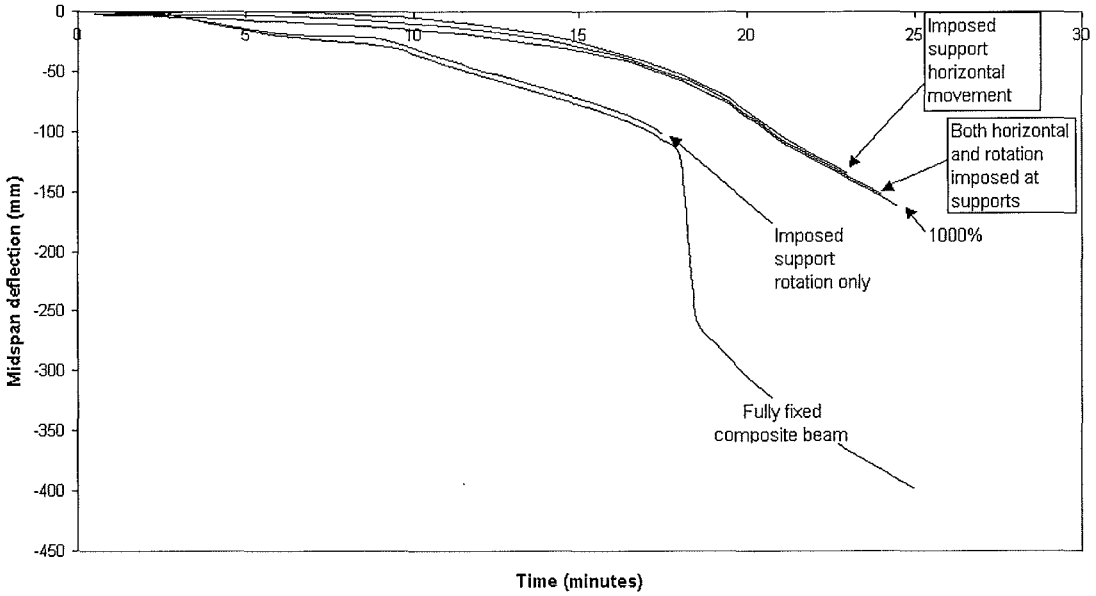

Figure 106) Comparison of 1000% column stiffness with fully fixed beam

Again, as was the case for the steel beam with columns, it was found that the horizontal movement at the beam-column joints seems to contribute the most to easing of beam axial compression, thereby reducing midspan deflections. Unlike the frame analysis for the steel beam of the previous section, the composite beam with imposed column rotation the midspan deflection is slightly less than the fully-fixed beam.

Horizontal deflection at the beam column joint

The trends observed for the horizontal movement at the beam column joint can be divided into two main categories. First, where the beam is stiffer than the column, and second, where the columns are stiffer than the beam.

- *Beam stiffer than the column*

In Figure 107 the pinned-roller's horizontal displacement is divided by 2. This is to allow for the fact that the pinned-roller supported beam is only able to expand axially at one end, compared with both ends of the beam supported within a frame. As the column stiffness drops, the beam column joint's movement becomes more similar to the movement noted for the pinned roller support of the same beam.

The reason that the weak columned frames behave similarly to the pinned-roller supported beam is because as the column stiffness is reduced more rotation and horizontal movement is possible at the ends of the beam. As previously observed with the steel beam with columns, the frame does not experience the same run-away failure as the pinned roller. This is because the columns are able to offer some horizontal resistance to the retracting beam.

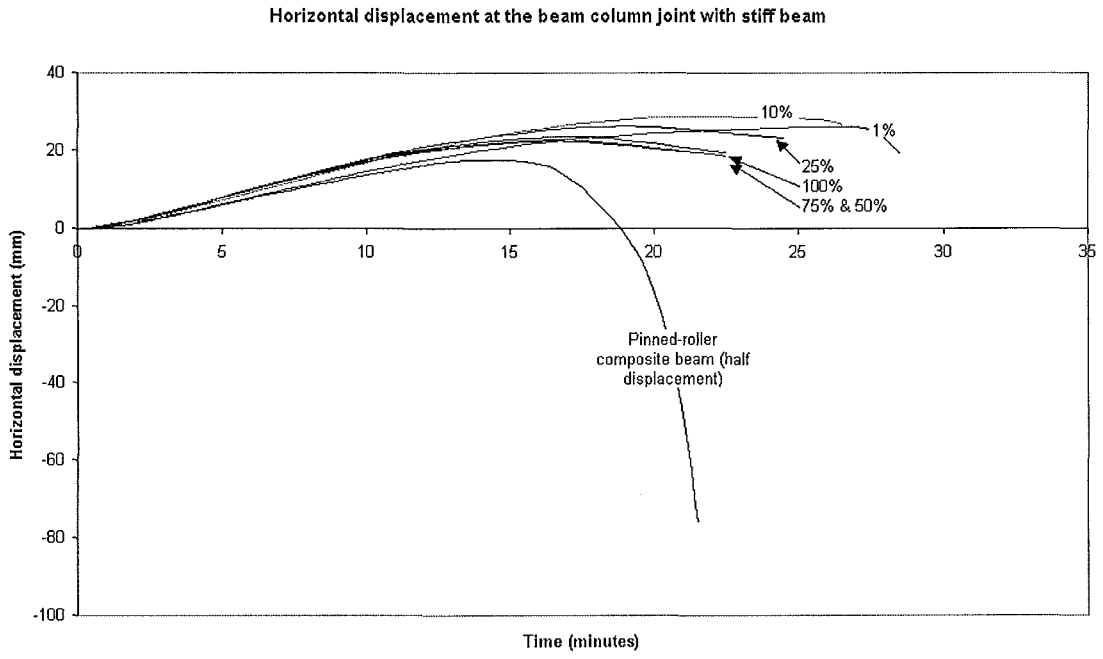

Figure 107) Horizontal displacement at the beam column joint with the beam stiffer than the columns

- *Columns stiffer than the beam*

The behaviour of the composite beams was found to be similar to that of the steel beams from the proceeding section when the columns are stiffer than the beam (see Figure 108). As the column stiffness is increased beyond 75% there is very little noticeable variation in the beam column joint horizontal displacement for the first 17 minutes. The stiffest beam analysed does not compare well with the fully fixed beam, which will not have any horizontal displacement at all. As was shown for the scenario of the frame with the steel beam in the previous section, this indicates that even with very stiff columns the axial force imposed by the expanding beam is likely to cause some support movement with columns.

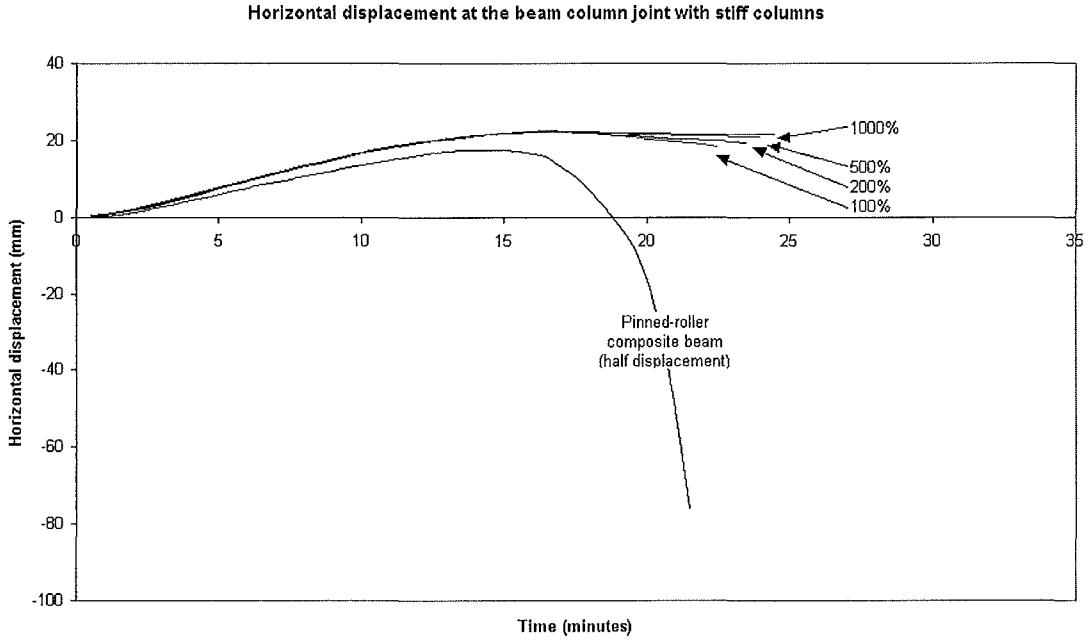

Figure 108) Horizontal displacement at the beam column joint with stiff columns for composite beamed frame

Bending moments

The composite beam showed the same trends for the beam end (Figure 110) and midspan (Figure 109) bending moments as did the steel beam. Throughout the fire duration it is noticeable that the ratio of the magnitude of bending moments at the supports compared with the midspan are typically of the order of 2:1. This is similar to what is observed for the fully-fixed beam, and is what is expected of fixed frame bending moments at cold conditions. As the beam is heated the bending moments at the beam column joints increase due to the P-δ effects of the beam's axial force. The midspan bending moments also change, maintaining the support to midspan beam bending moment of 2:1. After the bottom flange yields at the beam column joints, this axial force is substantially reduced, and the bending moments drop accordingly at both the ends and the midspan of the beam. The beam-column joint bending moments of the beam with 1% column stiffness is very small throughout the fire's duration. This is because the columns are so flexible that sufficient rotation at the supports occurs that the beam behaves similarly to the pin-pinned beam. The bending moments of the beam with 1% column stiffness also lacks the distinctive peak of the stiffer columned frames. This is because the columns deflect before large axial forces build-up within the beam. The bottom flange at the beam column joint does not yield in compression as occurs in the frames with stiffer columns because of the lower axial forces.

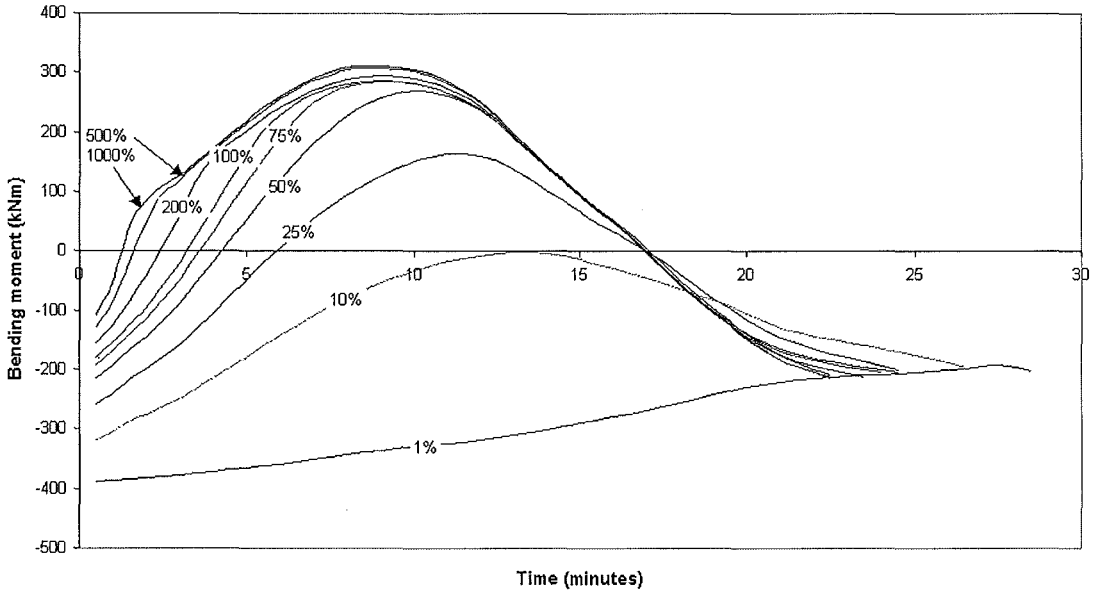

Figure 109) Midspan moments of the composite beam with varied column stiffness

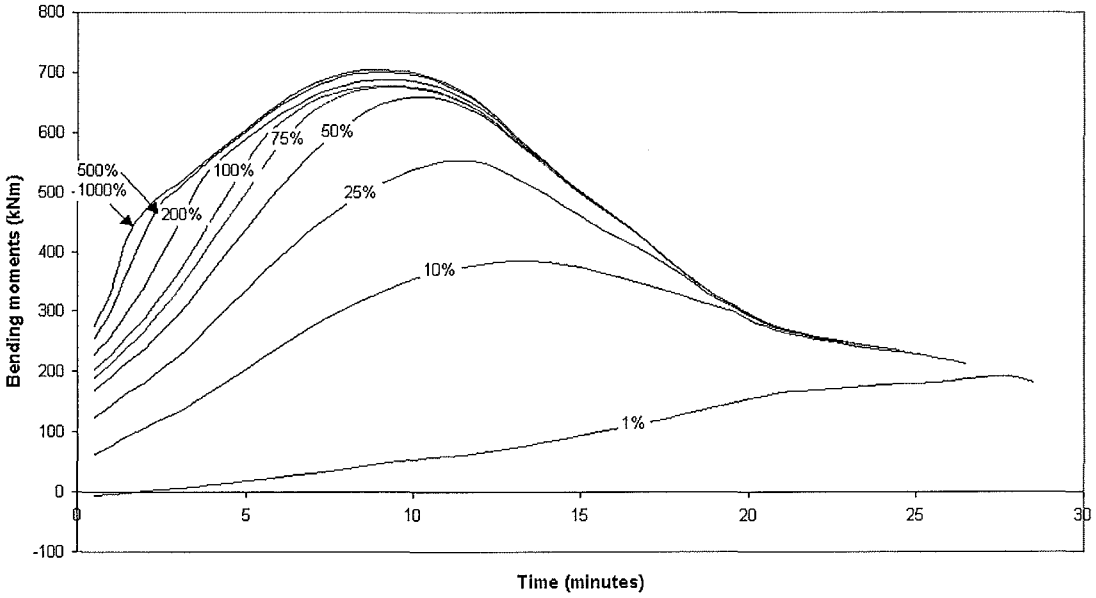

Figure 110) Beam end moments of the composite beam with varied column stiffness

Column stresses

The inner and outer column flanges, and locations within columns, as stated within this section are defined by paragraph 7.1.1, and Figure 84.

- *Bottom of columns*

It can be seen that the bottom of the columns of Figure 111, and Figure 112, have very large stresses due to the column bending moments resulting from the expanding beam. Because the inside flanges of the columns are in tension, and the outside flanges are in compression we can tell that the columns are bowing out as the beam expands. The flanges at the bottom of the columns both yield sooner for the stiffer columns than for the less stiff columns. This is because the less stiff columns are able to deflect, rather than resist the beam expansion with bending moments. The stiffer the columns, the less they are able to deflect with column expansion, and hence the higher their bending moments and associated stresses. This is also consistent with what was observed for the frames with steel columns from the previous section.

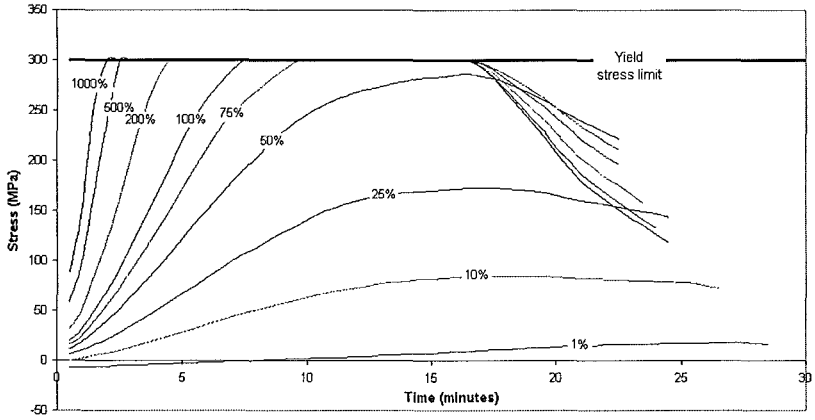

Figure 111) Stresses in inner flange at the bottom of columns

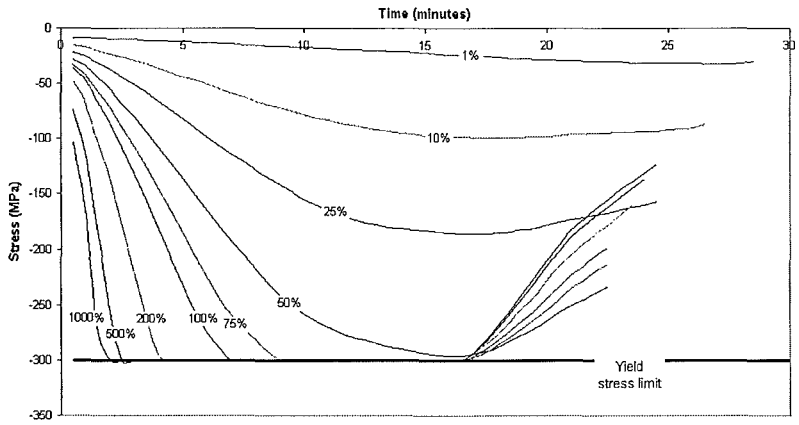

Figure 112) Stresses in outer flange at the bottom of columns

- *Top of column flange stresses*

The stresses at the top of the columns' flanges (Figure 113, and Figure 114) are similar to the stresses in the bottom of the columns' flanges. Again it can be seen that the tension of the inside flange, and the compression of the outside flange indicate that the columns are bowing out with the expanding beam. Note also that the flanges of the top of the columns yield sooner for the stiffer columns than for the less stiff columns, as was the case of the column base due to thermal expansion of the beam. This is consistent with what was observed for the frames with steel columns from the previous section.

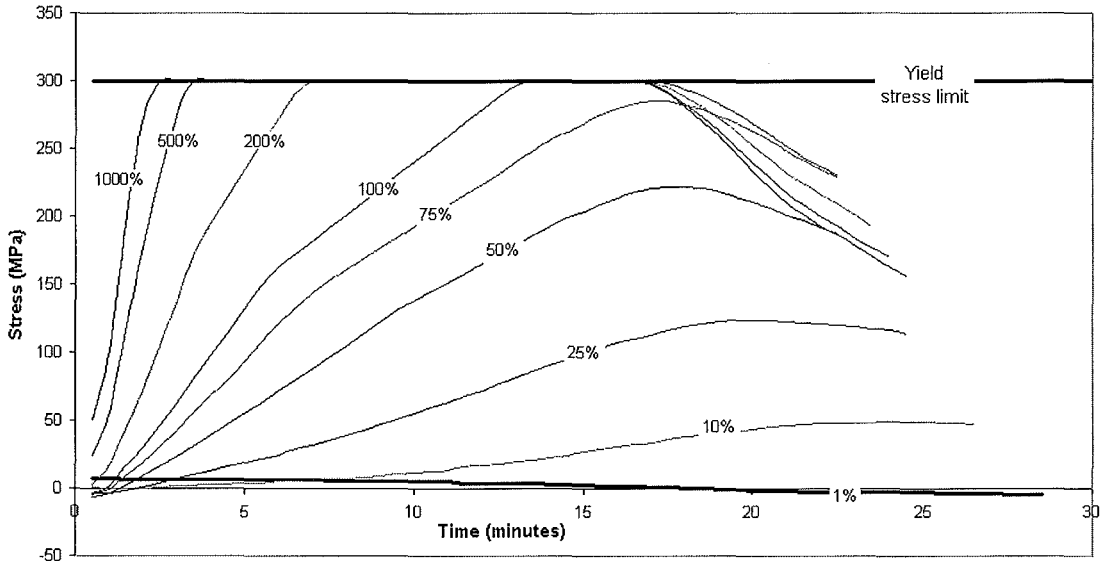

Figure 113) Stresses in inner flange at the top of columns

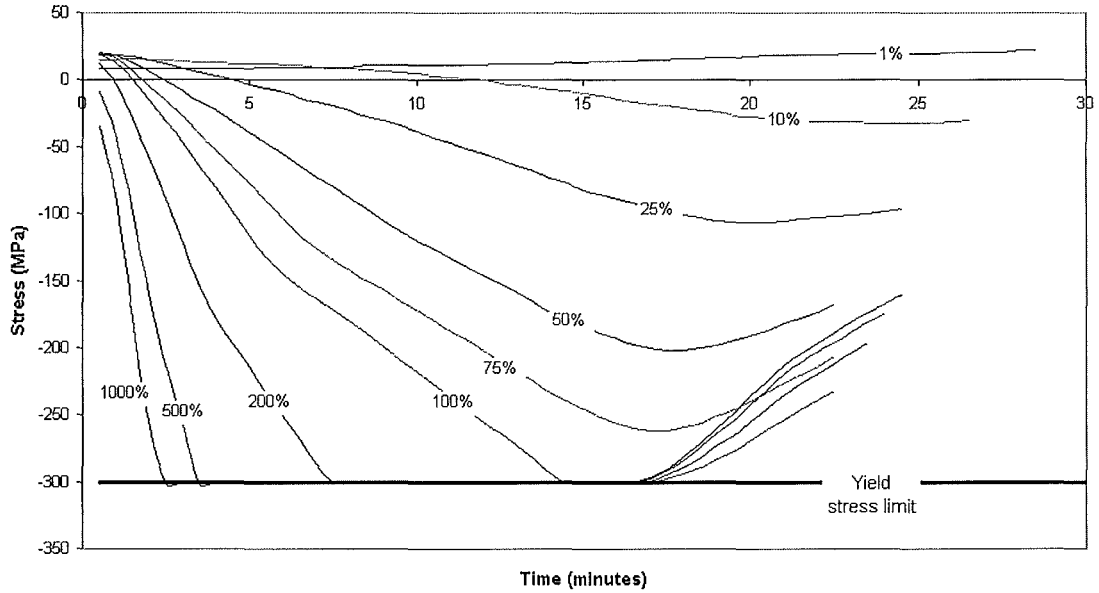

Figure 114) Stresses in outer flange at the top of columns

- *Beam-column joints*

Unlike the previous analysis of frames with steel beams, the stresses at the beam-column joints of the composite beam do reach yield (see Figure 115, and Figure 116). This is because the composite beam has a greater thermal bowing effect, which induces greater moments at the ends of the beams. The greater thermal bowing effects result from the differential heat of the top and bottom of the section due to the heat sink effects of the slab.

The inner flange stresses of the columns, measured just below the beam column joint, is in compression, while the outer flange is in tension. This behaviour is predictable, as the generated moment will resist the hogging moment at the end of the beam.

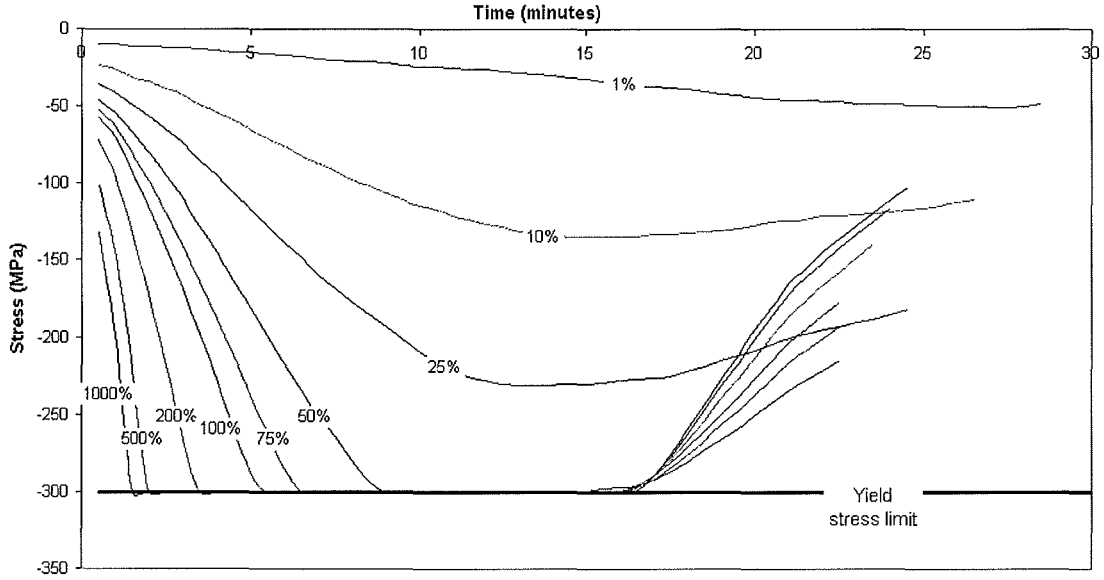

Figure 115) Stresses in inner flange at the beam column joint, within columns

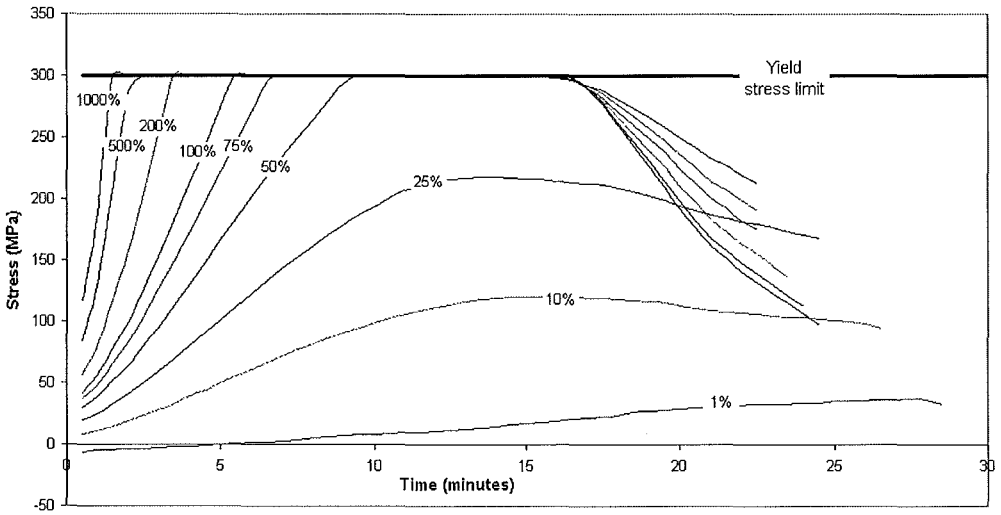

Figure 116) Stresses in outer flange at the beam column joint, within columns

Stresses within the composite beam at the beam column joint

- *Steel beam flange stresses at the beam column joint*

The beams connected to stiff columns increase in compression in the bottom flange (Figure 117) and tension in the top flange (Figure 118) initially at the beam column joints. This indicates that the beams with stiff columns have large induced moments resulting from the beam's thermal expansions. The compressive stresses of the bottom flange is relieved by the yield at the top, bottom, and the beam-column joint within the columns. As these compressive stresses again build up due to the continued beam expansion, some relief is found after reaching the proportional limit, but the stresses are most notably reduced by the yield of the bottom flange. The beams connected to less stiff columns, by contrast, tend to have both the top and bottom flanges in higher tension than was the case for the stiffer columns. This indicates that the bending moment within the composite beam with less stiff columns is more like the pin-pinned supported beam than the fully fixed beam. This is due to the relative ease that rotation occurs at the columns.

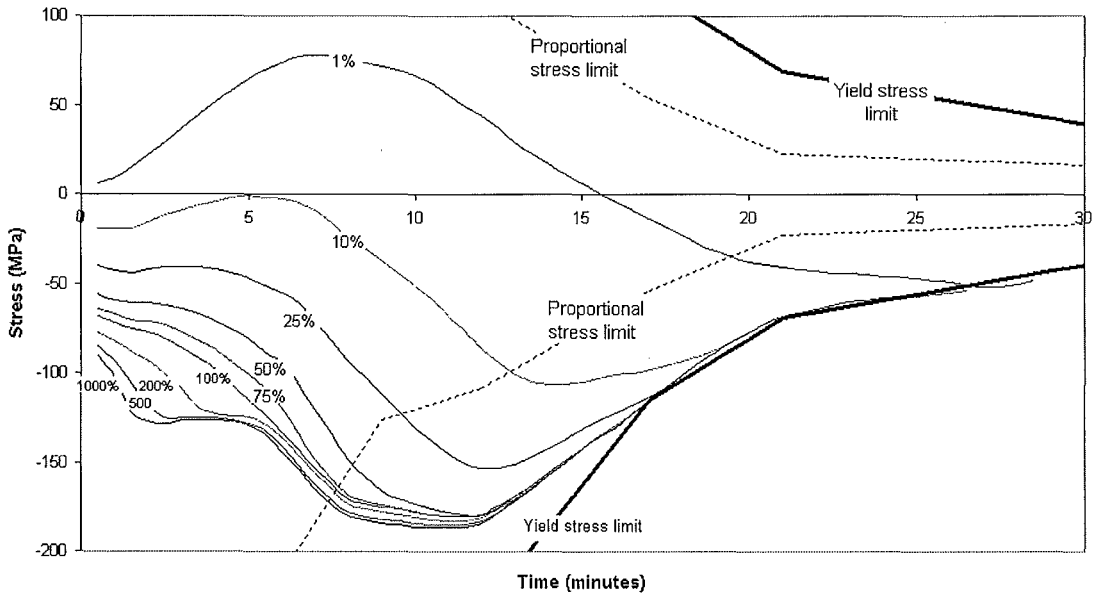

Figure 117) Beam bottom flange stress at beam column joint

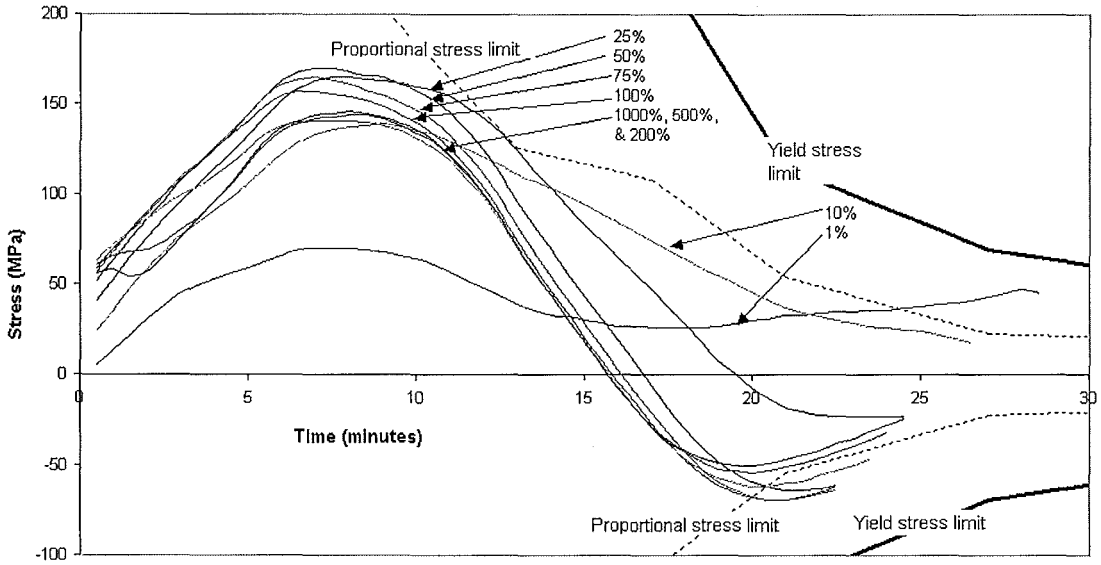

Figure 118) Beam top flange stress at beam column joint

- Mesh stresses at the beam-column joint

As the hogging moments increase at the beam-column joint, the top of the beam increases in tensile stresses. As can be seen in Figure 119, the steel mesh of the profiled slab reaches tensile yield within 6 minutes. The mesh remains at this yield stress for the rest of the fire's duration.

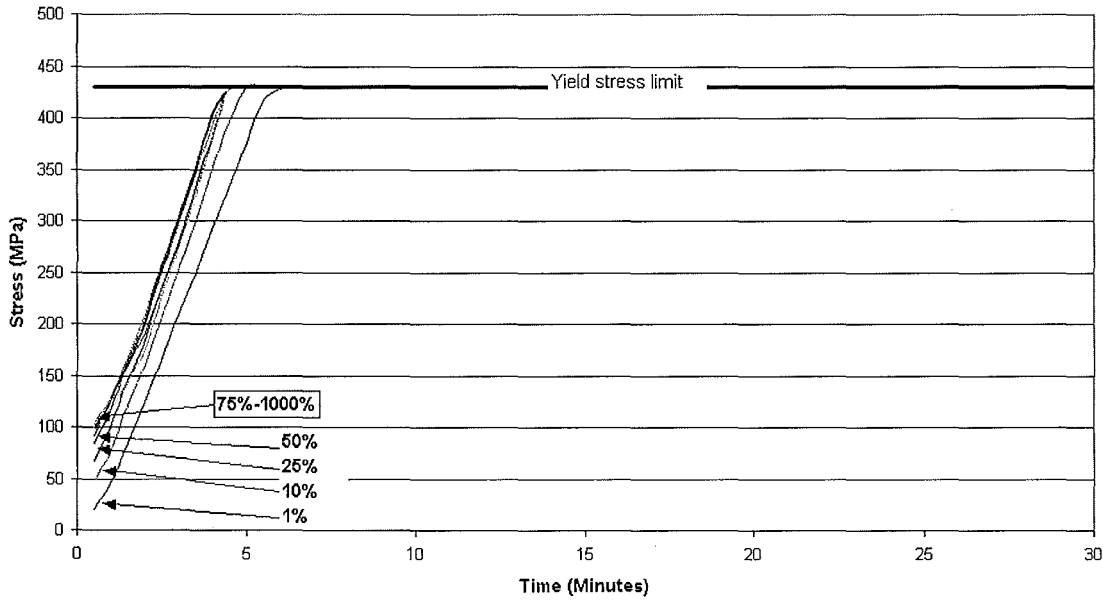

Figure 119) Composite beam's mesh stresses at beam-column joint

- Stresses within the concrete slab at the beam column joint

The slab is exposed to tensile stresses from hogging at time = 0, hence the concrete cracks. The concrete has no role in load carrying at the supports due to the hogging moments.

Stresses within the composite beam at the midspan

- Beam flange stresses at the midspan

The bottom flange (Figure 120) from cold, starts out in tension, and the top flange (Figure 121) in compression as is expected. The bottom flange increases in compression as it's thermal expansions are initially restrained by the stiff columns. These compressive stresses are reduced when the columns yield at the top and bottom, and then again when the web of the beam at the beam-column joints reaches the compressive proportional limit.

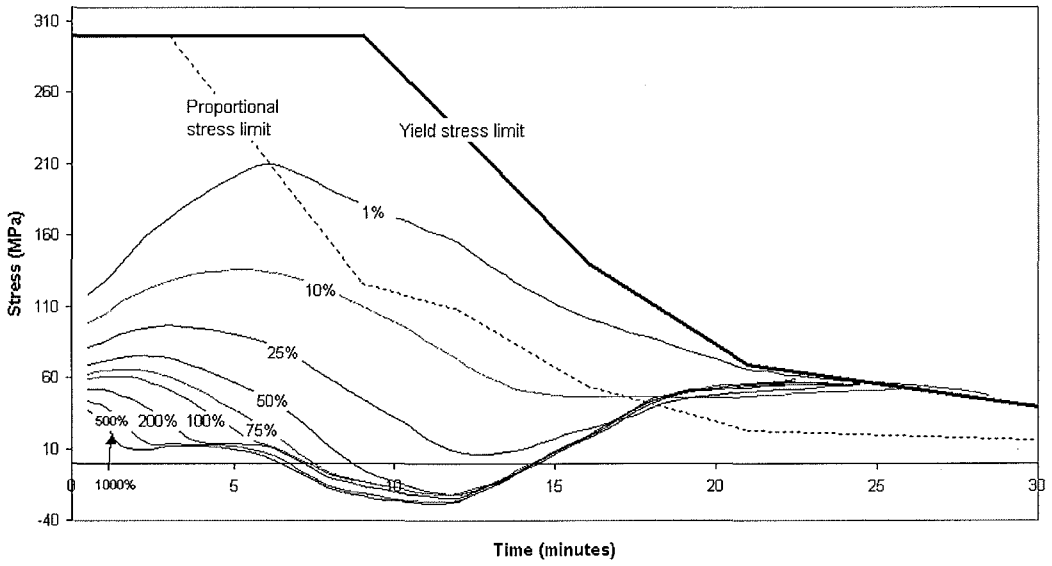

Figure 120) Bottom flange stresses at the midspan

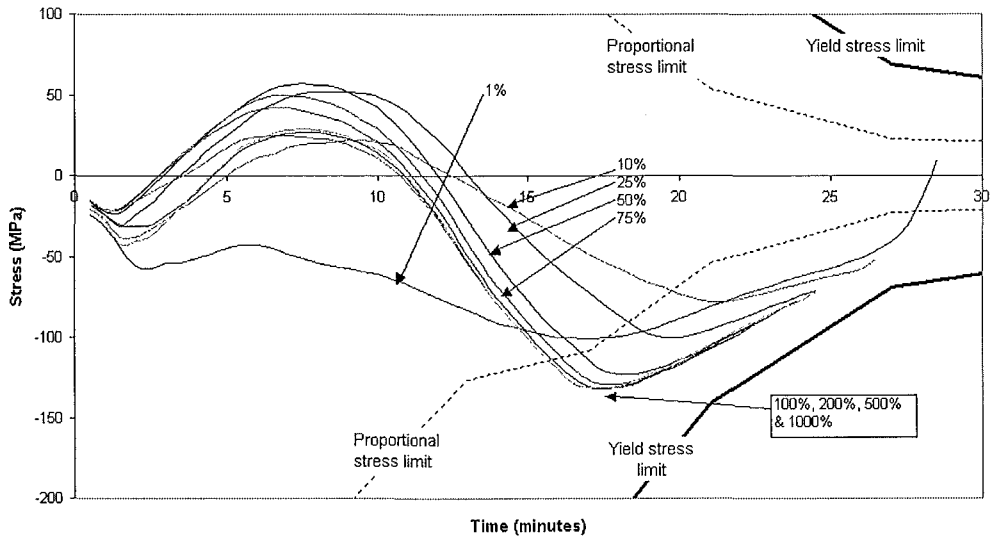

Figure 121) Top flange stresses within beam at the midspan

- Mesh stresses at the beam midspan

The midspan mesh is initially in compression before the fire as seen in Figure 122. This is expected for a sagging moment within the slab, which is at the top of the beam's cross-section. The mesh quickly increases in tensile stresses due to thermal bowing effects. When the bottom flange of the beam yields at the beam-column joint, the beam loses stiffness, and the midspan deflections increase. This drives the mesh at the midspan back into compression.

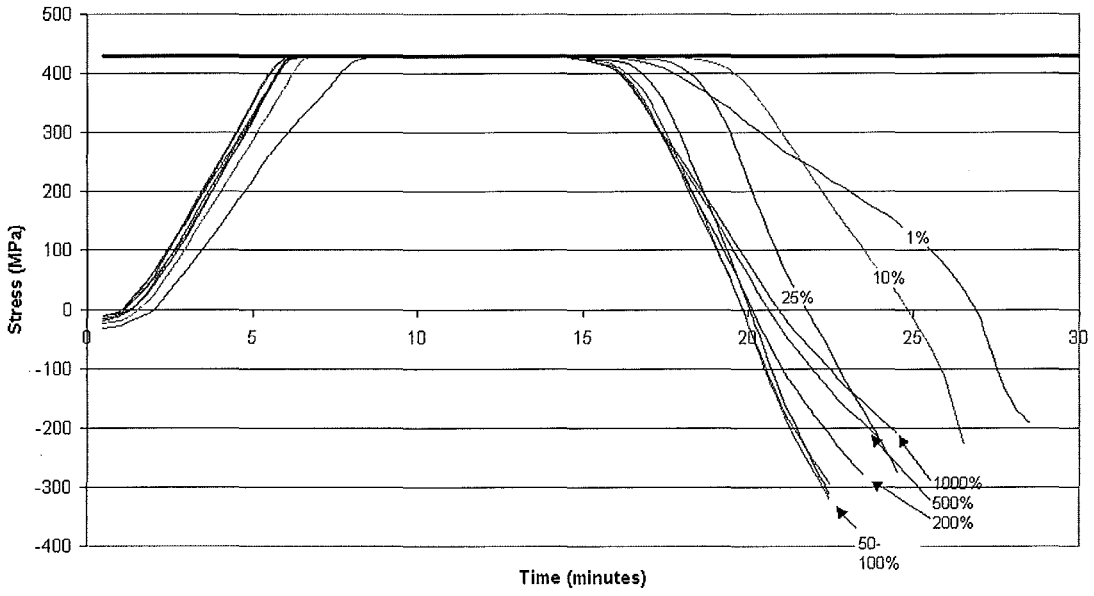

Figure 122) Mesh stresses at the beam midspan

- Slab stresses at the midspan

The slab, as shown in Figure 123, and Figure 124 initially starts out in compression with the midspan sagging moments in the same manner as the midspan mesh. As the thermal bowing effects increase the slab stresses drop to zero. This is because the concrete slab is unable to have tensile stresses. When the beam loses stiffness with the yield of the bottom flange at the beam-column joint the slab is driven into compression again. The stresses within the top and bottom of the slab are very similar, with the main difference being that the top of the slab has slightly higher compressive stresses. This is expected because the top of the slab is further from the beams neutral axis.

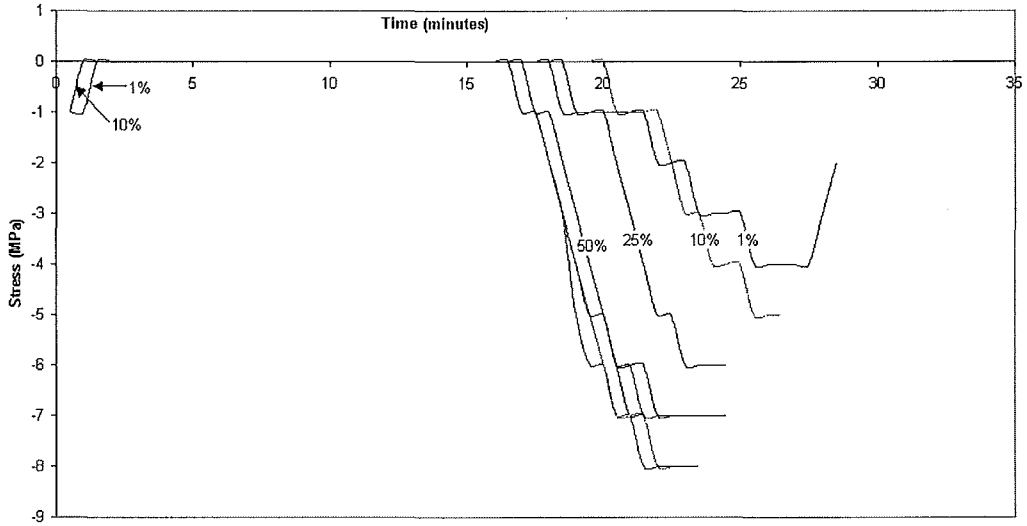

Figure 123) Bottom of slab stresses at the beam midspan

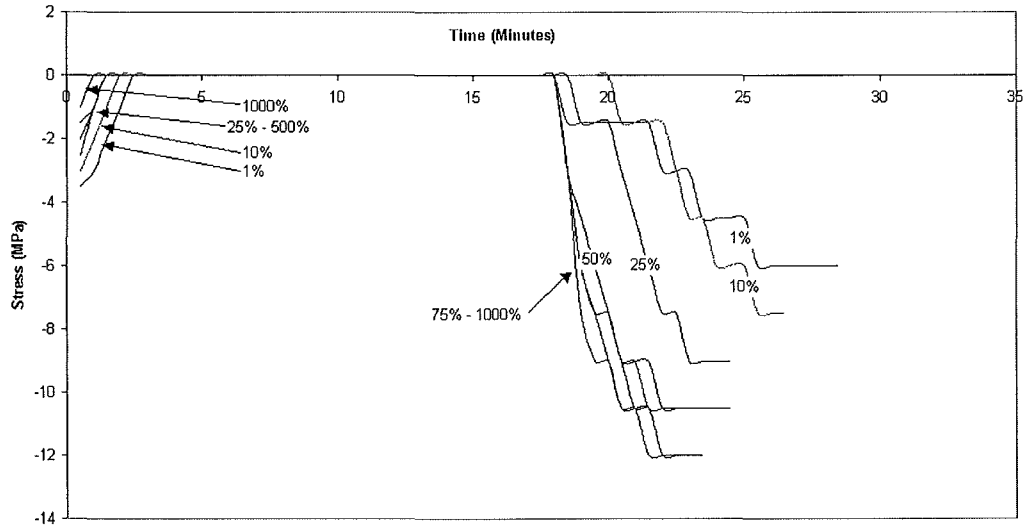

Figure 124) Top of slab stresses at the beam midspan

7.4 Discussion of frame action

The behaviour of the composite beam, and the steel beam were both significantly modified by the addition of columns compared to the idealised connections of chapter 6. The midspan deflection behaviour of the beams with frame effects can broadly be explained by dividing them into two main categories. The first is the category where the columns are stiffer than the beam, and second where the beam is stiffer than the columns. Both frame categories had a very low midspan deflection during the early stages of the fire. The midspan deflections were approximately linear with time during these initial stages. This compares well with the findings of the real fire single beam test of the Cardington fires (Clifton: 2001) where a single beam connected to protected columns was exposed to the ISO fire. This test is discussed in section 2.2 of this report.

7.4.1 Stiff columns

When the columns are very stiff, we would expect the behaviour of both the steel beam and the composite beam to approach that of the fully-fixed beam analysed in section 6.1. However, even with the stiffest columns considered, i.e. 1000% of the beam stiffness, the behaviour was found to be quite different. The fully-fixed beam's midspan deflections increase rapidly very early in the fire due to the bottom flange at the supports reaching the proportional limit. The stresses at the supports build up rapidly in the case of the fully-fixed beam as the fixed supports do not allow any axial expansion of the beam. The same beam with frame effects, by contrast, has varying degrees of flexibility permitted at the beam-column joint. Even when the column is very stiff, i.e. 1000% of the beam stiffness, the horizontal movement allowed at the support significantly reduces stresses within the beam. The frame instead develops large bending moments within the columns. The column bending moments result in plastic hinges forming at the columns top and base which allows more flexibility in the frame as the beam expands. The midspan deflections remain very low until yield occurs at the beam-column joint. The result is much reduced midspan deflection of the beam with frame effects over the beam with fully-fixed connections for most of the fire's duration.

7.4.2 Flexible columns

The frames with flexible columns behaved differently. With flexible columns; column deflection, rather than column bending moments accommodated the expansion of the beam. With very flexible columns, i.e. 1% of the beam stiffness, the beam-column joint of both the steel beam and the composite beam allowed significant rotation and horizontal movement at the beam ends. So, for the early stages of the fire, the frame behaved in similar manner to the pin-roller supported beam of section 6.4.2. However, in the later stages of the fire, after a plastic hinge had formed at the beam midpan, the behaviour of the frame and the pin-roller supported beam are again different. This differences is due to the columns allowing enough horizontal resistance to the beam to avoid the same run-away failure that was noted for the pin-roller supported beam in section 6.4.2.

7.4.3 Mechanisms of failure

The observed mechanisms of failure can be differentiated for frames according to the column stiffness.

7.4.3.1 Stiff columns

When the columns were stiffer than the beam, for the frames analysed exposed to the ISO fire, different collapse mechanisms for the composite and the steel beam were observed. Both had a variation of the frame mechanism as described in section 5.3.2.2. The plastic hinges that formed at the beam-column joint formed in the column for the frame with composite beams, and in the beam for the frame with steel beams. The order of plastic hinge formation for the frame with both the composite beam and the steel beam was:

- Top and bottom of both columns simultaneously
- Beam column joint, within the beam for the steel beam, and within the column for the composite beam
- At the beam's midspan

This completes the frame mechanism described in section 5.3.2.2.

7.4.3.2 Flexible columns

When the columns were more flexible, the columns were able to deflect elastically, hence they never yielded for the frame with either the composite, or the steel beam. The mechanism of failure for the frames with flexible columns was therefore the beam mechanism described in section 5.3.2.2. As the column stiffness decreased, for both the composite, and the steel beam, the bending moment increasingly resembled the bending moment expected for a simply supported beam. Hence, as the column stiffness decreased, the bottom flange at the supports increased in tension. The order of plastic hinge formation for the frame with both the composite beam and the steel beam was:

- Beam column joint, within the beam.
- At the beam's midspan.

This completes the beam mechanism described in section 5.3.2.2.

8 Conclusions

8.1 Introduction

This report set out to investigate the behaviour of unprotected structural steel members exposed to fire. The finite element software SAFIR has been used to model both a steel beam, and a composite beam exposed to the ISO fire. Firstly; the pin-pinned, fully-fixed, fixed slide, and pin-roller theoretically idealised connections were considered. Comparisons are made to earlier analyses by Welsh (2001) and Seputro (2001) where the same beams with idealised connections were exposed to fires with slower heating rates. Finally the composite beam, and the steel beam were exposed to the ISO fire when connected to columns of varied stiffness in a moment resisting frame. The columns in this analysis are treated as being fully protected, and therefore remain at ambient temperatures.

8.2 Idealised connections

The two beams with idealised connections exposed to the ISO fire behaved similarly to that determined by Welsh (2001) and Seputro (2001) for exposure to a fire with a slower linear heating rate. This section highlights these similarities and observed differences.

8.2.1 Failure mechanisms

As found by Welsh (2001) and Seputro (2001) the failure mechanisms for the idealised beam connections were as follows:

- Pin-pinned beam: a single plastic hinge at the midspan
- Fully-fixed beam: a plastic hinge forms at either end and the midspan
- Pin-roller: a single plastic hinge at the midspan
- Fixed-slide: a plastic hinge forms at either end and the midspan

It was also found that when the EC3 Proportional and EC3 Yield Limit stresses were reached in the steel section, displacements, axial force and bending moments along the section were affected.

8.2.2 Differences in behaviour due to rate of heating

The main differences noticed between the beams exposed to the ISO fire from this report, and the slower linear heating rate by Welsh (2001) and Seputro (2001) were due to the rate of heating. These differences were as follows:

8.2.2.1 Reduced duration of catenary action

The pin-pinned steel beam heated very quickly when exposed to the ISO fire, and did not last significantly longer than the fully-fixed steel beam. Suptro (2001) found this same beam lasted considerably longer with pinned supports than fixed supports due to catenary action after enough plastic hinges had resulted to form a mechanism. A less significant duration of catenary action was possible with the steel beam exposed to the ISO fire because the steel heated so rapidly that very little tensile strength was available for catenary action. This effect was less significant for the composite beam due to the heat sink effect of the concrete slab.

8.2.2.2 Sequence of plastic hinge formation

The sequence of plastic hinge formation was related to the rate of the beam's heating during the fire. It was found that both the composite and steel beams with fixed supports formed plastic hinges at the midspan before the supports when exposed to the ISO fire. In contrast, for slow heating, the first plastic hinges formed at the supports, then the midspan (Welsh, 2001) (Seputro, 2001). Because of the high axial compressive stress within the restrained beams, the compression zone yields in the beam before tension zone. The formation of plastic hinges are determined by the tensile yielding of the beam. This explains why the first plastic hinge when exposed to the ISO fire is due to yield in tension at the midspan bottom flange, where the yield limit is lower due to the thermal degradation at the bottom flange being faster than at the top flange. The second plastic hinge forms with the tensile yielding of top flange at the supports, where the yield limit is higher.

8.3 Frame effects

The steel and composite beams, as used for the idealised connection scenarios, were made into frames by replacing the beam supports with columns. The columns were assumed to remain at ambient temperatures and only the column stiffness was varied. For both the composite beam and the steel beam, the behaviour of the frames can be divided into two categories. The first category is where the columns are stiffer than the beam, and the second is where are columns more flexible than the beam. Both frame categories had a very low midspan deflection during the early stages of the fire. The midspan deflection was approximately linear with time. This compares well with the findings of the real fire single beam test of the Cardington fires (Clifton: 2001), as discussed in section 2.2 of this report.

8.3.1 Columns stiffer than the beam

Even with very stiff columns the beam's behaviour was significantly different to the fully-fixed beam for both the composite and the steel beam. The very small horizontal deflections of the beam-column joints with very stiff columns permitted enough axial expansion of the beam to delay the beam ends from reaching the proportional limit compared to the fully-fixed beam. As a result the midspan deflections were very low for the first 15 minutes of the fire's duration for both the composite and the steel beam. The collapse mechanism of the frame with stiff columns has a plastic hinge at the top and bottom of the columns, both beam column joints, and the beam midspan. The beam-column joint plastic hinge occurs in the columns for composite beam case, and the beam for the steel beam case.

8.3.2 Columns more flexible than the beam

When the columns are more flexible than the beam, the beam behaviour becomes more similar to the pinned-roller supported beam for both the composite beam and the steel beam in the early stages of the fire. In the later stages of the fire, after a plastic hinge has formed at the midspan, the columns offer tensile resistance to the collapsing beam. This causes it to last significantly longer than the pinned-roller supported beam. The collapse mechanism of the frame with flexible columns has plastic hinges at the beam-column joints, and at the beam midspan. The plastic hinges form at the beam-column

joints within the beam first, and then secondly at the beam midspan for both the composite beam and the steel beam scenarios. The sequence of plastic hinge formation for this beam mechanism varies from what was observed for the beams with axially restrained idealised connections. This was because the axial compression within the framed beams is less due to frame action.

8.4 Recommendations for further research

It is recommended that future research should include:

- Analysis of frames with pinned connections to the columns.
- The effects of unsymmetrical and partial loading
- The effect of continuity of the frame. 3 spans should be investigated with thermal exposure to the centre span, an end span and a centre and end span combination
- A study of the effects of different fire curves upon the frame
- A study comparing thermally protected beams with unprotected beams
- Analysis of frames with columns exposed to the fire
- 2-D frame analysis for a single storey of the building
- 3-D shell and beam element analysis including the effects of tensile membrane action and frame redundancy.
- Experimental verification of analytical results

9 References

Bailey C, et al, 1999; The Behaviour of Multistorey Steel Framed Buildings in Fire; British Steel plc, Sweden Technology Centre, Moorgate, United Kingdom

Becker R, 2000; Thermal and Structural Behaviour of Continuous Steel Construction under Fire Conditions; First International Workshop on Structures in Fire, Copenhagen, (as Report TM2).

Buchanan A.H., 2001; Structural Design for Fire Safety; John Wiley & Sons , West Sussex, England.

O'Callaghan D. J. and O'Connor M. A, 2000; Comparison of Finite Element Models of Composite Framed Buildings Behaviour in Fire; First International Workshop on Structures in Fire, Copenhagen, (as Report TM2).

Clifton C, 2001; Notes prepared for a seminar on The Behaviour and Design of Multi-Storey Steel Framed Buildings For Severe Fires; HERA Report R4-105, Manukau City, New Zealand

Dimond Industries, 1997; Hi Bond Design Manual. Manual No. 7 in the Dimond Design Information Series, Dimond Industries, New Zealand

EC2, 1993; Eurocode 2: Design of Concrete Structures. ENV 1992-1-2: General Rules – Structural Fire Design. European Committee for Standardisation, Brussels.

EC3, 1995; Eurocode 3: Design of Steel Structures. ENV 1993-1-2: General Rules – Structural Fire Design. European Committee for Standardisation, Brussels.

Fire Saftey Engineering Consultants (FSEC) Ltd., 1991, Structural Fire Engineering Investigation of Broadgate Phase 8 Fire; SCIF Fire Engineering Group, BHP Melbourne Research Laboratories, Australia

Franssen, J. M., Kodur, V. K. R. and Mason, J. (2001), Users's Manual for Safir2001; A Computer Program for Analysis of Structures Submitted to the Fire; University of Liege, Belgium.

NZS 3404:1992 Steel Structures Standard, Parts 1 & 2, Standards New Zealand, Wellington.

Rotter J.M. and Usmani A.S., 2000, Fundamental principles of structural behaviour under thermal effects; First International Workshop on Structures in Fire, Copenhagen, (as Report TM2).

Seputro, J. (2001), Effect of Support Conditions on Steel Beams Exposed of Fire. Fire Engineering Research Report 01/6. School of Engineering, University of Canterbury, Christchurch, New Zealand

Welsh, R. D. (2001), 2-D Analysis of Composite Steel-Concrete Beams in Fire. Fire Engineering Research Report 01/8. School of Engineering, University of Canterbury, Christchurch, New Zealand

10 Appendix

10.1 Appendix 1: Properties of steel and concrete at elevated temperatures from EC3 (1995) and EC2 (1993)

10.1.1 EC3 (1995) grade S 355 steel

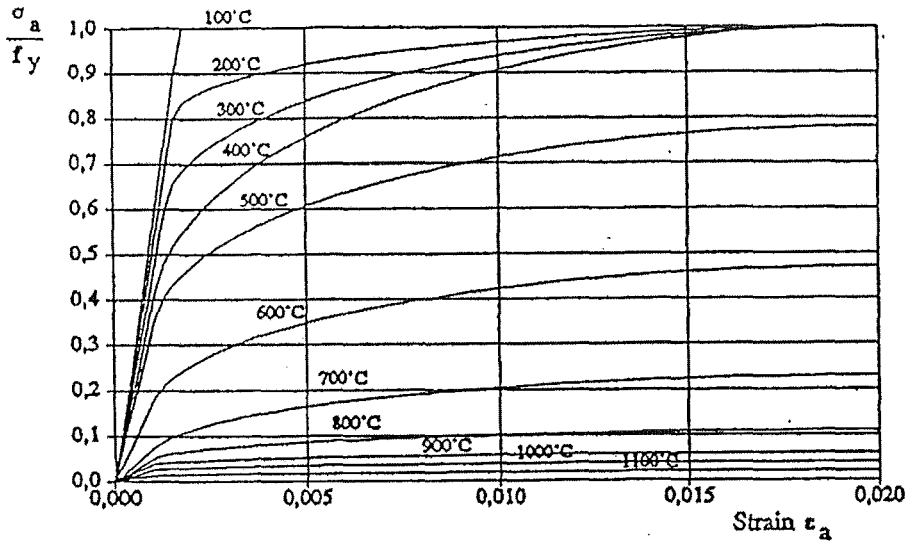

Figure A.1) EC3 (1995) variation of stress-strain relationship with temperature for grade S 355 steel (Strain hardening not included)

Steel temperature θ_a	Reduction factors at temperature θ_a relative to the value of f_y or E_a at 20°C		
	Reduction factor for effective yield strength	Reduction factor for proportional limit	Reduction factor for the elastic modulus.
20°C	1.000	1.000	1.000
100°C	1.000	1.000	1.000
200°C	1.000	0.807	0.900
300°C	1.000	0.613	0.800
400°C	1.000	0.420	0.700
500°C	0.780	0.360	0.600
600°C	0.470	0.180	0.310
700°C	0.230	0.075	0.130
800°C	0.110	0.050	0.090
900°C	0.060	0.0375	0.0675
1000°C	0.040	0.0250	0.0450
1100°C	0.020	0.0125	0.0225
1200°C	0.000	0.0000	0.0000

Table A.1) EC3 (1995) reduction factors for stress-strain relationship of steel at elevated temperatures

10.1.2 EC2 (1993) hot rolled reinforcing steels

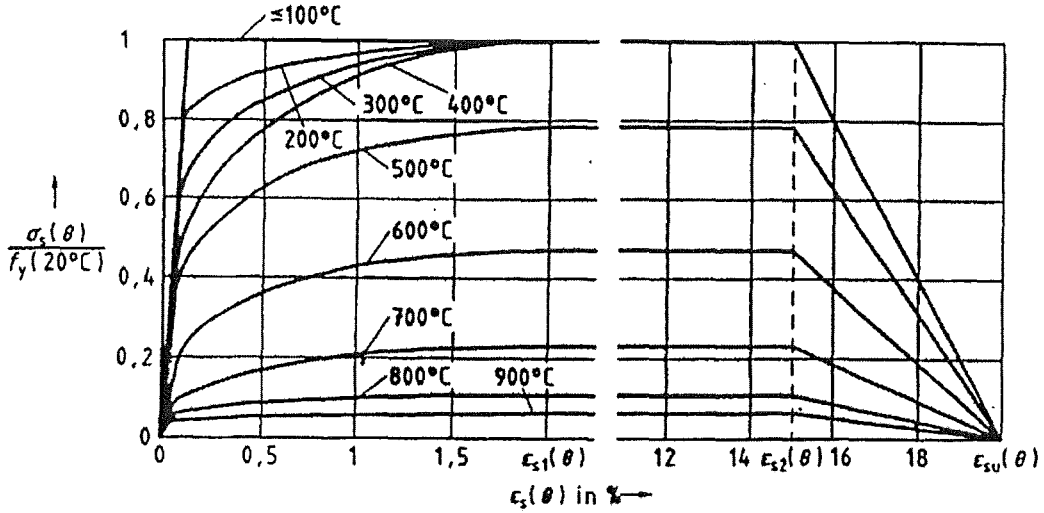

Figure A.2) EC2 (1993) variation of stress-strain relationship with temperature of hot rolled reinforcing steels at elevated temperatures

Steel temperature θ_a	Reduction factors at temperature θ_a relative to the value of f_y or E_a at 20°C		
	Reduction factor for effective yield strength	Reduction factor for proportional limit	Reduction factor for the elastic modulus.
20°C	1.000	1.000	1.000
100°C	1.000	0.960	1.000
200°C	1.000	0.920	0.870
300°C	1.000	0.810	0.720
400°C	0.940	0.630	0.560
500°C	0.670	0.440	0.400
600°C	0.400	0.260	0.240
700°C	0.120	0.080	0.080
800°C	0.110	0.060	0.060
900°C	0.080	0.050	0.050
1000°C	0.050	0.030	0.030
1100°C	0.030	0.020	0.020
1200°C	0.000	0.000	0.000

Table A.2) EC2 (1993) reduction factors for stress-strain relationship of hot rolled reinforcing steels at elevated temperatures

10.1.3 EC2 (1993) siliceous concrete

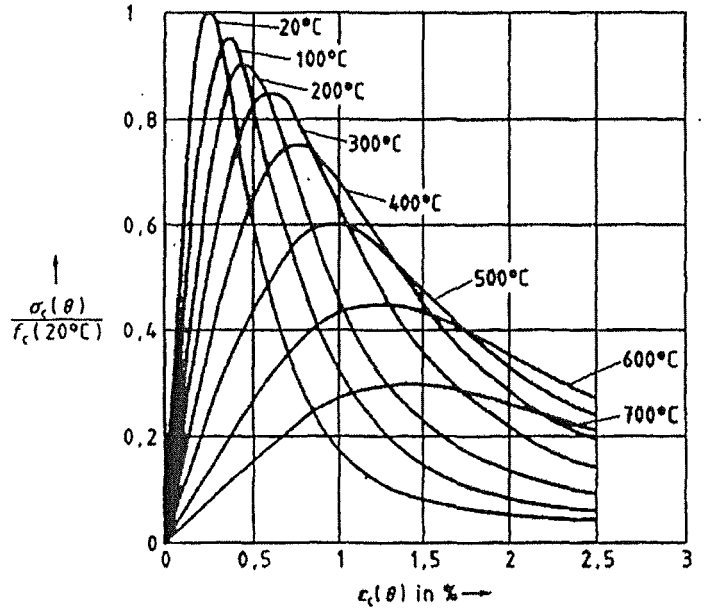

Figure A.3) EC2 (1993) stress-strain relationships of siliceous concrete under uniaxial compression at elevated temperatures

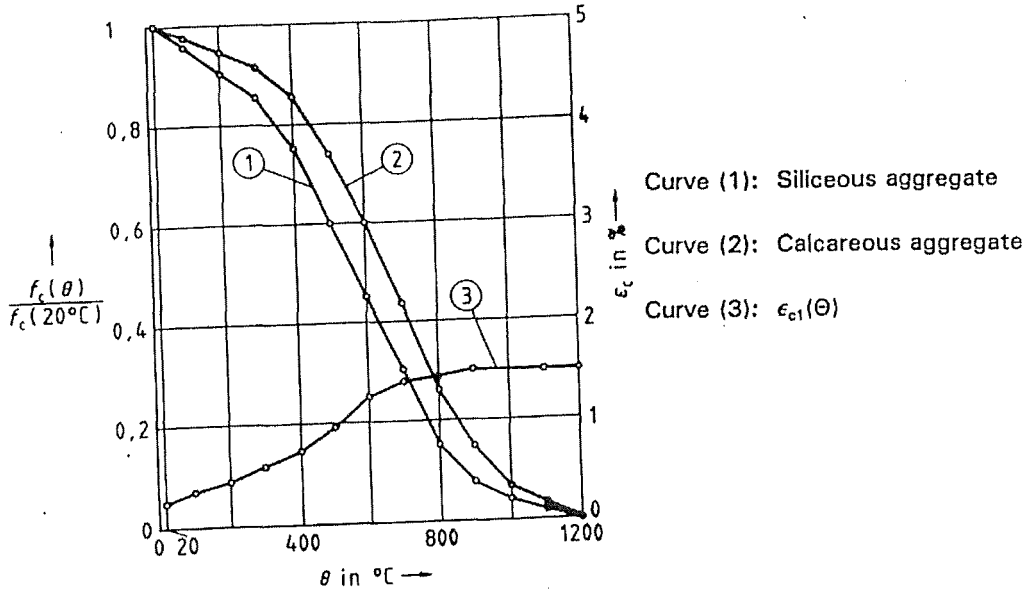

Figure A.4) EC2 (1993) Parameters for stress-strain relationships of concrete at elevated temperatures

Concrete Temperature (°C)	$f_c(\Theta)/f_c(20\,°C)$		$\epsilon_{c1}(\Theta) \times 10^{-3}$
	siliceous	calcareous	
20	1,00	1,00	2,5
100	0,95	0,97	3,5
200	0,90	0,94	4,5
300	0,85	0,91	6,0
400	0,75	0,85	7,5
500	0,60	0,74	9,5
600	0,45	0,60	12,5
700	0,30	0,43	14,0
800	0,15	0,27	14,5
900	0,08	0,15	15,0
1000	0,04	0,06	15,0
1100	0,01	0,02	15,0
1200	0,00	0,00	-

Table A.3) EC2 (1993) reduction factors for stress-strain relationship in compression of concrete at elevated temperatures

10.2 Appendix 2: Example Thermal SAFIR input files.

Note in this section of the appendix repetitive sections of the input code have been replaced with an arrow: ↓.

10.2.1 Steel Beam

This describes a 610UB101 steel beam exposed to the ISO (FISO) Fire curve on three faces

```
  NPTTOT     412
   NNODE  280
    NDIM   2
 NDIMMATER   1
  NDDLMAX   1
    FROM   1  TO  280 STEP   1 NDDL   1
 END_NDDL
 TEMPERAT
   TETA     0.9
 TINITIAL    20.0
 MAKE.TEM
LARGEUR11    40000
LARGEUR12     100
 NORENUM
Jenny.tem
   NMAT   1
 ELEMENTS
  SOLID  206
    NG   2
  NVOID   0
 END_ELEM
  NODES
   NODE   1   0.3010  -0.1140
   NODE   2   0.3010  -0.1056
   NODE   3   0.3010  -0.0972
```

```
   NODE   4   0.3010  -0.0888
                        ↓
   NODE 280  -0.3010   0.1140
 NODELINE          0       0
     YC_ZC         0       0
FIXATIONS
 END_FIX
NODOFSOLID
   ELEM   1   1  30  31   2   1   0
   ELEM   2   2  31  32   3   1   0
   ELEM   3   3  32  33   4   1   0
                        ↓
   ELEM 206 250 279 280 251   1   0
 FRONTIER
     F     1    FISO     NO      NO      NO
     F    29    FISO     NO      NO      NO
     F    57    FISO     NO      NO      NO
                        ↓
     F   206      NO     NO    FISO      NO
 END_FRONT
 SYMMETRY
 END_SYM
 PRECISION    1.E-3
 MATERIALS
 STEELEC3
25 9 0.5
   TIME
          1.     15.
         15.   1800.
         30.  10800.
 END_TIME
IMPRESSION
 TIMEPRINT     60.
```

10.2.2 Composite Beam

This describes a 610UB101 steel beam acting compositively with a 120mm thick profiled concrete slab exposed to the ISO (FISO) Fire curve on three faces.

```
  NPTTOT       2
   NNODE 1507
    NDIM   2
NDIMMATER   1
 NDDLMAX   1
    FROM   1  TO 1507 STEP   1 NDDL   1
 END_NDDL
 TEMPERAT
    TETA     0.90
 TINITIAL      20
 MAKE.TEM
LARGEUR11    50000
LARGEUR12     1000
 NORENUM
finishedslab.TEM
    NMAT   3
 ELEMENTS
   SOLID 1349
     NG   2
   NVOID   0
 END_ELEM
   NODES
NODE 1        0        0
NODE 2        -0.0125          0
                        ↓
NODE 1506   -0.72275        0.1056
NODE 1507   -0.72275        0.114
 NODELINE        -0.120        0
   YC_ZC           0        0
```

```
 FIXATIONS
  END_FIX
NODOFSOLID
ELEM 1      2      16     15     1      3      0
ELEM 2      3      17     16     2      3      0
                          ↓
ELEM 1349   1506   1507   1492   1491   1      0

 FRONTIER
F       1      NO     NO     f20.fct   NO
F       14     NO     NO     f20.fct   NO
                          ↓
F       1260   NO     NO     FISO      NO
 END_FRONT
 SYMMETRY
    YSYM
   ENDSYM
 PRECISION    0.001
 MATERIALS
 STEELEC3
25 9 0.5
 STEELEC2
25 9 0.5
SILCONCEC2
92 25 9 0.5
    TIME
          1.     10.
         10.   3600.
         15.   7200.
  END_TIME
IMPRESSION
 TIMEPRINT     60.
```

10.3 Appendix 3: Example structural SAFIR input files.

10.3.1 Pin-pinned steel beam

This describes the pin-pin supported steel beam

```
  NPTTOT    8240
   NNODE  41
    NDIM  2
NDIMMATER  1
 NDDLMAX  3
   FROM  1  TO  41 STEP  2 NDDL  3
   FROM  2  TO  40 STEP  2 NDDL  1
END_NDDL
 STATIC
  NLOAD  1
 OBLIQUE  0
 COMEBACK  0.000001
NARCLENGTH    0.05
LARGEUR11     500
LARGEUR12      50
 NORENUM
   NMAT  1
ELEMENTS
   BEAM  20  1
    NG  2
  NFIBER  206
END_ELEM
  NODES
   NODE  1  0.00000  0.00000  0.00000
   GNODE  41  8.00000  0.00000  0.00000
FIXATIONS
   BLOCK  1        F0     F0     NO
   BLOCK  41       F0     F0     NO
```

```
  END_FIX
NODOFBEAM
Jenny.tem
 TRANSLATE   1   1
 END_TRANS
    ELEM   1   1   2   3   1
   GELEM  20  39  40  41   1   2
PRECISION    1.e-3
   LOADS
 FUNCTION    FLOAD
DISTRBEAM      1   0. -25000   0.
DISTRBEAM      2   0. -25000   0.
                          ↓
DISTRBEAM     20   0. -25000   0.
 END_LOAD
MATERIALS
 STEELEC3
210.0E+9 0.3 300.0E+6
    TIME
            5.    600.
           10.   7200.
  ENDTIME
LARGEDISPL
   EPSTH
IMPRESSION
 TIMEPRINT      30.
PRINTREACT
  PRINTMN
PRNSIGMABM  10   2
```

10.3.2 Pin-pinned composite beam

This describes the pin-pin supported composite beam

```
  NPTTOT    53960
   NNODE   41
    NDIM    2
 NDIMMATER    1
  NDDLMAX    3
    FROM    1   TO   41 STEP    2 NDDL    3
    FROM    2   TO   40 STEP    2 NDDL    1
 END_NDDL
  STATIC
   NLOAD    1
 OBLIQUE    0
 COMEBACK 0.0000001
NARCLENGTH      0.05
 LARGEUR11       500
 LARGEUR12        50
  NORENUM
    NMAT    3
 ELEMENTS
    BEAM   20    1
     NG    2
  NFIBER 1349
 END_ELEM
   NODES
    NODE    1   0.00000   0.00000   0.00000
   GNODE   41   8.00000   0.00000   0.00000
 FIXATIONS
   BLOCK    1          F0       F0       NO
   BLOCK   41          F0       F0       NO
  END_FIX
 NODOFBEAM
```

finishedslab.tem

```
 TRANSLATE   1   1
 TRANSLATE   2   2
 TRANSLATE   3   3
 END_TRANS
    ELEM   1   1   2   3   1
   GELEM  20  39  40  41   1   2
 PRECISION    1.e-7
   LOADS
 FUNCTION    FLOAD
 DISTRBEAM       1       0.   -50.E3
GDISTRBEAM      20       0.   -50.E3    1
 END_LOAD
 MATERIALS
 STEELEC3
210.0E+9 0.3 300.0E+6
 STEELEC2
210.0E+9 0.3 430.0E+6
SILCONCEC2
 0.2 30.0E+6 0 0

    TIME
            1.      10.
            5.     600.
           10.   21600.
  ENDTIME
LARGEDISPL
   EPSTH
IMPRESSION
 TIMEPRINT      30.
PRINTREACT
  PRINTMN
PRNSIGMABM  10   2
```

10.3.3 Frame with steel beam (100% column stiffness)

This describes the frame with steel beam (100% column stiffness)

```
  NPTTOT   58080
   NNODE 123
    NDIM   2
NDIMMATER   1
 NDDLMAX   3
   FROM   1  TO  41 STEP   2 NDDL   3
   FROM   2  TO  40 STEP   2 NDDL   1
   FROM  42  TO  82 STEP   2 NDDL   3
   FROM  43  TO  81 STEP   2 NDDL   1
   FROM  83  TO 123 STEP   2 NDDL   3
   FROM  84  TO 122 STEP   2 NDDL   1
 END_NDDL
  STATIC
   NLOAD   1
 OBLIQUE   0
 COMEBACK  0.00001
NARCLENGTH    0.05
 LARGEUR11    1902
 LARGEUR12      50
  NORENUM
    NMAT   2
 ELEMENTS
   BEAM  60   2
    NG   2
  NFIBER 206
 END_ELEM
   NODES
   NODE   1 -4.00000   0.00000   0.00000
  GNODE  41   4.00000   0.00000   0.00000
   NODE  42 -4.00000   4.00000   0.00000
```

```
   GNODE  82 -4.00000 -4.00000  0.00000
    NODE  83  4.00000  4.00000  0.00000
   GNODE 123  4.00000 -4.00000  0.00000
 FIXATIONS
   BLOCK  42        F0     F0     F0
   BLOCK  82        F0     F0     F0
   BLOCK  83        F0     F0     F0
   BLOCK 123        F0     F0     F0
    SAME   1  62    YES    YES    YES
    SAME  41 103    YES    YES    YES
  END_FIX
 NODOFBEAM
Column.tem
 TRANSLATE   1   1
 END_TRANS
Jenny.tem
 TRANSLATE   1   2
 END_TRANS
    ELEM   1   1   2   3   2
   GELEM  20  39  40  41   2   2
    ELEM  21  42  43  44   1
   GELEM  40  80  81  82   1   2
    ELEM  41  83  84  85   1
   GELEM  60 121 122 123   1   2
 PRECISION    1.e-4
   LOADS
 FUNCTION    FLOAD
 DISTRBEAM        1      0.   -25.E3
 GDISTRBEAM      20      0.   -25.E3   1
 END_LOAD
 MATERIALS
 STEELEC3
210.0E+9 0.3 300.0E+6
 STEELEC3
```

```
210.0E+9 0.3 300.0E+6
    TIME
              5.    600.
             10.   7200.
  ENDTIME
LARGEDISPL
   EPSTH
IMPRESSION
 TIMEPRINT     30.
PRINTREACT
  PRINTMN
PRNSIGMABM  30   1
```

10.3.4 Frame with composite beam (100% column stiffness)

This describes the frame with composite beam (100% column stiffness)

```
  NPTTOT   70440
   NNODE 123
    NDIM  2
NDIMMATER  1
 NDDLMAX  3
   FROM  1  TO  41 STEP  2 NDDL  3
   FROM  2  TO  40 STEP  2 NDDL  1
   FROM  42  TO  82 STEP  2 NDDL  3
   FROM  43  TO  81 STEP  2 NDDL  1
   FROM  83  TO  123 STEP  2 NDDL  3
   FROM  84  TO  122 STEP  2 NDDL  1
 END_NDDL
  STATIC
   NLOAD  1
 OBLIQUE  0
 COMEBACK 0.000001
NARCLENGTH    0.05
 LARGEUR11    1902
 LARGEUR12     50
  NORENUM
    NMAT  4
 ELEMENTS
   BEAM  60  2
     NG  2
  NFIBER 1349
 END_ELEM
   NODES
    NODE  1 -4.00000  0.00000  0.00000
   GNODE  41  4.00000  0.00000  0.00000
```

```
   NODE  42 -4.00000  4.00000  0.00000
   GNODE  82 -4.00000 -4.00000  0.00000
   NODE  83  4.00000  4.00000  0.00000
   GNODE 123  4.00000 -4.00000  0.00000
FIXATIONS
   BLOCK  42        F0     F0     F0
   BLOCK  82        F0     F0     F0
   BLOCK  83        F0     F0     F0
   BLOCK 123        F0     F0     F0
   SAME  1  62    YES    YES    YES
   SAME  41 103    YES    YES    YES
 END_FIX
NODOFBEAM
Column2.tem
TRANSLATE  1  1
END_TRANS
finishedslab2.tem
TRANSLATE  1  2
TRANSLATE  2  3
TRANSLATE  3  4
END_TRANS
   ELEM  1  1  2  3  2
   GELEM  20  39  40  41  2  2
   ELEM  21  42  43  44  1
   GELEM  40  80  81  82  1  2
   ELEM  41  83  84  85  1
   GELEM  60 121 122 123  1  2
PRECISION   1.e-4
   LOADS
 FUNCTION   FLOAD
DISTRBEAM       1     0.   -50.E3
GDISTRBEAM      20      0.   -50.E3   1
 END_LOAD
MATERIALS
```

```
 STEELEC3
210.0E+9 0.3 300.0E+6
 STEELEC3
210.0E+9 0.3 300.0E+6
 STEELEC2
210.0E+9 0.3 430.0E+6
SILCONCEC2
0.2 30.0E+6 0 0
    TIME
            5.    600.
           10.   7200.
  ENDTIME
LARGEDISPL
   EPSTH
IMPRESSION
 TIMEPRINT     30.
PRINTREACT
  PRINTMN
PRNSIGMABM  40   2
```

FIRE ENGINEERING RESEARCH REPORTS

95/1	Full Residential Scale Backdraft	I B Bolliger
95/2	A Study of Full Scale Room Fire Experiments	P A Enright
95/3	Design of Load-bearing Light Steel Frame Walls for Fire Resistance	J T Gerlich
95/4	Full Scale Limited Ventilation Fire Experiments	D J Millar
95/5	An Analysis of Domestic Sprinkler Systems for Use in New Zealand	F Rahmanian
96/1	The Influence of Non-Uniform Electric Fields on Combustion Processes	M A Belsham
96/2	Mixing in Fire Induced Doorway Flows	J M Clements
96/3	Fire Design of Single Storey Industrial Buildings	B W Cosgrove
96/4	Modelling Smoke Flow Using Computational Fluid Dynamics	T N Kardos
96/5	Under-Ventilated Compartment Fires - A Precursor to Smoke Explosions	A R Parkes
96/6	An Investigation of the Effects of Sprinklers on Compartment Fires	M W Radford
97/1	Sprinkler Trade Off Clauses in the Approved Documents	G J Barnes
97/2	Risk Ranking of Buildings for Life Safety	J W Boyes
97/3	Improving the Waking Effectiveness of Fire Alarms in Residential Areas	T Grace
97/4	Study of Evacuation Movement through Different Building Components	P Holmberg
97/5	Domestic Fire Hazard in New Zealand	KDJ Irwin
97/6	An Appraisal of Existing Room-Corner Fire Models	D C Robertson
97/7	Fire Resistance of Light Timber Framed Walls and Floors	G C Thomas
97/8	Uncertainty Analysis of Zone Fire Models	A M Walker
97/9	New Zealand Building Regulations Five Years Later	T M Pastore
98/1	The Impact of Post-Earthquake Fire on the Built Urban Environment	R Botting
98/2	Full Scale Testing of Fire Suppression Agents on Unshielded Fires	M J Dunn
98/3	Full Scale Testing of Fire Suppression Agents on Shielded Fires	N Gravestock
98/4	Predicting Ignition Time Under Transient Heat Flux Using Results from Constant Flux Experiments	A Henderson
98/5	Comparison Studies of Zone and CFD Fire Simulations	A Lovatt
98/6	Bench Scale Testing of Light Timber Frame Walls	P Olsson
98/7	Exploratory Salt Water Experiments of Balcony Spill Plume Using Laser Induced Fluorescence Technique	E Y Yii
99/1	Fire Safety and Security in Schools	R A Carter

99/2	A Review of the Building Separation Requirements of the New Zealand Building Code Acceptable Solutions	J M Clarke
99/3	Effect of Safety Factors in Timed Human Egress Simulations	K M Crawford
99/4	Fire Response of HVAC Systems in Multistorey Buildings: An Examination of the NZBC Acceptable Solutions	M Dixon
99/5	The Effectiveness of the Domestic Smoke Alarm Signal	C Duncan
99/6	Post-flashover Design Fires	R Feasey
99/7	An Analysis of Furniture Heat Release Rates by the Nordtest	J Firestone
99/8	Design for Escape from Fire	I J Garrett
99/9	Class A Foam Water Sprinkler Systems	D B Hipkins
99/10	Review of the New Zealand Standard for Concrete Structures (NZS 3101) for High Strength and Lightweight Concrete Exposed to Fire	M J Inwood
99/12	An Analytical Model for Vertical Flame Spread on Solids: An Initial Investigation	G A North
99/13	Should Bedroom Doors be Open or Closed While People are Sleeping? - A Probabilistic Risk Assessment	D L Palmer
99/14	Peoples Awareness of Fire	S J Rusbridge
99/15	Smoke Explosions	B J Sutherland
99/16	Reliability of Structural Fire Design	JKS Wong
99/17	Heat Release from New Zealand Upholstered Furniture	T Enright
00/1	Fire Spread on Exterior Walls	FNP Bong
00/2	Fire Resistance of Lightweight Framed Construction	PCR Collier
00/3	Fire Fighting Water: A Review of Fire Fighting Water Requirements (A New Zealand Perspective)	S Davis
00/4	The Combustion Behaviour of Upholstered Furniture Materials in New Zealand	H Denize
00/5	Full-Scale Compartment Fire Experiments on Upholstered Furniture	N Girgis
00/6	Fire Rated Seismic Joints	M James
00/7	Fire Design of Steel Members	K R Lewis
00/8	Stability of Precast Concrete Tilt Panels in Fire	L Lim
00/9	Heat Transfer Program for the Design of Structures Exposed to Fire	J Mason
00/10	An Analysis of Pre-Flashover Fire Experiments with Field Modelling Comparisons	C Nielsen
00/11	Fire Engineering Design Problems at Building Consent Stage	P Teo
00/12	A Comparison of Data Reduction Techniques for Zone Model Validation	S Weaver
00/13	Effect of Surface Area and Thickness on Fire Loads	H W Yii
00/14	Home Fire Safety Strategies	P Byrne
00/15	Accounting for Sprinkler Effectiveness in Performance Based Design of Steel Buildings in Fire	M Feeney

00/16	A Guideline for the Fire Design of Shopping Centres	J M McMillan
01/1	Flammability of Upholstered Furniture Using the Cone Calorimeter	A Coles
01/2	Radiant Ignition of New Zealand Upholstered Furniture Composites	F Chen
01/3	Statistical Analysis of Hospitality Industry Fire Experience	T Y A Chen
01/4	Performance of Gypsum Plasterboard Assemblies Exposed to Real Building Fires	B H Jones
01/5	Ignition Properties of New Zealand Timber	C K Ngu
01/6	Effect of Support Conditions on Steel Beams Exposed of Fire	J Seputro
01/7	Validation of an Evacuation Model Currently Under Development	A Teo
01/8	2-D Analysis of Composite Steel - Concrete Beams in Fire	R Welsh
01/9	Contribution of Upholstered Furniture to Residential Fire Fatalities in New Zealand	C R Wong
01/10	The Fire Safety Design of Apartment Buildings	S Wu
01/11	Smoke Alarm Ownership in Relation to Socio-Economic Factors in Christchurch	N Buchanan
01/12	Accounting for Sprinkler Effectiveness in Performance Based Design of Steel Buildings for Fire	M Feeney
01/13	Equivalent Fire Resistance Ratings of Construction Elements Exposed to Realistic Fires	J Nyman
02/1	Performance of Expanded Polystyrene Insulated Panel Exposed to Radiant Heat	G Baker
02/2	A Comparison Between Predicted and Actual Behaviour of Domestic Smoke Detectors in a Realistic House Fire	D Brammer
02/3	Development of Bench-Scale Testing of Sprinkler and Smoke Detector Activation/Response Time	K S Chin
02/4	The Effect of Door Angle on Fire Induced Flow Through a Doorway	L R Clark
02/5	Implementation of a Glass Fracture Module for the BRANZ Fire Compartment Fire Zone Modelling Software	R Parry
02/6	Assessing the Feasibility of Reducing the Grid Resolution in FDS Field Modelling	N Patterson
02/7	Fire Safety Design of Ferrymead Heritage Park	M Rangi
02/8	Experimental Results for Pre-Flashover Fire Experiments in Two Adjacent ISO Compartments	L Rutherford
02/9	Measurement of Magnitude and Direction of Hot Gas Flow in a Fire Compartment with a Fire-hole Probe	J Schulz
02/10	Assessment of the Current False Alarm Situation from Fire Detection Systems in New Zealand and the Development of an Expert System for Their Identifications	Y F Tu
02/11	Performance of Unprotected Steel and Composite Steel Frames Exposed to Fire	C Wastney

School of Engineering
University of Canterbury
Private Bag 4800, Christchurch, New Zealand

Phone 643 364-2250
Fax 643 364-2758